Fractional-Order Signal Processing and Signal Generating Circuits

A thesis submitted to the
Delhi Technological University
for the award of the degree

of

Doctor of Philosophy

in

Electronics & Communication

by

Garima Varshney
(2K18/PHDEC/506)

Under the supervision of

Prof. Neeta Pandey

Prof. Rajeshwari Pandey

Delhi Technological University
Bawana Road, Shahbad Daulatpur Village,
Rohini, New Delhi-110042, India

June 2023

Dedicated to,

My beloved family, without whose endless love and support, I could not achieve this.

DELHI TECHNOLOGICAL UNIVERSITY
formerly Delhi College of Engineering
(under Delhi Act 6 of 2009, Govt. of NCT of Delhi)

CERTIFICATE

This is to certify that the thesis entitled "**Fractional-Order Signal Processing and Signal Generating Circuits**", submitted by **Garima Varshney** (2K18/PHDEC/506) to the Department of Electronics and Communication Engineering, Delhi Technological University, for the award of the degree of Doctor of Philosophy is based on the original research work carried out by her under our guidance and supervision. In our opinion, the thesis has reached the standards fulfilling the requirements of the regulations relating to the degree. It is further certified that the work presented in this thesis is not submitted to any other university or institution for the award of any degree or diploma.

Date:

Place:

Prof. Neeta Pandey
Professor
Delhi Technological University
New Delhi
India

Prof. Rajeshwari Pandey
Professor
Delhi Technological University
New Delhi
India

DECLARATION

I hereby certify that the research work, which is being presented in this thesis, titled, "**Fractional-Order Signal Processing and Signal Generating Circuits**", in fulfillment of requirements of the award of the degree of Doctor of Philosophy is an authentic record of my research work carried under the supervision of Prof. Neeta Pandey and Prof. Rajeshwari Pandey. The matter presented in this thesis has not been submitted elsewhere in part or fully to any other University or Institute for the award of any degree.

Date:

Place:

Garima Varshney
(2K18/PHDEC/506)

Acknowledgments

I am sincerely grateful for the support and expert guidance provided by my supervisors, Prof. Neeta Pandey and Prof. Rajeshwari Pandey, from the Department of Electronics and Communication Engineering at Delhi Technological University (DTU). Their invaluable supervision, unwavering motivation, and genuine care have played a significant role in my academic journey. I am truly thankful for their mentorship and the humanitarian values they consistently demonstrate.

I extend my heartfelt appreciation to Prof. O. P. Verma, Head of the Department of Electronics and Communication Engineering at DTU, for providing me with the essential resources and facilities to successfully complete my work. I would also like to express my sincere thanks to all the faculty members of the ECE Department at DTU for their ongoing assistance and support whenever I needed it.

I am also grateful to Prof. J. P. Saini, Vice-Chancellor of DTU, Delhi, and Prof. Yogesh Singh, former Vice-Chancellor of DTU, Delhi, for fostering a conducive research environment within the institute. Their visionary leadership and support have contributed significantly to creating an atmosphere that encourages and promotes research activities. I am thankful for their contributions in establishing an environment that nurtures academic and research excellence.

I would like to extend my heartfelt thanks to my colleagues and seniors in the electronics department, namely Dr. K. Gurumurthy, Dr. Rakesh Verma, Ms. Parveen, Ms. Damyanti, Ms. Sweta, Ms. Kavita, and Mr. Lokesh for their unwavering support throughout my journey. Their guidance and encouragement have been invaluable.

I would also like to express my deep respect and gratitude to my mother, Smt. Pratima, for her constant support in every aspect of my life. Her unwavering belief in me has been a source of strength and inspiration. I am truly grateful to my husband, Vijay, for his consistent motivation and encouragement during my doctoral studies. His support has played a significant role in keeping me motivated and focused.

I would also like to thank my brother, Purav for supporting me through this long journey. Last but not the least, I want to thank my wonderful son, Dev, and my charming daughter, Devanya, for their patience and understanding during my academic journey. Their love and support have been instrumental in helping me navigate through the challenges.
I am truly grateful to all these individuals who have played a significant role in my academic and personal growth.

Date:

Place:

Garima Varshney
(2K18/PHDEC/506)

Abstract

Fractional calculus is the branch of mathematics concerning differentiations and integrations of non-integer orders. The inherent ability of fractional calculus to provide more accurate descriptions of real-world phenomena compared to classical integer methods is making it a preferred choice among system designers. Fractional-order systems are found in diverse scientific disciplines including thermodynamics, electrical engineering, control systems, biomedical science, mechanics, electronics, communication, and image encryption. As a result, there is significant potential for multidisciplinary research and exploration in the field of fractional-order systems.

Electronic filters are essential components of modern electronic systems. The order of a filter is characterized by the slope it offers in transition band. Fractional-order filters (FOF) are more general case of classical integer-order filters, with order of the filter $(n + \alpha)$, where n is the integer and α is the fractional part $(0 < \alpha < 1)$. FOF offers more precise control over the transitional slope between pass band and stop band, as the slope is given by $-20(n+\alpha)$ dB/decade, while for classical filters it is 20 dB/decade. Fractional order provides an extra degree of freedom, which increase flexibility of the design.

In many applications, such as telecommunication, biomedical signal processing etc., the cascading of voltage-mode and current-mode filters necessitates the use of a voltage-to-current (V-I) converter. The total efficacy of the filter can be increased if signal processing can be combined with V-I converter interfacing. A transadmittance-mode filter is suitable for such applications. As OTA exhibits high impedance at both input and output terminals, it is an ideal choice for implementing trans-admittance mode (TAM) signal processing applications. Thus, a resistor-less, α-order TAM FOF utilizing two OTAs and one fractional-order capacitor is presented to improve the cascadibility between voltage-mode and current-mode filters. The electronic tuning of the proposed TAM FOF's parameters is achieved through transconductance gain of OTA.

There are two main methods to achieve the electronic tuning of filter's parameter.

The first method involves adjusting the transconductance/current/voltage gain of the constituent active elements. The second method utilizes controlling the gain of the external amplifier introduced in the feedback loop of the core filter. The later approach is known as the shadow concept, and filters employing this method are referred to as shadow filters. The theory of shadow filters, originally developed for integer-order filters, is generalized to fractional domain. Mathematical formulas are drafted for pole frequency and pole quality factor of the fractional-order shadow filters. The proposed theory is validated through OTA-based two active filters.
Sinusoidal oscillators are extensively used in the field of communication, control systems, testing and measurements. Fractional-order oscillators (FOOs) offer the advantage of achieving higher oscillation frequencies compared to their integer-order counterparts, while still maintaining the same values of passive components. FOOs also offer arbitrary phase shifts between their output signals, providing added flexibility. OTA based three new sinusoidal FOOs and one fractional-order multivibrator are presented. The first two circuits of the sinusoidal FOO are designed using the trans-admittance mode FAPF with a trans-impedance mode integrator/differentiator topology. The third circuit of the sinusoidal FOO features a unique design that enables independent control of the phase difference between its two output voltages. Further, an electronically tunable fractional-order multivibrator based on OTA has been generalized to fractional domain. The mathematical formula for the time period has been derived using Reimann-Liouville fractional integral.
As all the circuits of FOFs and FOOs, proposed in this thesis employs fractional-order elements (FOEs), specifically fractional-order capacitor (FOC), thus a compact design to approximate the behaviour of FOC based on active inductor is proposed. The circuit is modular in nature and allows for the higher order approximations through parallel connection or impedance multiplication to realize FOC. Furthermore, a circuit is presented that implements a floating version of the higher order FOE ($1 < \alpha < 2$) using OTA based IIMC.
The functionality of all the proposed structures has been verified through SPICE simulations with 180 nm CMOS technology parameters. Mathematical formulation for sensitivity of the proposed FOFs and FOOs is included. The robustness of the proposed FOFs and FOOs is also investigated through corner and Monte-Carlo analysis.

Table of Contents

List of Figures

List of Tables

Chapter 1

Introduction

1.1 Introduction

The concept of fractional-order calculus, addresses integrals and derivatives of fractional order(i.e., non-integer orders), is well known to the mathematical/scientific world. Fractional derivatives and integrals provide a remarkable representation of natural phenomena, making them an effective tool for understanding and communicating with the natural world. Fractional-order calculus, although originating at the same time as classical integer-order calculus [1], has only recently gained significant attention in various fields of applied science such as: biomedical [6]–[8], thermodynamics [2], control system [4], [5], electrical engineering [2], [3], electronics engineering [9]–[11], communication engineering [12], [13] and image encryption and decryption [14]. Therefore, there is a vast opportunity for interdisciplinary research in fractional-order systems.

The definition of fractional derivative for fractional order α $(0 < \alpha < 1)$ that is widely accepted and based on the Riemann-Liouville definition [15] is provided in (1.1). The Laplace transform is a valuable instrument employed for the purpose of designing and analyzing electronic circuits. The main purpose of Laplace transform is the transformation of circuits from the time domain to the frequency domain, which facilitates analyzing the circuit algebraically rather than working with differential equations. It is pertinent to mention that Laplace transform is applicable to fractional derivatives also. Applying the Laplace transform to (1.1) with zero initial conditions gives (1.2):

$$\frac{d^{\alpha}}{dt^{\alpha}} f(t) \equiv D_t^{\alpha} f(t) = \frac{1}{\Gamma(1-\alpha)} \frac{d}{dt} \int_0^t (t-\tau)^{-\alpha} f(\tau)\, d\tau \tag{1.1}$$

$$L\left\{D_t^{\alpha} f(t)\right\} = s^{\alpha} F(s) \tag{1.2}$$

The s^{α} denotes fractional-order Laplacian operator of α order, facilitates the design and analysis of electronic systems using fractional calculus principles, thereby avoiding the need to solve complex time-domain representations.

On the circuit theory and design front, a fractional order element (FOE) has an generalized impedance expressed as [16]:

$$Z(s) = ks^{\alpha} = k(\omega)^{\alpha} e^{j(\frac{\alpha\pi}{2})} = k(\omega)^{\alpha} \left(\cos\left(\frac{\alpha\pi}{2}\right) + jsin\left(\frac{\alpha\pi}{2}\right)\right) = |z|\angle\phi \tag{1.3}$$

Here α and ϕ denote the order and phase of the FOE respectively. The phase (ϕ) of FOE is computed as $\alpha\pi/2$, which does not depend on frequency and for a particular value of α remains constant; hence, a FOE can also be referred to as a constant phase element (CPE) and the phase can be referred to as the constant phase angle (CPA). The FOE exhibits fractional-order capacitor (FOC) behavior for values of α within the range of $-1 < \alpha < 0$, and it behaves as a fractional-order inductor (FOI) for values of α within the range of $0 < \alpha < 1$. For the specific values of α being -1, 0, and 1, the FOE behaves as a pure capacitor, resistor and inductor, respectively. However, when α equals -2, the FOE exhibits the quality of frequency-dependent negative resistance (FDNR) [17]. The representative diagram, which categorizes these elements based on CPA, is depicted in Fig. 1.1 [18].

Signal processing and signal generating circuits are the most vital elements of analog circuit design. In view of advantages offered by fractional-order calculus, researchers in the field of analog circuit design have proposed a wide range of

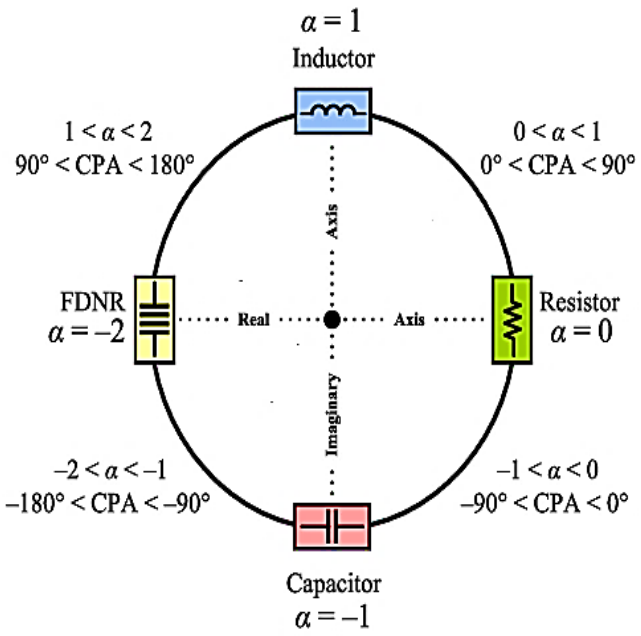

Figure 1.1: Categorization of fractional order elements [18]

fractional-order circuits, including but not limited to: fractional-order active and passive filters [17], [57]–[93], fractional-order controllers [5], [19], [20] fractional-order sinusoidal

oscillators [94]–[111], and fractional-order multivibrators [112]–[115] etc.

1.2 Related Literature

Regardless the fact, the fractional-order calculus is about three century old subject [1], the circuit design in this area has freshly captured noteworthy research interest. Thus, there are tremendous possibilities in the design and synthesis of fractional-order circuits. The candidate has concentrated on fractional-order signal processing and signal generating circuits along with the FOE. The available literature in these

areas has been discussed below.

1.2.1 Fractional-Order Element (FOE)

Literature survey suggests that numerous efforts have been made to realize/design a FOE. At present there are two techniques to realize a FOE: single-component realization (i.e., fabrication) [20]–[31] and multi-component realization (i.e., emulation) [19], [32]–[56].

The major inspiration behind the development of single-component FOE is to make it commercially available, just like a conventional capacitor. The fabrication of FOE is based on various methods such that: the rough surface of metal electrodes coated with lithium ions [20], development of fractal structures on silicon surface [21], polymer coated probe capacitive in nature is dipped in a polarized medium [22], electrolytic process [23]–[26], replacing the dielectric of a conventional capacitor by a polymer composite, percolated with reduced graphene oxide [27], ferroelectric polymer based [28], dipping CNT-polymer nanocomposite coated probes in ionic gel [29] and carbon black based [30], [31]. Despite these efforts, these are still in the early stages and require much effort before meeting the criteria of circuit designers.

Meanwhile, noteworthy research efforts have been made for the development of structures which emulate behavior of FOE. The emulation process finds a suitable mathematical approximation for the fractional-order Laplacian operator $s^{\pm\alpha}$ that remains valid within the desired frequency range and also determines the corresponding passive or active circuit with integer-order elements. Some commonly used

approximations for emulating the fractional-order Laplacian operator include: Continued Fraction Expansion (CFE) [32], Carlson approximation [32], Matsuda approximation [32], Oustaloup Recursive approximation [32], Valsa approximation [116] and Modified Oustaloup [33]. After obtaining an approximated impedance function using FOE approximation methods, it is possible to synthesize it using R-C networks [19], [34], [35]. The values of the components in the R-C network used for emulating the FOE depend on the desired magnitude and order of the FOE, so these do not provide electronic tuning of magnitude and fractional order (α).

Numerous research papers are accessible that demonstrate the utilization of active building blocks (ABBs) for realizing FOE, making them flexible and compatible with integrated circuits (ICs) [36]–[55]. Operational transconductance amplifier (OTA) based emulators use functional block diagram approach [36]–[40], cascading of bilinear immittances [41]–[44] and replacing the resistors by OTA in R-C ladder network [45]. In MOS based emulators the active inductor [46] and low/high pass filter sections [47] are utilized to achieve the desired FOE characteristics. Current mirror-based integrator/differentiator emulators utilizes MOS capacitors in [48]–[50]. Further, immittance simulators are also proposed using generalized impedance converter (GIC) [51], [52], inverted impedance multiplier circuit (IIMC) [53], frequency dependent negative resistance (FDNR) [54] and mutator [55] which are later used for fractional-order filter (FOF) implementation. By proper selection of bias currents of OTA, fractional order α of FOE [38]–[40], [48], [50], and magnitude of FOE [37]–[42], [48], [50], [53], [56], can be electronically tuned. Further, magnitude scaling can also be achieved by connecting FOE in parallel, series or combination of both [36]. However, there exists a trade-off between the

desired operating frequency range and the number of circuit elements required in FOE design. This limitation restricts the use of passive or active emulators in many applications.

1.2.2 Fractional-Order Filters (FOF)

Filters are the circuits that process signals in a frequency-dependent manner. Filters are designed to pass certain frequencies and stop other frequencies. The frequency range between passband and stopband frequencies is called the transition band. The order of a filter is typically characterized by the slope it provides in the transition band. The FOFs are more generalized form of classical integer-order filters. The filter order of FOFs is denoted by $(n+\alpha)$, where n represents the integer part and α represents the fractional part $(0 < \alpha < 1)$. FOFs provide enhanced control over the slope of the transition band in comparison to classical integer-order filters. $-20(n+\alpha)$ dB/decade is the slope of the transition band for FOFs, whereas classical integer-order filters have a fixed slope of -20 dB/decade. This allows for greater flexibility in designing filters with non-integer orders, providing more precise control over the filter characteristics. [17], [57].

There are two primary design approaches for developing FOFs. In the first design approach a FOE with impedance $Z(s)= ks^{\alpha}$ (FOI for $\alpha > 0$ and FOC for $\alpha < 0$) is realized using any one of the approximation methods listed in section 1.2.1. The FOE structure replaces the corresponding integer-order passive element in existing integer-order filter circuits [17], [57]–[75]. In the second design approach, the fractional-order Laplacian operator s^{α} with $0 < \alpha < 1$ is approximated using

an integer order approximation with order m. This approximation transforms the $(1+\alpha)$-order FOF into an integer-order $(1+m)$-order FOF. Subsequently, the final transfer function of FOF, derived from this approximation is implemented using active blocks and integrators [76]–[93]. These components are utilized to create a circuit that realizes the desired filter response and emulates the behavior of the FOF.

1.2.2.1 FOFs using first approach:

Some of the widespread second order filter circuits [58]–[65] explored in the fractional domain are Tow-Thomas (TT) biquad [58], [59], [63], [65], Kerwin-Huelsman-Newcomb (KHN) biquad [60]–[62], Sallen-Key biquad filter [62], [64], and RLC filter [64]. Researchers have also applied this approach to derive FOFs from first-order filters [66], [67], second-order filters [68]–[71] and even third-order filters [72]. In respective references, the FOFs with Chebyshev characteristics [65], Inverse Chebyshev characteristics [73] and Butterworth characteristics [59], [69] are reported. Other than these, IIMC [53], mutator [55] and GIC [64] based immittance simulators are also proposed, which are subsequently used for FOF realizations. The FOFs designed using this approach utilize different ABBs such as: OTA [53], [67], [68], [71], operational amplifier (Opamp) [58]–[60], [62]–[65], [73], differential voltage current conveyor (DVCC) [66], [69], MOS [70], current differencing buffered amplifier (CDBA) [72] and second-generation current conveyor (CCII) [55], [61], [74], [75].

1.2.2.2 FOFs using second approach:

As in the second approach, the $(1+\alpha)$-order FOF's transfer function modifies to $(1+m)$-order integer order transfer function. A 2^{nd}-order approximation for FOC converts $(1+\alpha)$ order transfer function to 3^{rd}-order integer order transfer function which is realized by cascading of 1^{st} and 2^{nd}-order filters [76]. Functional block diagram of follow the leader feedback topology [77]–[86], inverse follow the leader feedback topology [87]–[91], and signal flow graph [92] are used in respective references. The FOFs implemented using this approach employs various ABBs such as: OTA [77], [78], [84], [87], [88], [90], [91], current-feedback operational amplifier (CFOA) [80], [86], current mirror [85], differential difference current conveyor (DDCC) [89], adjustable current amplifier (ACA) [77], [78], [81]–[84], [87], [88], [90], CDBA [92] and Opamp [76], [93],.

1.2.3 Fractional-Order Oscillators (FOO)

Oscillators are one of the most frequently used electronic devices in communication systems. Hence, electronic oscillator is an enthralling topic among researchers. The utilization of fractional-order calculus has transformed the design procedure of oscillator circuits. There are two primary types of oscillators: sinusoidal oscillators and relaxation oscillators (multivibrators), both of which leverage the advantages of fractional-order α in perfecting their performance. The presence of the fractional order α in the FOO design provides more degree of freedom. This additional parameter can be used to alter frequency of oscillation and condition of oscillation,

without disturbing the other circuit parameters (i.e., resistances and capacitances). Literature survey for sinusoidal FOOs and fractional-order multivibrators have been given below:

1.2.3.1 Sinusoidal FOO

In [94], the concept of FOO was first substantiated using popular Wein oscillator. In [95] and [96], the Barkhausen criterion for FOO was derived and confirmed through Colpitts oscillator, Wien oscillator, LC tank resonator and phase-shift oscillator. Reference [97] studies the integration of two-port network concept in oscillator with fractional calculus. In [98], a comprehensive design procedure was proposed specifically for third-order oscillators in the fractional domain. This design procedure outlines a systematic approach to achieve oscillations with a desired phase and frequency. In [99], authors discuss all the possible topologies of Wein-bridge oscillator in fractional domain.

Multiphase FOO was introduced in [100], the authors proposed multiphase FOO based upon fractiona-order all pass filter (FAPF) and APF connected in a feedback loop with an amplifier. In [101] authors utilized the multiple node structure for FOO with multiple FOE and hence multiple phase difference could be implemented. In [102] and [103], multiple phase FOO was realized using double integrator topology and current mirrors respectively.

Different FOOs were introduced in literature [104]–[109] based on various ABBs such as operational transresistance amplifier (OTRA), current-controlled current follower transconductance amplifiers (CCCFTA), DVCC, MOS-RC, DDCC and

OTA. Stability analysis of various oscillatory circuits was presented in [110], [111].

1.2.3.2 Fractional-order multivibrator (fractional-order relaxation oscillator)

Compared to the sinusoidal FOO, fractional-order multivibrator is less commonly discussed in the literature. The reference [112] investigated the impact of incorporating a FOC in the widely used single opamp multivibrator circuit. The potential application of a commercial super-capacitor in the construction of a very low frequency oscillator was explored in [113]. A general design methodology was suggested for two types of fractional-order relaxation oscillators that utilize OTRA in [114]. The proposed methodology involves solving the FOC's charging and discharging equations using the Mittag-Leffler function. In [115], a fractional-order multivibrator was introduced that utilizes a multi-output current follower transconductance amplifier (MO-CFTA) and relies on the saturation current of the transconductance amplifier (TA) block for the charging and discharging of the FOC.

1.3 Research Gaps

After conducting a literature survey, several research gaps have been identified, including the following:

In numerous applications, there is a requirement to cascade voltage-mode and current-mode filters, necessitating the use of a voltage-to-current converter (V-I) interface. It is observed from the literature survey that filters topologies to improve

cascadibility in fractional domain are need to be explored.

Further, limited literature is available for electronic tuning of filter parameters such as pole frequency and pole quality factor in fractional domain. To investigate electronic tuning of filter parameters, with the help of external amplifier without affecting filter's core structure, the shadow concept can be generalized in fractional domain.

The signal generating circuits, such as: sinusoidal oscillators and multivibrators, are less explored in fractional domain. These circuits need to be generalized in terms of frequency of oscillation in the fractional domain. Moreover, limited literature is available for independent tuning of phase difference between the two outputs of a sinusoidal FOO.

The main components of fractional-order systems are FOEs. Thus, the realization of FOE using simpler techniques with lesser number of components is always in the scope. Further, it is clear from literature survey that limited work has been done to realize higher order FOEs.

1.4 Research Objectives

Based on a thorough review of the literature and identified research gaps, the following objectives have been established:

1. To explore FOF topologies with better cascadibility features.

2. To develop electronically tunable FOFs, where tuning is done using the

external parameter.

3. To develop new designs for FOO with electronic tunability.

4. To implement FOE using simpler techniques with reduced active block/component count.

5. To develop higher order FOE topologies.

1.5 Organization of the Thesis

The primary focus of this research is on fractional-order circuits for signal processing and signal generation. The organization of the research work is presented in a chapter-wise format in this thesis, as follows:

Chapter 1

The purpose of this chapter is to provide an overview of the background and motivation that underlies the research conducted in the thesis. A comprehensive literature survey of existing analog fractional-order circuits (i.e. FOE, FOF and FOO) is put up. Based on this survey, the research gaps are identified, which serve as the foundation for establishing the objectives of the work. After establishing the objectives, a brief overview of the thesis layout is provided.

Chapter 2

In this chapter, a concise overview of the realization of FOE using CFE approximation and Valsa's algorithm is provided. Further, it includes the procedure to analyse the stability of fractional-order circuits. It also contains a preliminary analysis of

the active block used in this work. Furthermore, the functionality of the circuits introduced in this chapter is confirmed through the use of SPICE simulations.

Chapter 3

This chapter presents a new α-order multifunction transadmittance mode (TAM) FOF based upon OTA. The proposed structure provides fractional-order high-pass filter (FHPF), fractional-order low-pass filter (FLPF), and fractional-order all-pass filter (FAPF). The functionality of the proposed TAM FOF is confirmed using both SPICE simulations and experimental testing. The sensitivities of the transfer functions with the changes in various circuit parameters are analyzed using MATLAB. The robustness of the proposed TAM FOF is studied using PVT and Monte-Carlo analysis.

Chapter 4

The objective of this chapter is to extend the design principles of shadow filters to the fractional domain. Mathematical equations have been drafted to determine the pole frequency and pole quality factor of the shadow FOF when different types of feedback signals, such as low-pass, high-pass, band-pass, or band-stop are applied to the external amplifier in the feedback loop and demonstrated using MATLAB simulations. To validate the proposed theory, SPICE simulations are conducted using two active FOFs and it is observed that the obtained results closely align with the theoretical predictions, indicating the effectiveness of the proposed theory. The parameters of shadow FOF such as pole frequency and pole quality factor, are adjusted with the help of external amplifier's gain, without altering the active or passive components of the basic FOF. For both of the shadow FOF circuits the THD is calculated. Further, corner and Monte-Carlo analysis have been performed

to verify the robustness of the shadow FOF circuits.

Chapter 5

This chapter is devoted to fractional-order signal generating circuits. The first two circuits of the sinusoidal FOO are designed using the trans-admittance mode FAPF with a trans-impedance mode integrator/differentiator topology. Additionally, the third circuit of the sinusoidal FOO features a unique design that enables independent control of the phase difference between its two output voltages. The proposed circuits are analyzed for stability, sensitivity of the frequency of oscillation to changes in various circuit parameters, and robustness.

Further, a multivibrator circuit based on three OTAs is generalized in the fractional domain. The time period of the proposed fractional-order multivibrator has been derived mathematically and confirmed via SPICE simulations. The robustness of the circuit is scrutinized through Monte-Carlo and corner analyses. The chapter also explores the potential application of the fractional-order multivibrator as a versatile modulator. This includes exploring its use as an amplitude modulator (AM), frequency modulator (FM), delta modulator (DM), and sigma-delta modulator (SDM).

Chapter 6

This chapter proposes a new active inductor-based realization to approximate the behavior of FOC is proposed. Proposed structure enables higher order approximation of FOC either by parallel connection or by impedance multiplication. Further, an application of the proposed FOC to realize a FOO is shown. Moreover, the realization of floating FOE based upon OTA based IIMC is presented. Higher order $(n-1+\alpha)$, floating FOI and floating FOC are realized and electronic tuning

of the magnitude of FOE using external bias currents to OTA is verified.

Chapter 7

This chapter presents a summary of the research work presented in the thesis and offers suggestions for the future work.

Chapter 2

Preliminaries of Fractional-Order Circuits

2.1 Introduction

As discussed in Chapter 1, FOEs are crucial components of fractional-order circuits. Among FOEs, FOCs hold particular significance. This thesis employs two methods, namely CFE approximation [34] and Valsa's algorithm [116], to emulate the FOC behavior, both of which are explained in detail in this chapter. Furthermore, a concise guide to conducting stability analysis for fractional-order systems [117] is provided. Finally, characterization of OTA [118] is presented, which is utilized for the verification of all the propositions put forth in this work.

2.2 Approximation of Fractional-Order Capacitor

The impedance of a FOC is described by the following equation:

$$Z(s) = \frac{1}{s^{\alpha} C_{\alpha}} \tag{2.1}$$

The variable α $(0 < \alpha < 1)$ (2.1) is the order of the FOC, while C_{α} is capacitance expressed in $\mho sec^{\alpha}$. The magnitude of FOC depends on frequency and the value of α. Its value varies with -20α decibels per decade of frequency. The phase of the FOC is equal to $-\alpha\pi/2$.

In this section, two methods to approximate the behaviour of FOC are discuused, first method is CFE based approximation [34] while second is based on Valsa's algorithm [116].

2.2.1 Approximated FOC Based on CFE

The series expansion of $(1+x)^{\alpha}$ by using CFE [119] is given by (2.2).

$$\cfrac{1}{1-\cfrac{\alpha x}{1+\cfrac{(1+\alpha)x}{2+\cfrac{(1-\alpha)x}{3+\cfrac{(2+\alpha)x}{2+\cfrac{5}{(2-\alpha)x}}}}}} \tag{2.2}$$

alternatively, (2.2) can also be written as

$$(1+x)^{\alpha} = \cfrac{1}{1-}\,\cfrac{\alpha x}{1+}\,\cfrac{(1+\alpha)x}{2+}\,\cfrac{(1-\alpha)x}{3+}\,\cfrac{(2+\alpha)x}{2+}\,\cfrac{(2-\alpha)x}{5+\ldots} \tag{2.3}$$

The expansion of fractional-order Laplacian operator s^{α} can be achieved by substituting $x{=}(s-1)$. As it is an infinite series, the required accuracy depends upon the finite number of terms to represent s^{α}. The highest power of s in the final expression of the approximation determines the order of the CFE approximation for s^{α}, i.e., if n is the highest power of s in the final expression then it is a n^{th} order approximation. Performing routine algebraic analysis, $1^{st}, 2^{nd}, 3^{rd}$, 4^{th} and 5^{th} order CFE approximation for s^{α} may be obtained and are given in Table 2.1 [120].

An impedance function is depicted by a n^{th}-order CFE approximation function and it can be approximated with the help of partial fraction by R-C network, shown in Fig. 2.1 [121]. The expression of the impedance $Z(s)$ of the R-C network shown

Table 2.1: CFE approximation for s^{α} [120]

Order	Approximated transfer function	
1^{st}	$\frac{P_0 s+P_1}{Q_0 s+Q_1}$	$P_0 = Q_1 = 1+\alpha$ $P_1 = Q_0 = 1-\alpha$
2^{nd}	$\frac{P_0 s^2+P_1 s+P_2}{Q_0 s^2+Q_1 s+Q_2}$	$P_0 = Q_2 = \alpha^2+3\alpha+2$ $P_1 = Q_1 = -2\alpha^2+8$ $P_2 = Q_0 = \alpha^2-3\alpha+2$
3^{rd}	$\frac{P_0 s^3+P_1 s^2+P_2 s+P_3}{Q_0 s^3+Q_1 s^2+Q_2 s+Q_3}$	$P_0 = Q_3 = \alpha^3+6\alpha^2+11\alpha+6$ $P_1 = Q_2 = -3\alpha^3-6\alpha^2+27\alpha+54$ $P_2 = Q_1 = 3\alpha^3-6\alpha^2-27\alpha+54$ $P_3 = Q_0 = -\alpha^3+6\alpha^2-11\alpha+6$
4^{th}	$\frac{P_0 s^4+P_1 s^3+P_2 s^2+P_3 s+P_4}{Q_0 s^4+Q_1 s^3+Q_2 s^2+Q_3 s+Q_4}$	$P_0 = Q_4 = \alpha^4+10\alpha^3+35\alpha^2+50\alpha+24$ $P_1 = Q_3 = -4\alpha^4-20\alpha^3+40\alpha^2+320\alpha+384$ $P_2 = Q_2 = 6\alpha^4-150\alpha^3+864$ $P_3 = Q_1 = -4\alpha^4+20\alpha^3+40\alpha^2-320\alpha+384$ $P_4 = Q_0 = \alpha^4-10\alpha^3+35\alpha^2-50\alpha+24$
5^{th}	$\frac{P_0 s^5+P_1 s^4+P_2 s^3+P_3 s^2+P_4 s+P_5}{Q_0 s^5+Q_1 s^4+Q_2 s^3+Q_3 s^2+Q_4 s+Q_5}$	$P_0 = Q_5 = -\alpha^5-15\alpha^4-85\alpha^3-225\alpha^2-274\alpha-120$ $P_1 = Q_4 = 5\alpha^5+45\alpha^4+5\alpha^3-1005\alpha^2-3250\alpha-3000$ $P_2 = Q_3 = -10\alpha^5-30\alpha^4+410\alpha^3+1230\alpha^2-4000\alpha-12000$ $P_3 = Q_2 = 10\alpha^5-30\alpha^4-410\alpha^3+1230\alpha^2+4000\alpha-12000$ $P_4 = Q_1 = -5\alpha^5+45\alpha^4-5\alpha^3-1005\alpha^2+3250\alpha-3000$ $P_5 = Q_0 = \alpha^5-15\alpha^4+85\alpha^3-225\alpha^2+274\alpha-120$

in Fig. 2.1 is given in (2.4).

$$Z(s) = R_0 + \sum_{i=1}^{i=n} \frac{\frac{1}{C_i}}{s + \frac{1}{R_i C_i}} \tag{2.4}$$

In general form (2.4) may be expressed as

$$Z(s) = c + \sum_{i=1}^{i=n} \frac{r_i}{s + p_i} \tag{2.5}$$

Where c and r_i are the constants and p_i represent impedance function's poles. The values of components in Fig. 2.1 may be find out by using (2.6).

$$R_0 = c, \qquad C_i = 1/r_i, \qquad R_i = 1/(C_i|p_i|) \qquad (i = 1, 2...n) \tag{2.6}$$

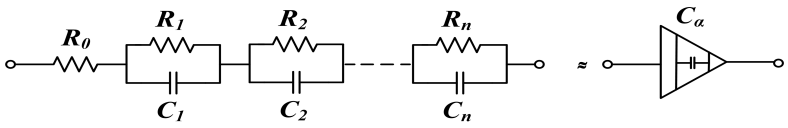

Figure 2.1: n^{th} order R-C network to emulate FOC's behaviour based on CFE approximation

The final value of the magnitude ($C_\alpha \; in \; \mho sec^\alpha$) of FOC and the center frequency (ω_c) around which the FOC's behaviour is valid may not matched with the desired values. Thus to obtain the FOC with desired value of magnitude C_α and ω_c, scaling operation, with the help of magnitude scaling factor (k_m) and frequency scaling factor (k_f), is performed on the components of R-C network.

$$k_m = \frac{1}{C_\alpha \omega_c^\alpha}, \qquad k_f = \omega_c \tag{2.7}$$

The relationship between scaled values ($R_s,\ C_s$) and unscaled values ($R,\ C$) of components is given as

$$R_s = k_m R, \qquad C_s = \frac{C}{k_f k_m} \tag{2.8}$$

2.2.2 Simulation Results for FOCs Based on CFE Approximation

To verify the behaviour of FOC based on CFE approximation, SPICE simulations have been carried out. A 5^{th}-order CFE based FOC is emulated using series connection of 5 sections of parallel connected resistance and capacitance as shown in Fig. 2.2. The passive components' values to realize approximated FOCs of magnitude 1 $\mu\mho sec^{\alpha}$ with α=0.2, 0.5 and 0.8 and center frequency as 1 kHz are given in Table 2.2.

Table 2.2: Passive component's values used to realize 5^{th}-order CFE approximated FOC shown in Fig. 2.2

α	R_0	R_{s1} C_{s1}	R_{s2} C_{s2}	R_{s3} C_{s3}	R_{s4} C_{s4}	R_{s5} C_{s5}
0.2	69.33 $k\Omega$	44.69 $k\Omega$ 224.17 pF	34.26 $k\Omega$ 1.59 nF	37.96 $k\Omega$ 4.70 nF	59.69 $k\Omega$ 10.21 nF	190.40 $k\Omega$ 22.69 nF
0.5	1.15 $k\Omega$	2.49 $k\Omega$ 5.51 nF	3.24 $k\Omega$ 20.28 nF	5.35 $k\Omega$ 39.63 nF	13.29 $k\Omega$ 57.41 nF	113.25 $k\Omega$ 67.98 nF
0.8	12.18 Ω	57.54 Ω 312.67 nF	119.18 Ω 660.43 nF	293.14 Ω 863.53 nF	1.23 $k\Omega$ 800.65 nF	67.04 $k\Omega$ 324.31 nF

Figure 2.3 illustrates the corresponding theoretical and simulated responses. In the frequency range of 100 Hz to 10 kHz, the errors between the simulated magnitude

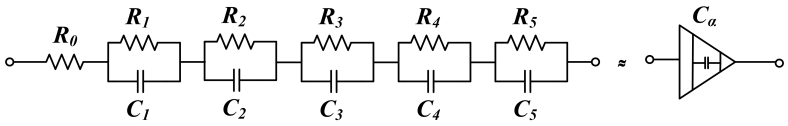

Figure 2.2: 5^{th} order R-C network to emulate FOC's behaviour based on CFE approximation

of FOC from the desired magnitude (i.e., 1 $\mu\mho sec^{\alpha}$) are found to be within 0.3%, 0.6% and 0.5% for α=0.2, 0.5 and 0.8 respectively, as shown in Fig. 2.3 (a). From Fig. 2.3 (b) it is noticed that the simulated phase of FOC diverges from theoretical phase by approximately 0.3%, 2.1% and 0.8% for α=0.2, 0.5 and 0.8 respectively, in the frequency range of 100 Hz to 10 kHz. From Fig. 2.3 (c), the deviation of 0.09%, 0.5% and 0.25% is noticed between the theoretical and simulated slopes of magnitude response of orders 0.2, 0.5 and 0.8 respectively. The valid frequency range of the FOC response improves with increase in the number of R-C sections.

2.2.3 Approximated FOC Based on Valsa's Algorithm

In this section, Valsa's algorithm [116] to emulate the behaviour of FOC is discussed. It generates a network of R_s and C_s, equivalent to the behaviour of the FOC with required fractional-order α. The emulated FOC's behaviour is valid over a certain frequency range $[\omega_l, \omega_u]$ Thus, first the lower end of frequency range (ω_l) is set to the desired value. The upper end of frequency range (ω_u) depends upon many other factors such as: number of R-C sections (m), ω_l and desired value of allowable phase ripple ($\Delta\phi$) (phase of the FOC oscillates around its average value ϕ with an

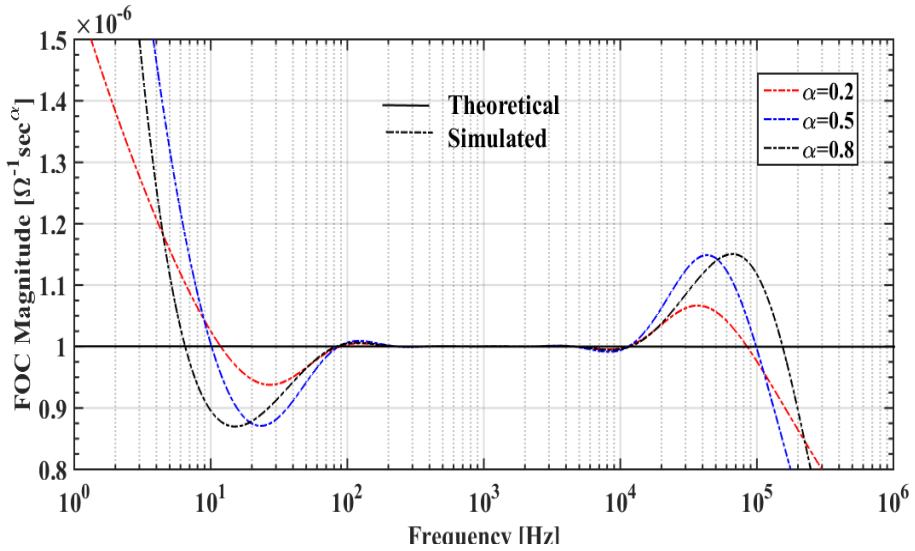

(a)

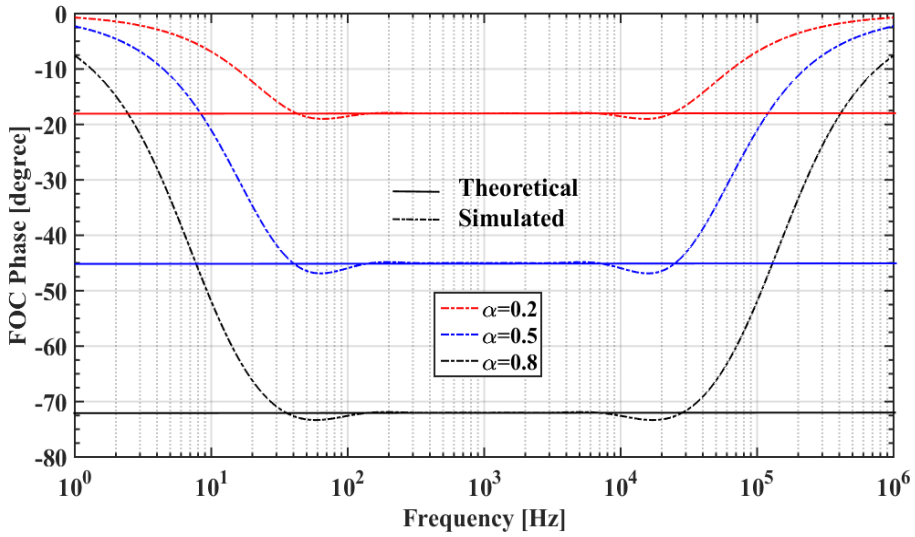

(b)

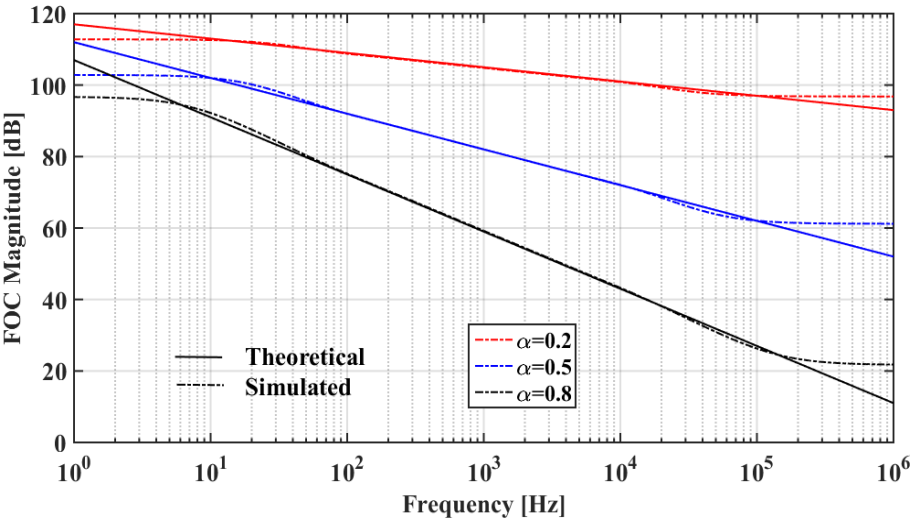

(c)

Figure 2.3: Frequency response for FOC, based on 5^{th}-order CFE approximation (a) Magnitute in $\mho sec^{\alpha}$ (b) phase response in degrees (c) Magnitude in dBs

amplitude of $\pm\Delta\phi$).

$$\omega_u = \frac{\omega_l}{(ab)^m}, \quad ab \approx \frac{0.24}{(1+\Delta\phi)}$$

Here a and b depend upon allowable phase ripple $\Delta\phi$ and lie in the range of $(0, 1)$. The individual values of a and b can be obtained as

$$a = 10^{\alpha log(ab)},\ b = \frac{0.24}{(1+\Delta\phi)a}$$

By using the value of ω_l, the values of R_1 and C_1 can be chosen. The values of the components of the R-C network shown in Fig. 2.4 depend on R_1 and C_1 and can be calculated as follows:

$$R_1 C_1 = \frac{1}{\omega_l}$$

$$R_p = \frac{R_1(1-a)}{a},\ C_p = \frac{C_1 b^m}{(1-b)}$$

$$R_{sk} = R_1 a^{k-1},\ C_{sk} = C_1 b^{k-1},\ k = 1, 2, ...m$$

The resultant magnitude D of this R-C network is given as below.

$$D = Z_{av}(\omega_{av}^{-(\phi/90)})$$

$$\text{here, } Z_{av} = 1/|Y_{av}| \quad \text{and } \omega_{av} = \frac{1}{[R_1 C_1 (ab)^{h-1}]}\sqrt{a}, \quad h = int(m/2)$$

$$Y_{av} = \frac{1}{R_p} + j\omega_{av} C_p + \sum_{k=1}^{m} \frac{j\omega_{av} C_k}{1+j\omega_{av} R_k C_k}$$

Typically, the value of D obtained may not match the desired magnitude of FOC. To address this, it is necessary to use a scaling factor $S_d = D_p/D$, where D_p is the desired magnitude of the FOC. Multiply all resistances in sections (R_s and R_p) by S_d, and divide all capacitances (C_s and C_p) by the same scaling factor. This

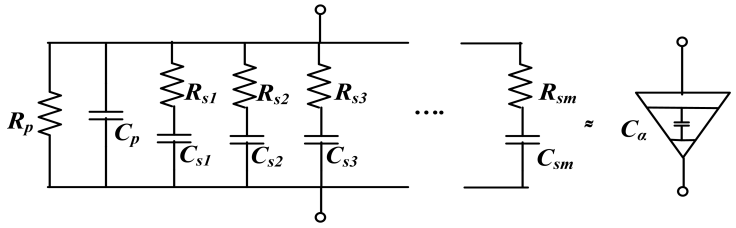

Figure 2.4: m^{th} order R-C network to emulate FOC's behaviour based on Valsa's algorithm

adjustment will not affect the lower and upper limits of the frequency range.

2.2.4 Simulation Results for FOCs Based on Valsa's Algorithm

To verify the behaviour of FOC based on Valsa's algorithm, SPICE simulations have been carried out. The FOCs are realized with fractional orders 0.2, 0.5 and 0.8 using parallel connected 7 sections of series R-C network shown in Fig. 2.5.

First, ω_l is set as 100 rad/sec and $\Delta\phi$ as 0.5°. By using the value of ω_l the initial values of R_1 and C_1 are selected as 400 $k\Omega$ and 25 nF, respectively. The passive components' values to emulate FOCs of magnitude 1 $\mu\mho sec^{\alpha}$ with fractional orders 0.2, 0.5 and 0.8 are given in Table 2.3.

Figure 2.6 illustrates the corresponding theoretical and simulated responses. In the frequency range of 10 Hz to 10 MHz, the errors between the simulated

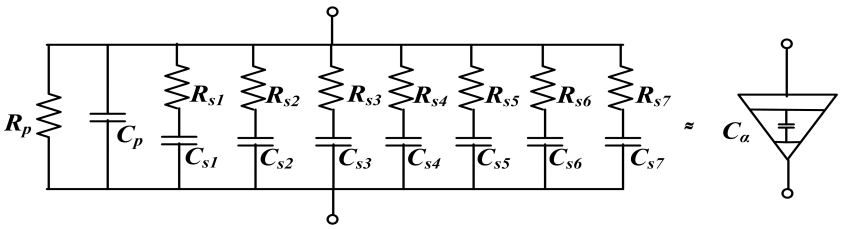

Figure 2.5: 7^{th} order R-C network to emulate FOC's behaviour based on Valsa'a algorithm

Table 2.3: Passive component's values used to realize 7^{th}-order Valsa's algorithm based approximated FOC shown in Fig. 2.5

α	R_p C_p	R_{s1} C_{s1}	R_{s2} C_{s2}	R_{s3} C_{s3}	R_{s4} C_{s4}	R_{s5} C_{s5}	R_{s6} C_{s6}	R_{s7} C_{s7}
0.2	122.00 $k\Omega$ 68.40 nF	36.60 $k\Omega$ 272.30 nF	8.50 $k\Omega$ 189.22 nF	1.95 $k\Omega$ 131.20 nF	450.50 Ω 90.90 nF	103.99 Ω 63.00 nF	24.00 Ω 43.71 nF	5.54 Ω 30.28 nF
0.5	257.09 $k\Omega$ 159.32 pF	171.39 $k\Omega$ 58.35 nF	68.56 $k\Omega$ 23.34 nF	27.42 $k\Omega$ 9.35 nF	10.97 $k\Omega$ 3.73 nF	4.39 $k\Omega$ 1.49 nF	1.76 $k\Omega$ 597.47 pF	702.02 Ω 238.99 pF
0.8	244.10 $k\Omega$ 34.20 nF	73.26 $k\Omega$ 136.51 nF	16.91 $k\Omega$ 94.62 nF	3.90 $k\Omega$ 65.59 nF	901.00 Ω 45.46 nF	207.98 Ω 31.51 nF	48.00 Ω 21.84 nF	11.08 Ω 15.14 nF

magnitude of FOC from the desired magnitude of FOC (i.e., 1 $\mu\mho sec^{\alpha}$) is 2.2%, 4.8% and 2.7% for α=0.2, 0.5 and 0.8 respectively, as shown in Fig. 2.6 (a). In the frequency ranges of (66 $Hz - 0.54\ MHz$), (39 $Hz - 0.41\ MHz$) and (9.3 $Hz - 0.28\ MHz$), the simulated phase deviates from theoretical phase by $\pm 0.50^{\circ}$ for FOCs with α=0.2, 0.5 and 0.8, respectively, as observed from Fig. 2.6 (b). From Fig. 2.6 (c), the deviation of 1.3%, 3.6% and 3.3% is noticed between the simulated slope and theoretical slope of magnitude response of FOCs with α=0.2, 0.5 and 0.8 respectively. The valid frequency range of the FOC response improves with increase in the number of R-C sections.

2.3 Stability Analysis

By mapping of s-plane into W-plane, the stability of any fractional-order system with fractional order $\alpha = \frac{p}{q}$ is investiated, here p and q are positive integers and $q \neq 0$ [117]. Lets define $W = s^{\frac{1}{q}}$, the $\pm j\omega$ axes (i.e., $|\theta_s| = \frac{\pi}{2}$) in the s-plane are mapped onto the lines $|\theta_W| = \frac{\pi}{2q}$ and the negative axis (i.e., $\theta_s = \pi$) of s-plane onto the line $|\theta_W| = \frac{\pi}{q}$, as shown in Fig. 2.7. The unstable region (i.e., $|\theta_s| < \frac{\pi}{2}$)

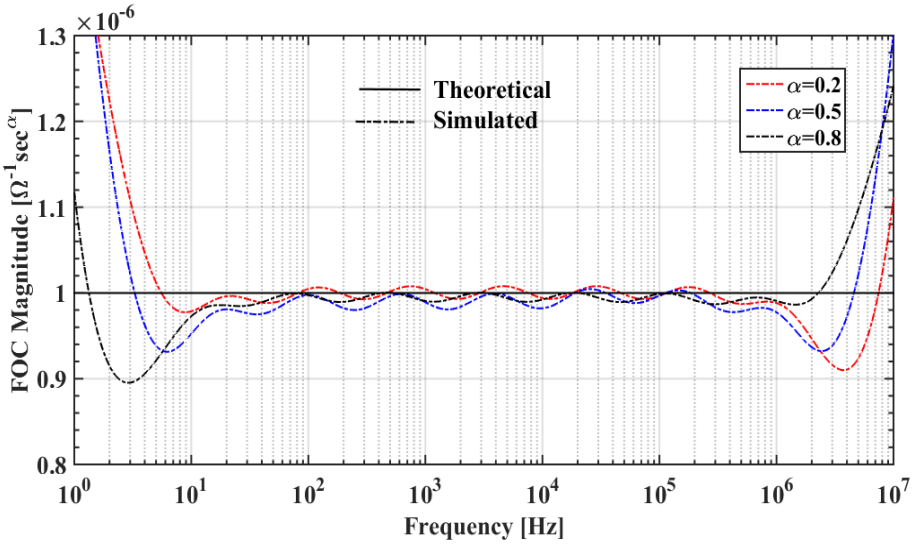

(a)

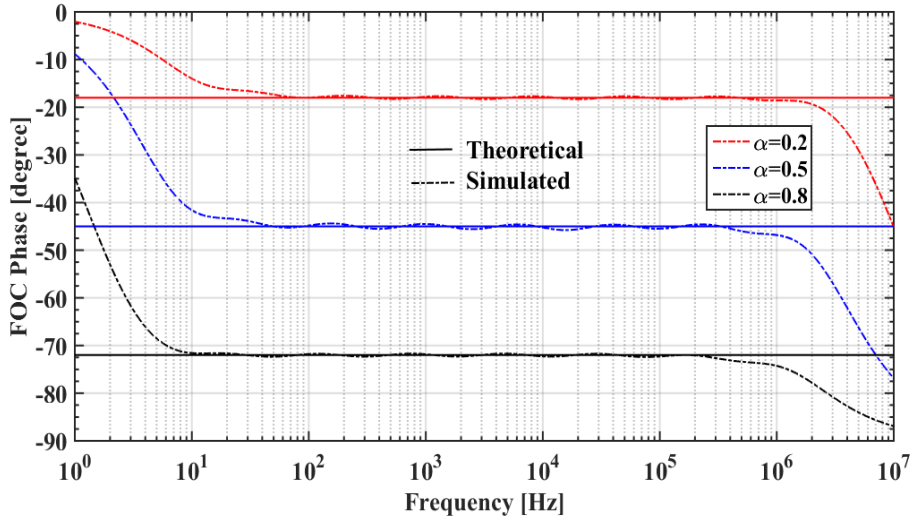

(b)

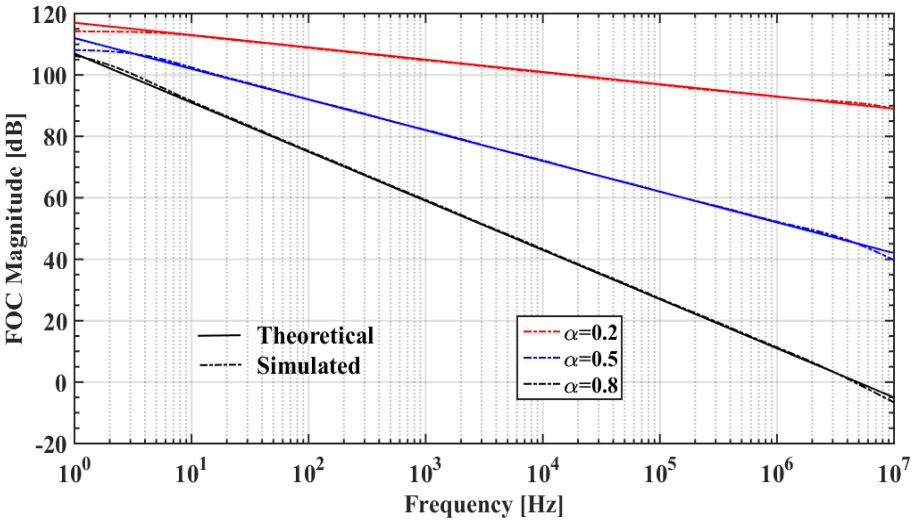

(c)

Figure 2.6: Frequency response for FOC, based on 7^{th}-order Valsa's algorithm (a) Magnitute in $\mho sec^{\alpha}$ (b) phase response in degrees (c) Magnitude in dBs

and stable regions (i.e., $\frac{\pi}{2}<|\theta_s|<\pi$) in the s-plane transform into $|\theta_W|<\frac{\pi}{2q}$ and $\frac{\pi}{2q}<|\theta_W|<\frac{\pi}{q}$ respectively. Therefore, the system is considered stable when all the roots lie in the region $|\theta_W|>\frac{\pi}{2q}$. Additionally, if at least one root lies on the lines $|\theta_W| = \frac{\pi}{2q}$ while all other roots remain in the stable region, the system will exhibit oscillatory behavior.

In this work, the stability analysis has been performed by plotting the roots of the fractional-order system's characteristic equation in the W-plane, using *forlocus* function of MATLAB [122]. By examining the location of roots, one can assess the system's stability. If all the roots are located in the stable region, the system is considered stable.

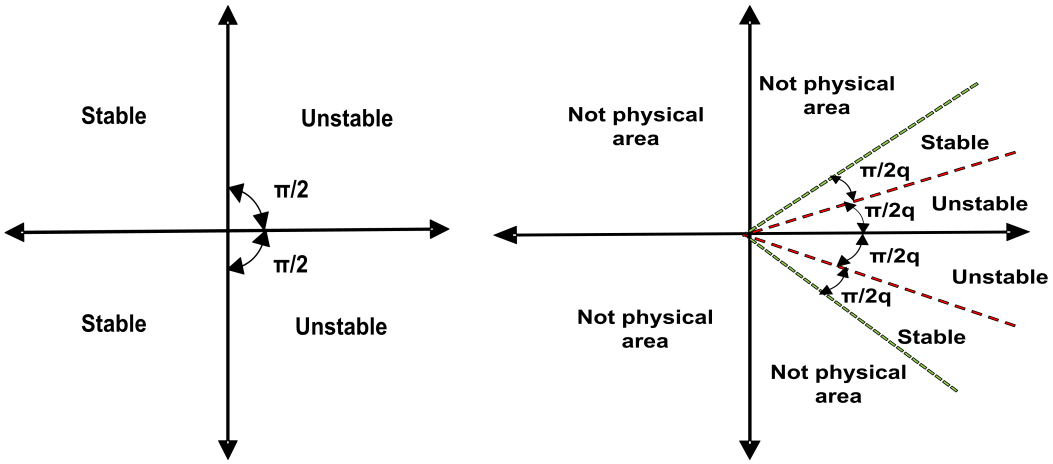

Figure 2.7: Stability region in complex plane (a) s-plane (b) W-plane

2.4 Active Block OTA

The OTA processes differential voltage at its two input ports and delivers output current. The block diagram of OTA and its CMOS schematic are illustrated

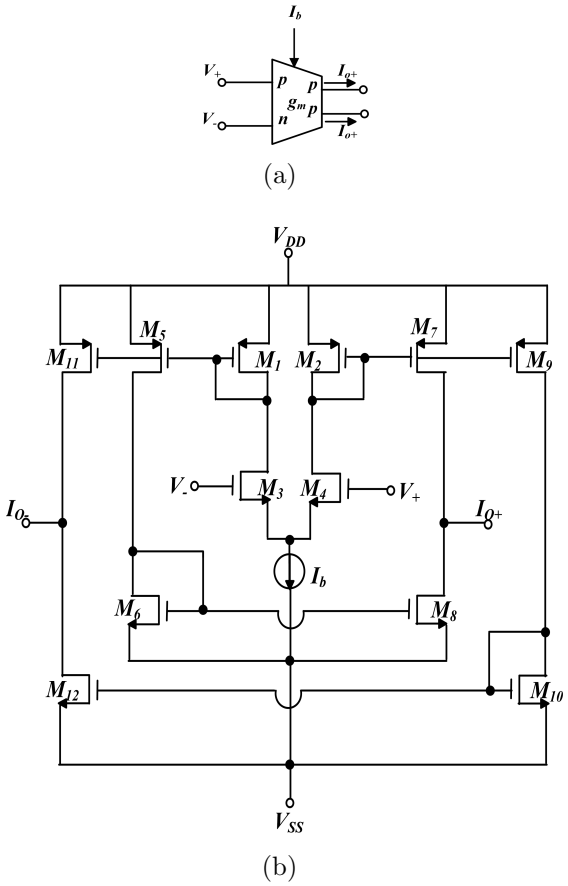

Figure 2.8: OTA's (a) Block diagram (b) CMOS schematic

in Figs. 2.8 (a) and (b) respectively. The relationship between input and output ports of the OTA is given by (2.9).

$$I_{O\pm} = \pm g_m(V_+ - V_-) \tag{2.9}$$

Here g_m is the transconductance gain of OTA and its relationship with the bias current (I_b) is given as

$$g_m = \sqrt{\mu_n C_{ox} \frac{W}{L} I_b} \tag{2.10}$$

The electron mobility and gate oxide capacitance per unit area are denoted by

symbols μ_n and C_{ox} respectively, while W/L is the aspect ratio of differential pair (M_3 and M_4). The relationship between the transconductance (g_m) and bias current can be utilized to introduce electronic tunability into the design parameters of the circuit.

2.4.1 Simulation Results for the verification of OTA

The OTA of Fig. 2.8 (b) has been simulated using 180 nm CMOS model parameters with supply voltages as $\pm 1.8\ V$. The aspect ratios assigned to the transistors $M_{3,4}$ are as 5.76 $\mu m/0.72\ \mu m$, while the aspect ratios of the transistors $M_{1,2,5,7,9,11}$ are set as 2.16 $\mu m/0.72\ \mu m$ and $M_{6,8,10,12}$ are set as 1.44 $\mu m/0.72\ \mu m$. The DC response is shown in Fig. 2.9 (a) for a bias current of 15 μA and the transconductance gain (g_m) is measured as 162.7 $\mu A/V$. Figure 2.9 (b) depicts the electronic tuning of transconductance gain (g_m) in relation to the bias current (I_b). The reduction in transconductance occurs when the bias currents exceed approximately 450 μA. This decrease can be attributed to the transistors M_3 and M_4 transitioning from the saturation region to the linear region of operation. The maximum transconductance gain of the OTA is about 798 $\mu A/V$. Figure 2.9 (c) presents the frequency response for the same bias current as used for plotting the DC response, i.e., 15 μA. The measured half-power frequency of the OTA is 243.2 MHz. Further, the simulations reveal that the parasitic capacitance at the output port of the OTA is observed to be approximately 65.3 pF.

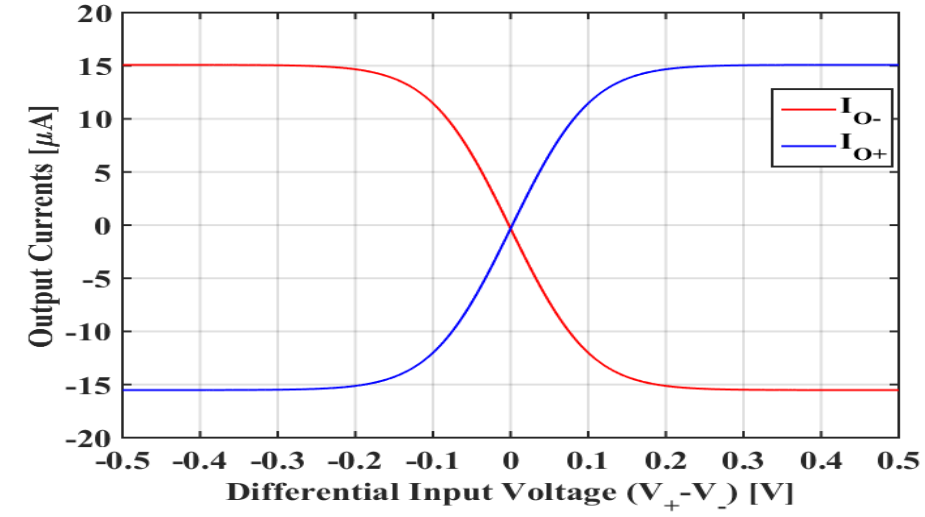

(a)

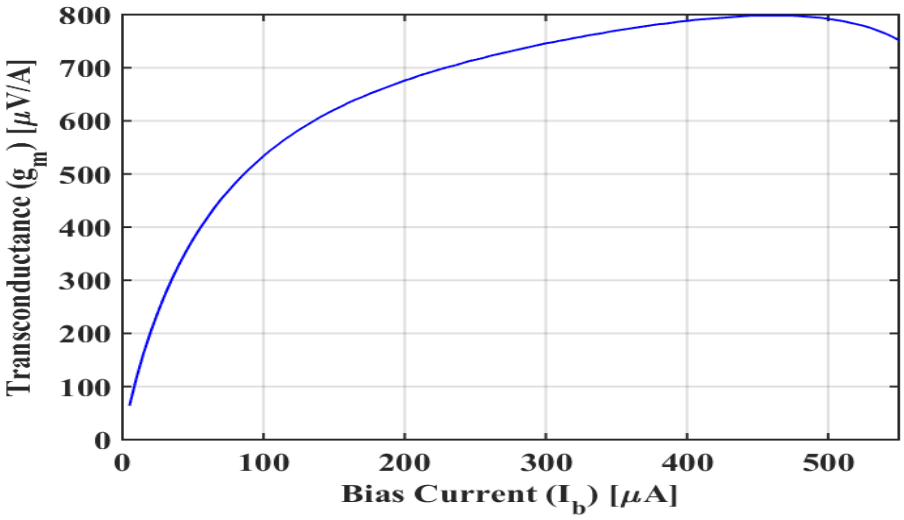

(b)

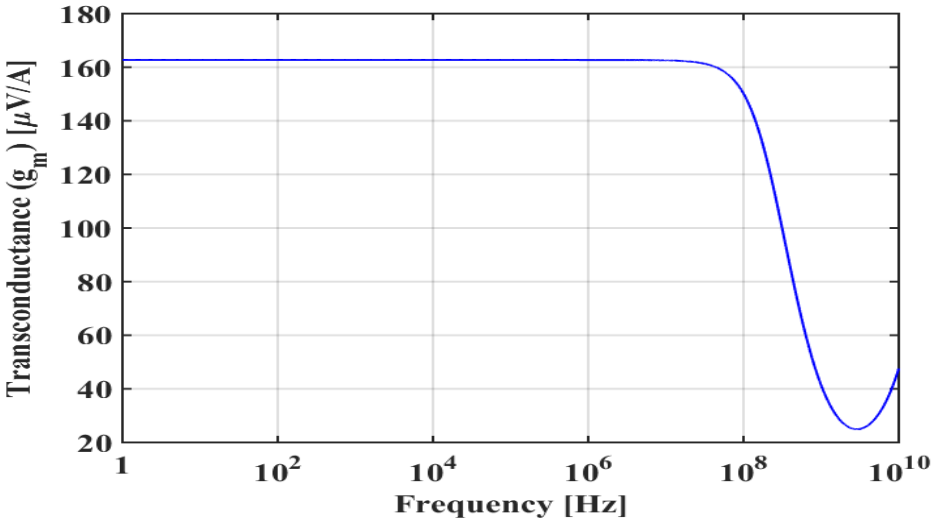

(c)

Figure 2.9: OTA's (a) DC response (b) Variation of transconductance gain with bias current I_b (c) AC response

2.5 Conclusion

In this chapter, approximated FOC realization using CFE approximation and Valsa's algorithm have been reviewed. The discussion also covers the circuit implementation for emulating FOC with α values of 0.2, 0.5, and 0.8 using 5^{th} order CFE approximation and 7^{th} order Valsa's algorithm. The stability analysis of fractional-order systems is also discussed and a preliminary analysis of the active block used in this work i.e., OTA, is included. Furthermore, the functionality of the circuits presented in this chapter is confirmed through SPICE simulations.

Chapter 3

FOF with Better Cascadibility Feature

This chapter presents the results and content of the following paper:

[1] **G. Varshney,** N. Pandey and R. Pandey, "Electronically Tunable Multifunction Transadmittance-Mode Fractional-Order Filter," in Arab Journal of Science and Engineering, vol. 46, pp. 1067–1078, 2021, doi: 10.1007/s13369-020-04841-8. **(SCIE indexing, 2.807 IF)**

3.1 Introduction

Electronic filters are essential components in modern electronic systems, used to manipulate and process analog signals. Filters can be classified based on their frequency response as high-pass filters (HPF), low-pass filters (LPF), band-pass filters (BPF), all-pass filters (APF) and band-stop filters (BSF). Fractional-order filters (FOFs) are a superclass of integer-order filters, which are characterized by transfer functions of non-integer order, such as fractional-order high-pass filters (FHPF), fractional-order low-pass filters (FLPF), fractional-order band-pass filters (FBPF), fractional-order all-pass filters (FAPF) and fractional-order band-stop filters (BSF).

On the other hand, filters can also be classified based on their input and output signals. Voltage mode (VM) filters operate on voltage signals, while current mode (CM) filters operate on current signals. Trans-admittance mode (TAM) filters use a voltage signal at the input and provide a current signal at the output, while trans-impedance mode (TIM) filters use a current signal at the input and provide a voltage signal at the output.

In numerous applications, there is a requirement to cascade voltage-mode and current-mode filters, necessitating the use of a voltage-to-current converter (V-I) interface. Combining signal processing with voltage-to-current converter interfacing can enhance the overall effectiveness of electronic filters. In this regard, the utilization of a TAM filter proves to be beneficial. One notable application of TAM filters is in the receiver baseband blocks of modern radio systems [123]. Numerous integer-order TAM filters have been documented in [124], [125] and

references cited therein, but there are no reports of a TAM FOF in the existing literature.

This chapter presents OTA-based α-order multifunction TAM FOF. As the OTA exhibits high impedance at both input and output terminals, it is an ideal choice for implementing TAM signal processing applications. The proposed TAM FOF is capable of generating FLPF, FHPF, and FAPF responses. The proposed TAM FOF employs two OTAs and one grounded FOC, the proposed structure is resistor-less. The electronic tunability of the parameters of the FOF is achieved by using transconductance gain of OTA. To validate the the functionality of the proposed TAM FOF SPICE simulations and experimental testing have been conducted.

3.2 Generalization of First-Order Filters

The expression of generalized transfer function of α-order FOF, with α ranging between 0 and 1, as mentioned in [17], is given as:

$$T^{\alpha}(s) = \frac{bs^{\alpha} + c}{as^{\alpha} + 1} \tag{3.1}$$

Where the coefficients a, b, c are the constant terms. By appropriately selecting values for a, b, and c, it is possible to realize various filter responses such as FHPF, FLPF or FAPF. The conditions for selecting these coefficients are summed up in Table 3.1.

The Magnitude response and phase response of FOFs, represented in (3.1) are

Table 3.1: Conditions for coefficient a, b, c along with the corresponding FOFs

Condition on a, b, c	FOF response
b=0	FLPF
c=0	FHPF
b=$-ac$	FAPF

given below:

$$|T^{\alpha}(s)| = \sqrt{\frac{b^2\omega^{2\alpha} + c^2 + 2bc\omega^{\alpha}cos(\frac{\alpha\pi}{2})}{\omega^{2\alpha} + a^2 + 2a\omega^{\alpha}cos(\frac{\alpha\pi}{2})}} \tag{3.2}$$

$$\angle T^{\alpha}(s) = \tan^{-1}\left[\frac{b\omega^{\alpha}\sin(\frac{\alpha\pi}{2})}{b\omega^{\alpha}\cos(\frac{\alpha\pi}{2}) + c}\right] - \tan^{-1}\left[\frac{\omega^{\alpha}\cos(\frac{\alpha\pi}{2}) + a}{\omega^{\alpha}\sin(\frac{\alpha\pi}{2})}\right] \tag{3.3}$$

The critical frequencies for FOF, as mentioned in [17], are defined as follows:

ω_m : The frequency of maxima/minima, corresponds to the frequency where the magnitude response of the FOF is maximum or minimum.

ω_{rp} : The right-phase frequency, corresponds to the frequency where the phase response of the FOF is $\pm 90°$.

ω_h : The half-power frequency, corresponds to the frequency where the magnitude of the FOF is $1/\sqrt{2}$ times of its maximum value.

3.3 Proposed α-Order Trans-Admittance Mode FOF

The proposed α-order multifunction TAM FOF is illustrated in Fig. 3.1. The proposed circuit is resistor-less, employing two OTAs with one grounded FOC and capable of generating FLPF, FHPF and FAPF responses. The output current of

the proposed TAM FOF is given as

$$I_o = g_{m2}\left[\frac{-g_{m1}V_{in1} + s^{\alpha}C_{\alpha}V_{in2}}{g_{m2} + s^{\alpha}C_{\alpha}}\right] \tag{3.4}$$

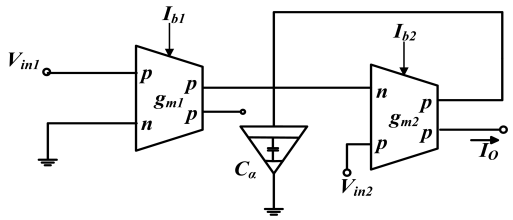

Figure 3.1: Proposed α-order TAM FOF

Table 3.2: Various inputs to the proposed TAM FOF and the related outputs

V_{in1} and V_{in2}	Transfer Function of FOF	Type of FOF
V_{in1}=V_{in}; V_{in2}=0	$T^{\alpha}(s)_{FLPF}$=-$g_{m1}[\frac{1}{1+s^{\alpha}(C_{\alpha}/g_{m2})}]$	FLPF (a=C_{α}/g_{m2},b=0,c=$-g_{m1}$)
V_{in2}=V_{in}; V_{in1}=0	$T^{\alpha}(s)_{FHPF}$=$g_{m2}[\frac{s^{\alpha}(C_{\alpha}/g_{m2})}{1+s^{\alpha}(C_{\alpha}/g_{m2})}]$	FHPF (a=C_{α}/g_{m2},b=C_{α},c=0)
V_{in1}=V_{in2}; g_{m1}=g_{m2}=g_m	$T^{\alpha}(s)_{FAPF}$=$g_m[\frac{s^{\alpha}(C_{\alpha}/g_{m2})-1}{s^{\alpha}(C_{\alpha}/g_{m2})+1}]$	FAPF (a=C_{α}/g_m,b=C_{α},c=$-g_m$)

For various conditions on inputs (V_{in1} and V_{in2}), different outputs may be obtained, as mentioned in Table 3.2. The critical frequencies of FLPF, FHPF and FAPF are computed and given in (3.5)–(3.7) respectively.

$$\begin{aligned}
\omega_{m(FLPF)} &= \omega_{0(FLPF)}\left[-cos(\frac{\alpha\pi}{2})\right]^{\frac{1}{\alpha}} \\
\omega_{rp(FLPF)} &= \omega_{0(FLPF)}\left[\frac{-1}{cos(\frac{\alpha\pi}{2})}\right]^{\frac{1}{\alpha}} \\
\omega_{h(FLPF)} &= \omega_{0(FLPF)}\left[\sqrt{1+cos^2(\frac{\alpha\pi}{2})} - cos(\frac{\alpha\pi}{2})\right]^{\frac{1}{\alpha}}
\end{aligned} \tag{3.5}$$

$$\begin{aligned}
\omega_{m(FHPF)} &= \omega_{0(FHPF)} \left[\frac{-1}{cos(\frac{\alpha\pi}{2})}\right]^{\frac{1}{\alpha}} \\
\omega_{rp(FHPF)} &= \omega_{0(FHPF)} \left[-cos(\frac{\alpha\pi}{2})\right]^{\frac{1}{\alpha}} \\
\omega_{h(FHPF)} &= \omega_{0(FHPF)} \left[\sqrt{1+cos^2(\frac{\alpha\pi}{2})}+cos(\frac{\alpha\pi}{2})\right]^{\frac{1}{\alpha}}
\end{aligned} \tag{3.6}$$

$$\begin{aligned}
\omega_{m(FAPF)} &= \omega_{rp(FAPF)} = \omega_{0(FAPF)} \\
\omega_{h(FAPF)} &= \omega_{0(FAPF)} \left[2cos(\frac{\alpha\pi}{2})+\sqrt{4cos^2(\frac{\alpha\pi}{2})-1}\right]^{\frac{1}{\alpha}}
\end{aligned} \tag{3.7}$$

Here $\omega_{0(FLPF)}$=$\omega_{0(FHPF)}$=$\omega_{0(FAPF)}$=ω_0=$(g_{m2}/C_\alpha)^{1/\alpha}$ and ω_0 is the pole frequency of the proposed TAM FOF.

3.3.1 Functional Verification

To validate the functionality of the proposed TAM FOF, SPICE simulations are performed using the 180 nm CMOS model parameters with supply voltages taken as $\pm 1.8\ V$. Section 2.4 provides the details of the transistors used to construct OTA, and its corresponding CMOS schematic is illustrated in Fig. 2.8 (b). By changing the bias current of OTA, g_m is adjusted, and provides electronic tunability to the pole frequency of the proposed TAM FOF.

The FOC utilized in the proposed TAM FOF is implemented using a 12^{th} order R-C ladder network based on CFE approximation [35]. The schematic of the R-C ladder network is depicted in Fig. 3.2. The values for R_0, R_i and C_i (i=1, 2, ...11) to emulate FOC with α=0.5 and C_α=3.75 $\mu\mho sec^\alpha$ are given below:

R_0=18.2 Ω, R_1=330 $k\Omega$, R_2=82 $k\Omega$, R_3=33 $k\Omega$, R_4=12 $k\Omega$, R_5=4.7 $k\Omega$, R_6=2 $k\Omega$, R_7=736 Ω, R_8=270 Ω, R_9=120 Ω, R_{10}=47 Ω, R_{11}=8.2 Ω, C_1=4.7 μF, C_2=3.1 μF,

C_3=1 μF, C_4=470 nF, C_5=168 nF, C_6=68 nF, C_7=27 nF, C_8=10 nF, C_9=4.7 nF, C_{10}=1 nF, C_{11}=2.2 nF.

Simulations are performed for C_α=3.75 $\mu\mho sec^\alpha$ and α=0.5. The values of g_{m1} and

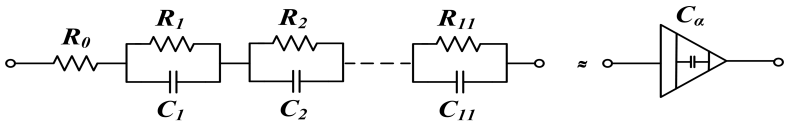

Figure 3.2: 12^{th} order R-C ladder network to realize FOC (based on CFE approximation)

g_{m2} are taken as same and the value is set to 162.3 $\mu A/V$. Magnitude and phase response for FLPF and FHPF are shown in Figs. 3.3 and 3.4 respectively. The half-power frequencies from the responses are found to be 88.43 Hz and 999 Hz for FLPF and FHPF respectively, while the theoretical values for the same are 83.7 Hz and 1.11 kHz respectively.

The magnitude of FAPF at ω_0=ω_{rp} exhibits a minimum value if $\alpha < 1$, a maximum value if $\alpha > 1$ and remains flat if α=1 (integer-order case) [17]. As the value of α has been chosen as 0.5 that is lesser than 1, a minima will show up at ω_{rp} and the value of ω_{rp} is same as ω_0. From Fig. 3.5, the frequency of minima for FAPF is observed as 271.46 Hz and its theoretical value is calculated as 298.12 Hz. The above observations show that both simulated and theoretical values of the half-power frequency of the proposed TAM FOF are in close approximation.

The effect of α on FLPF response has been shown in Fig. 3.6 for three values of α (0.4, 0.5 and 0.6). Increasing the value of α leads to an increased slope of the transition band in the magnitude response of FOF as the transition band slope for α-order FOF is -20α dB/decade. The similar study has been done for other responses also, and the variation in slope of the transition band shows the same

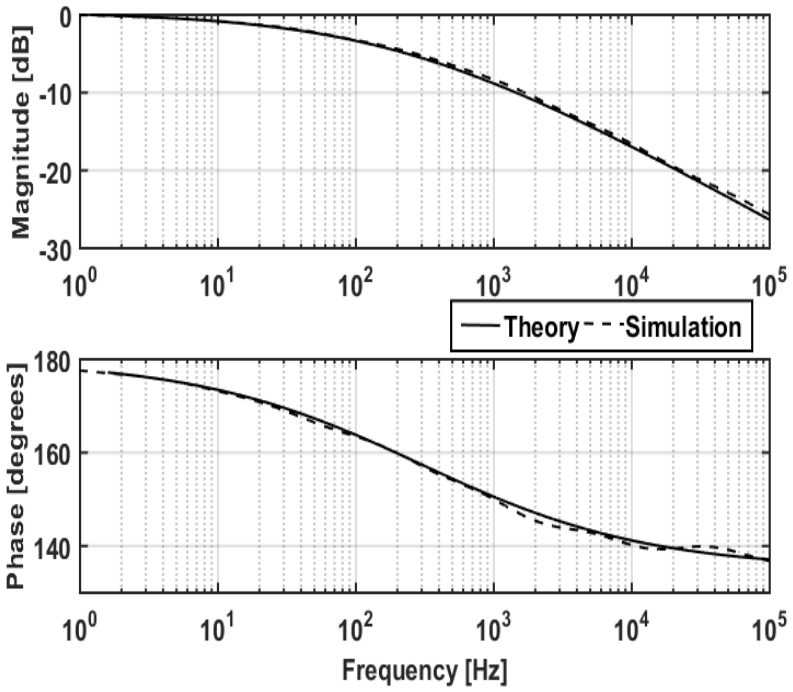

Figure 3.3: Magnitude response and phase response of proposed TAM FLPF

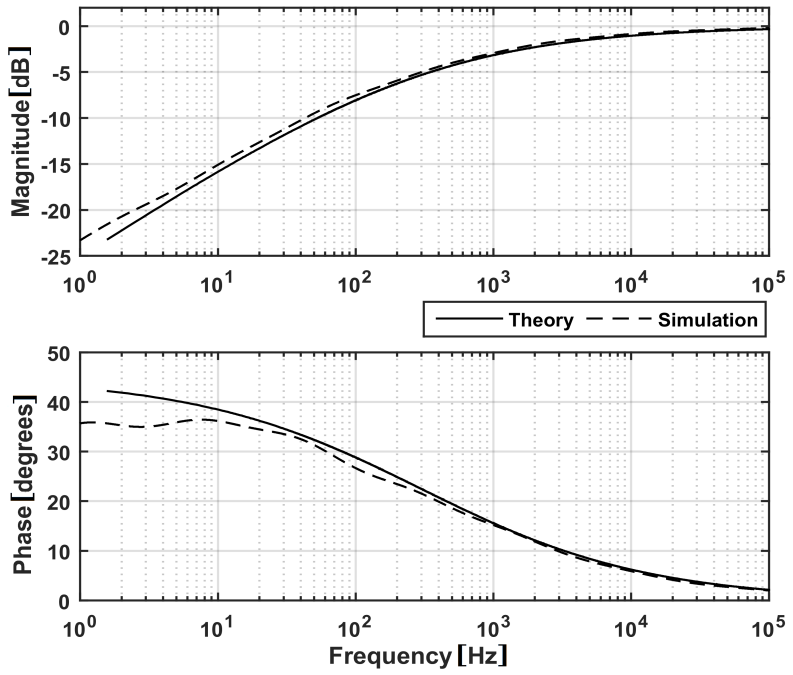

Figure 3.4: Magnitude response and phase response of proposed TAM FHPF

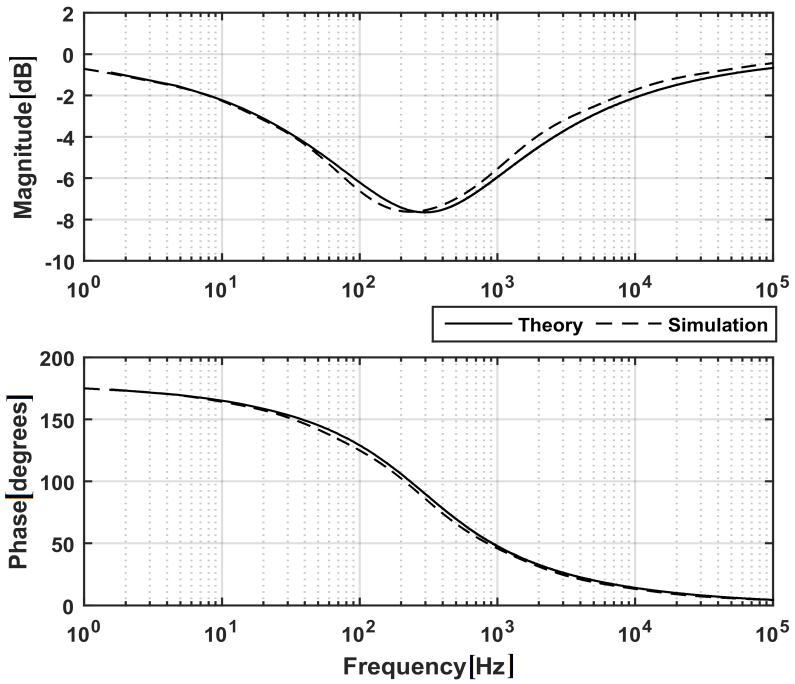

Figure 3.5: Magnitude response and phase response of proposed TAM FAPF

trend.

Time domain behavior for proposed FAPF is also observed for the sinusoidal input signal of 1 mV, 271.46 Hz and α=0.5 in Fig. 3.7 (a), corresponding Lissajous pattern is also depicted in Fig. 3.7 (b). As the frequency of the input sinusoid is equal to ω_0 of the FAPF, which is also the ω_{rp}, the Lissajous pattern shows a 90° phase shift between input and output. To ensure electronic tunability, Magnitude response and phase response of FAPF for I_b=5 μA, 15 μA and 25 μA are plotted in Fig. 3.8, the corresponding pole frequencies are 45.8 Hz, 298 Hz and 646.2 Hz respectively. The phase plot undergoes a shift along the frequency axis while preserving its shape, by adjusting the pole frequency, the same is evident from Fig. 3.8.

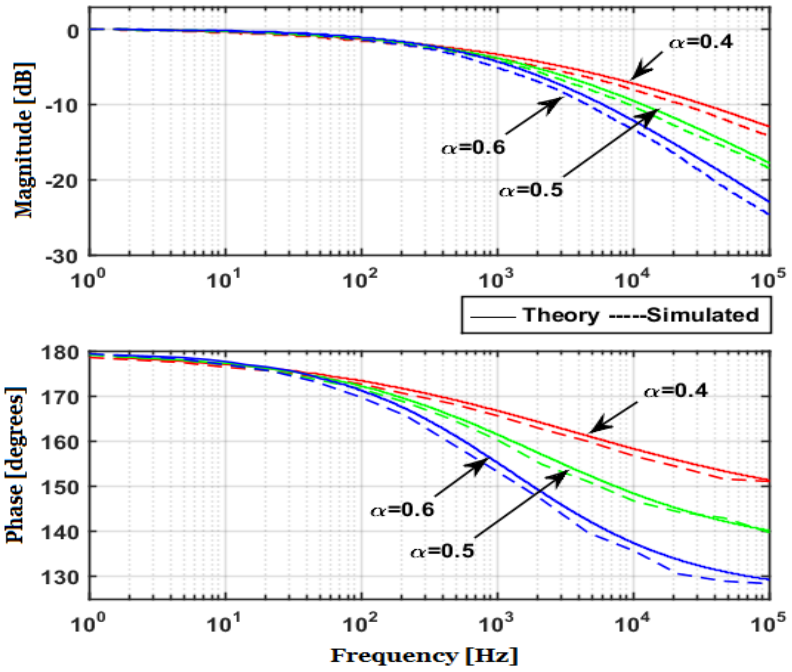

Figure 3.6: Magnitude response and phase response of proposed TAM FLPF for different values of α

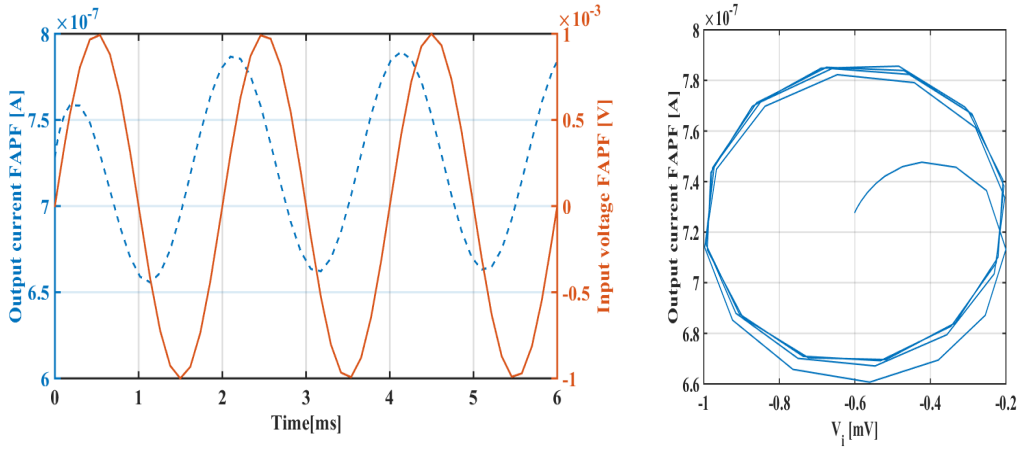

(a) (b)

Figure 3.7: Time domain behaviour of proposed TAM FAPF (a) Transient response with 1 mV, 271.46 Hz input sinusoid signal (b) Corresponding Lissajous pattern

3.3.2 Stability Analysis

The stability of the proposed TAM FOF has been verified using root locus method for the linear fractional-order system outlined in section 2.3 [117]. Pole plot for the characteristic equation of the proposed TAM FOF is acquired through *forlocus* function of MATLAB [122] for p=1 and q=2 (as $\alpha=\frac{p}{q}$=0.5) and is shown in Fig. 3.9. The boundaries for the stable and unstable regions are separated by $\pm\frac{\pi}{2q}$ and shown as dotted dash lines. As it may be witnessed from Fig. 3.9 that, both the roots lie outside $\pm\frac{\pi}{2q}$ region, the proposed TAM FOF is stable.

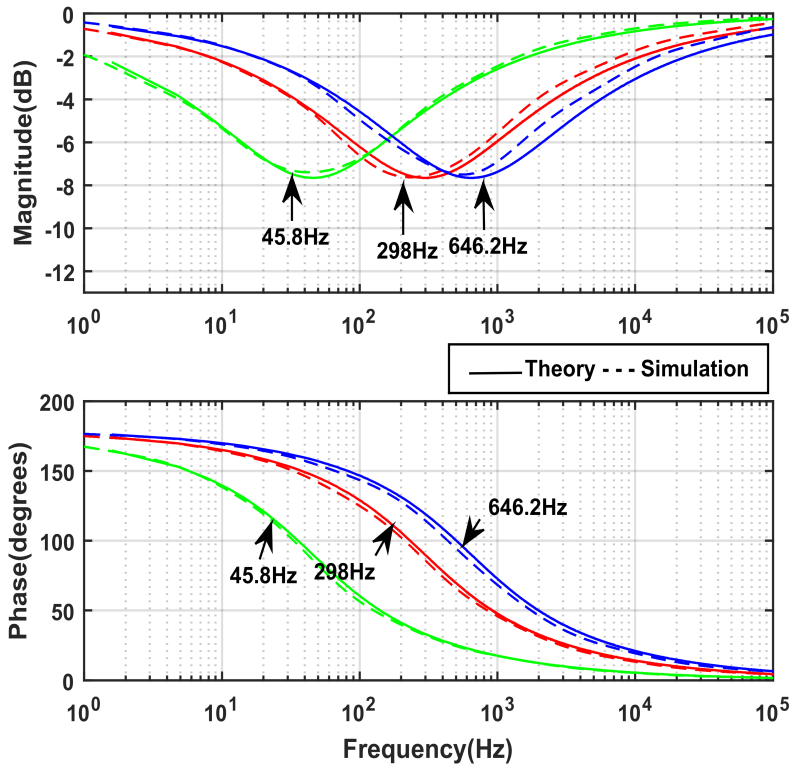

Figure 3.8: Magnitude response and phase response for FAPF for I_b=5 μA (45.8 Hz), 15 μA (298 Hz) and 25 μA (646.2 Hz), ensuring electronic tunability

3.3.3 Sensitivity Analysis

Transfer function of the proposed TAM FOF may change with the variations in component's value. The sensitivity analysis shows the relative variation in output responses of the circuit with respect to changes in its components values. The sensitivity of parameter (U) with respect to change in the value of parameter (V) is defined as [126]:

$$S_V^U = \frac{V}{U}\frac{\delta U}{\delta V} \tag{3.8}$$

The sensitivities of the transfer functions of the proposed FLPF, FHPF and FAPF with respect to various circuit components (i.e., α, C_α, g_{m1} and g_{m2}) have been derived mathematically and presented in (3.9), (3.10) and (3.11) respectively.

$$\begin{aligned} S_{\alpha}^{T^{\alpha}(s)_{FLPF}} &= -\frac{\alpha s^{\alpha} ln(s)}{(s^{\alpha}+g_{m2}/C_{\alpha})} \\ S_{C_{\alpha}}^{T^{\alpha}(s)_{FLPF}} &= S_{g_{m2}}^{FLPF} = \frac{s^{\alpha}}{(s^{\alpha}+g_{m1}/C_{\alpha})} \\ S_{g_{m1}}^{T^{\alpha}(s)_{FLPF}} &= 1 \end{aligned} \tag{3.9}$$

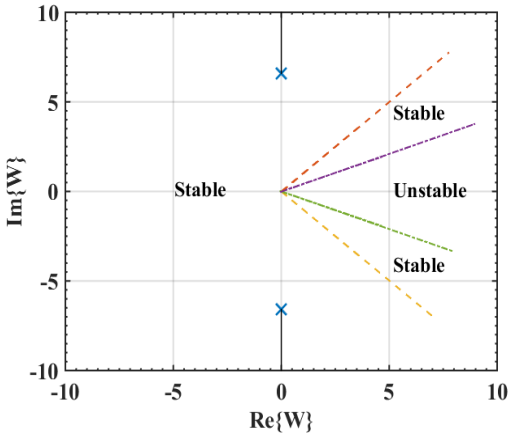

Figure 3.9: Pole plot in W-plane for proposed TAM FOF for α=0.5

$$
\begin{aligned}
S_{\alpha}^{T^{\alpha}(s)_{FHPF}} &= \frac{\frac{g_{m2}}{C_{\alpha}}\alpha ln(s)}{(s^{\alpha}+g_{m2}/C_{\alpha})} \\
S_{C_{\alpha}}^{T^{\alpha}(s)_{FHPF}} &= S_{g_{m2}}^{FHPF} = \frac{\frac{g_{m2}}{C_{\alpha}}}{(s^{\alpha}+g_{m2}/C_{\alpha})} \\
S_{g_{m1}}^{T^{\alpha}(s)_{FHPF}} &= 0
\end{aligned}
\tag{3.10}
$$

$$
\begin{aligned}
S_{\alpha}^{T^{\alpha}(s)_{FAPF}} &= \frac{\frac{2g_m}{C_{\alpha}}\alpha s^{\alpha} ln(s)}{(s^{2\alpha}-g_{m2}^2/C_{\alpha}^2)} \\
S_{C_{\alpha}}^{T^{\alpha}(s)_{FAPF}} &= \frac{\frac{2g_m}{C_{\alpha}}s^{\alpha}}{(s^{2\alpha}-g_{m2}^2/C_{\alpha}^2)} \\
S_{g_m}^{T^{\alpha}(s)_{FAPF}} &= \frac{(s^{2\alpha}-\frac{2g_m}{C_{\alpha}}s^{\alpha}-\frac{g_m^2}{C_{\alpha}^2})}{(s^{2\alpha}-g_{m2}^2/C_{\alpha}^2)}
\end{aligned}
\tag{3.11}
$$

The sensitivities for the proposed FLPF, FHPF and FAPF given in (3.9), (3.10) and (3.11) respectively, are plotted using MATLAB and shown in Fig. 3.10. To plot the sensitivity with respect to C_{α}, three different values of C_{α} are taken such as 1 $\mu\mho sec^{\alpha}$, 3.75 $\mu\mho sec^{\alpha}$ and 5 $\mu\mho sec^{\alpha}$ while keeping α and g_m (g_{m1}=g_{m2}) as constant at 0.5 and 162.3 $\mu A/V$ respectively. The corresponding simulated plots for FLPF, FHPF and FAPF are shown in Figs. 3.10 (a), (d) and (g) respectively. Sensitivity curves against g_m (for three different values of g_m such as: 63.6 $\mu A/V$, 162.3 $\mu A/V$ and 238.9 $\mu A/V$) while α is chosen as 0.5 and C_{α} as 3.75 $\mu\mho sec^{\alpha}$ are presented in Figs. 3.10 (b), (e) and (h) for FLPF, FHPF and FAPF respectively. The sensitivity curves with respect to α are plotted in Figs. 3.10 (c), (f) and (i) for FLPF, FHPF and FAPF respectively, keeping C_{α} as 3.75 $\mu\mho sec^{\alpha}$ and g_m (g_{m1}=g_{m2}) as 162.3 $\mu A/V$. The three different values of α are taken as 0.3, 0.5 and 0.8.

It is witnessed that sensitivity with respect to C_{α} is lowest in pass-band and highest in stop-band for both FLPF and FHPF and within unity which is desirable feature, same trend is followed by the sensitivity with respect to g_m for both FLPF

and FHPF. FAPF sensitivity with respect to C_α is highest at the pole frequency (slightly higher than unity), while sensitivity with respect to g_m is slightly higher than unity for lower frequencies and eventually for higher frequency it approaches to unity. As FLPF, FHPF and FAPF all are quite sensitive to α, the value of α must be selected very accurately. From (3.9), (3.10) and (3.11) the sensitivity with respect to α can be depicted as high due to the natural log of frequency term in the numerator.

3.3.4 Robustness

Process-Voltage-Temperature (PVT) and Monte-Carlo analyses have been conducted to examine the robustness of the proposed TAM FOF, and the results are discusse below.

3.3.4.1 PVT analysis

In order to assess the robustness of the proposed TAM FOF, the circuit structure is subjected to simulations under various conditions, including different process corners, variations in supply voltage, and temperature changes.

Process corners are named using two-letter identifiers, where the first letter represents the NMOS corner and the second letter represents the PMOS corner. The three main corners are typical, fast, and slow. The fast corner has higher carrier mobilities, oxide thickness, and doping concentration compared to the typical corner, while the slow corner has lower values. Therefore, there are five possible

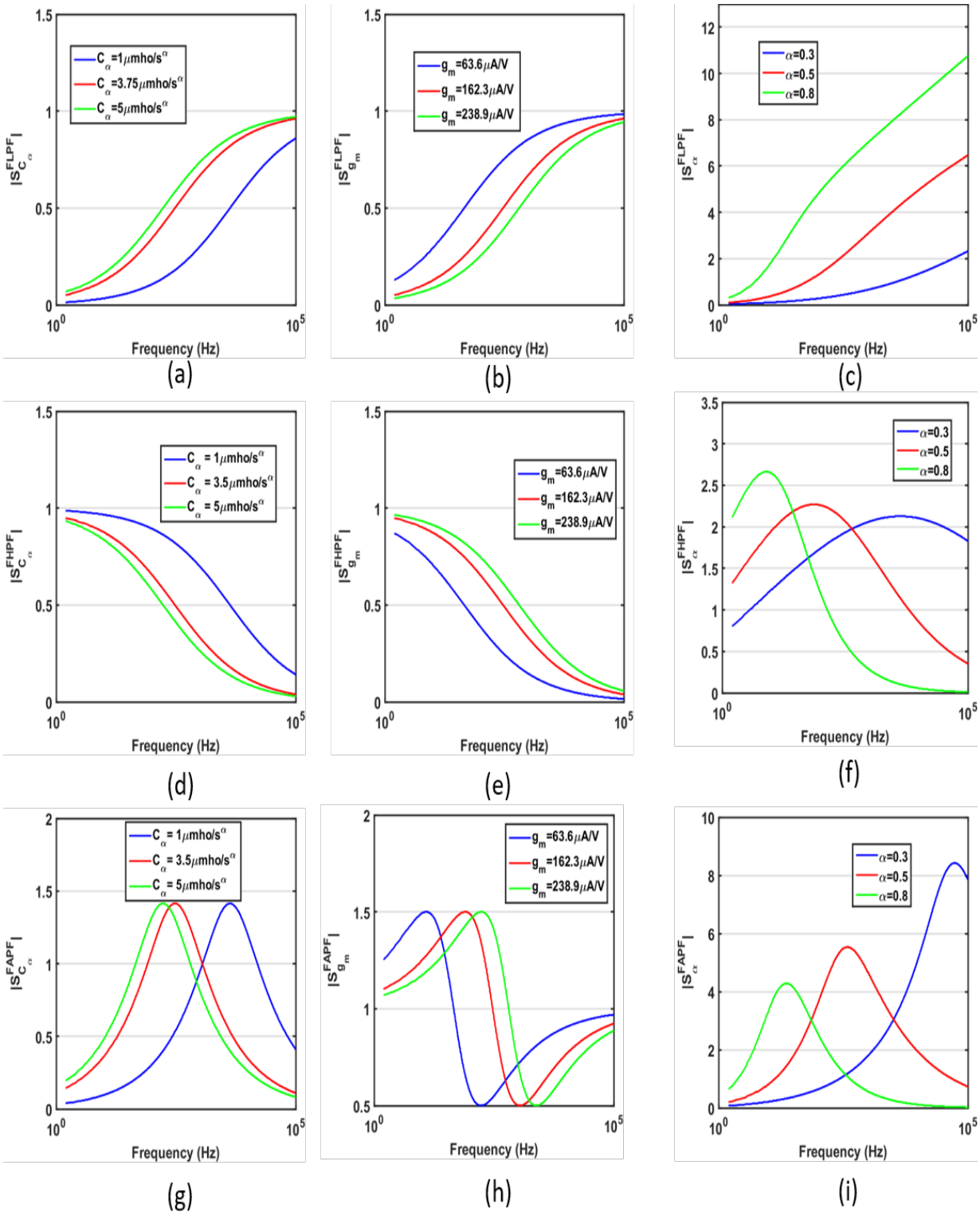

Figure 3.10: Sensitivity of the proposed TAM FOF: (a) $|S^{FLPF}_{C_\alpha}|$(b) $|S^{FLPF}_{g_{m2}}|$(c) $|S^{FLPF}_{\alpha}|$(d) $|S^{FHPF}_{C_\alpha}|$(e) $|S^{FHPF}_{g_{m2}}|$(f) $|S^{FHPF}_{\alpha}|$(g) $|S^{FAPF}_{C_\alpha}|$(h) $|S^{FAPF}_{g_m}|$(i) $|S^{FAPF}_{\alpha}|$

Table 3.3: Half-power frequency/frequency of minima of the proposed TAM FOF for all five process corners for α=0.5

Process corner	FLPF half-power frequency (% error from TT corner)	FHPF half-power frequency (% error from TT corner)	FAPF frequency of minima (% error from TT corner)
FF	84.45 (4.5%)	950.05 (4.9%)	258.39 (4.8%)
FS	84.899 (4%)	961.04 (3.8%)	261.11 (3.8%)
TT	88.43 -	999 -	271.42 -
SF	85.07 (3.8%)	958.04 (4.1%)	260.02 (4.2%)
SS	84.01 (5%)	249.55 (4.95%)	257.85 (5%)

corners: fast-fast (FF), fast-slow (FS), typical-typical (TT), slow-fast (SF), and slow-slow (SS) corners.

The values of half-power frequencies of FLPF and FHPF, and frequency of minima for FAPF with the percentage error from TT corner point for all the remaining four corner points are listed in Table 3.3. Further Tables 3.4 and 3.5 comprise the values of half-power frequencies of FLPF and FHPF, and frequency of minima for FAPF in presence of supply voltage variations (1.8 V, 1.8 V±2.5% and 1.8 V±5%) and temperature variations (0°C, 27°C and 70°C) respectively for the proposed TAM FOF.

It is clear from Tables 3.3, 3.4 and 3.5 that the percentage error from the base parameter (i.e., TT corner for corner analysis, 1.8 V for power supply variations and 27°C for temperature variations) lie within 6% , which verifies the robustness of the proposed circuit for PVT variations.

Table 3.4: Half-power frequency/frequency of minima of the proposed TAM FOF for power supply variation for $\alpha = 0.5$

Power supply	FLPF half-power frequency (% error from 1.8 V)	FHPF half-power frequency (% error from 1.8 V)	FAPF frequency of minima (% error from 1.8 V)
1.8 V	88.43 -	999 -	271.42 -
1.8 V±2.5%	89.1 (0.76%)	1000.25 (0.13%)	271.01 (0.15%)
1.8 V±5%	86.89 (1.74%)	995.1 (0.39%)	272.3 (0.38%)

Table 3.5: Half-power frequency/frequency of minima of the proposed TAM FOF for for temparature variation for α=0.5

Temp.	FLPF half-power frequency (% error from 27°C)	FHPF half-power frequency (% error from 27°C)	FAPF frequency of minima (% error from 27°C)
0°C	92.85 (5.9%)	1048.95 (5%)	287.47 (5.9%)
27°C	88.43 -	999 -	271.42 -
70°C	84.89 (3.8%)	939.06 (6%)	257.85 (5%)

3.3.4.2 Monte-Carlo analysis

To gain a deeper understanding of the sensitivity of the proposed TAM FOF with respect to random variations in FOC i.e., C_α, Monte-Carlo simulation is done on 100 random samples. The values of passive components, used for FOC realization, are randomly varied in uniform Gaussian distribution with a tolerance of ±5%. Magnitude response and phase response for the proposed TAM FOF are shown in Fig. 3.11. For FLPF, the maximum spread for magnitude (phase) in pass-band, stop-band and at half-power frequency is observed to be 0.088 dB (0.5°), 1.55 dB (9.2°) and 0.74 dB (3.7°). Similar observations for FHPF are obtained and it is

clear that maximum spread for magnitude (phase) in pass-band, stop-band and at half-power frequency is 0.092 dB (0.56°), 1.32 dB (6.2°) and 0.58 dB (3.7°). For FAPF, the spread for magnitude (phase) is calculated at the frequency of minima and the range for the same is within 2.08 dB (14.6°). It is observed from the above analysis that the spread in magnitude and phase is within a small range, which confirms the smaller component sensitivity of the proposed TAM FOF.

The observations from the sensitivity analysis and Monte-Carlo analysis for FLPF, FHPF and FAPF responses with respect to C_α are summed up in Table 3.6. It is noteworthy that sensitivity has a direct bearing on spread in Monte-Carlo analysis. A higher sensitivity leads to higher spread in the magnitude response, whereas lower sensitivity results in lower spread.

Table 3.6: Summary of Sensitivity and Monte-Carlo Analysis of the proposed TAM FOF

Filter Response	Sensitivity from Sensitivity analysis		Spread region in Monte-Carlo analysis	
	Maximum	Minimum	Maximum	Minimum
FLPF	Stop band	Pass band	Stop band	Pass band
FHPF	Stop band	Pass band	Stop band	Pass band
FAPF	Near pole frequency	Lower and higher frequencies	Near pole frequency	Lower and higher frequencies

3.3.5 Experimental Results

The proposed TAM FOF is verified experimentally also using commercially available OTA IC LM13700N with supply voltage of $\pm 10\ V$. The FOC is realized using the R-C ladder network of Fig. 3.2 with component values as specified in section

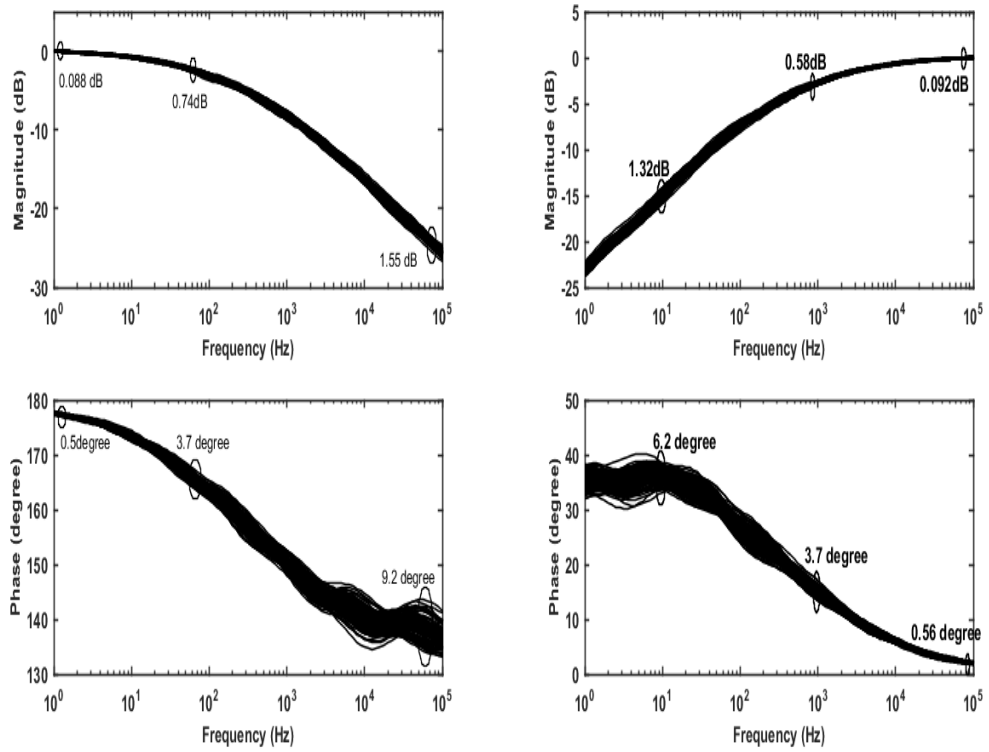

(a) (b)

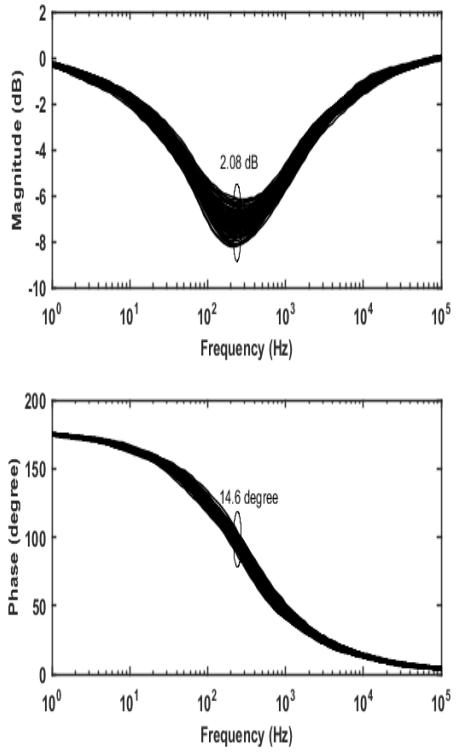

(c)

Figure 3.11: Magnitude response and phase responses under Monte-Carlo analysis for the proposed TAM FOF (a) FLPF (b) FHPF (c) FAPF

3.3.1. Figure 3.12 shows the experimental setup for the proposed TAM FOF. The transconductance gains of both the OTAs are set as g_{m1}=g_{m2}=0.46 mA/V. The frequency response, transient response and Lissajous pattern for FLPF, FHPF and FAPF are shown in Figs. 3.13, 3.14 and 3.15 respectively. The input signal frequencies for obtaining transient responses for FLPF and FHPF are so chosen that they fall in their respective pass-bands i.e., 100 Hz and 100 kHz, respectively for FLPF and FHPF, whereas for FAPF, the input signal frequency is selected at which the minima in the magnitude response is obtained i.e., 4.6 kHz. It may

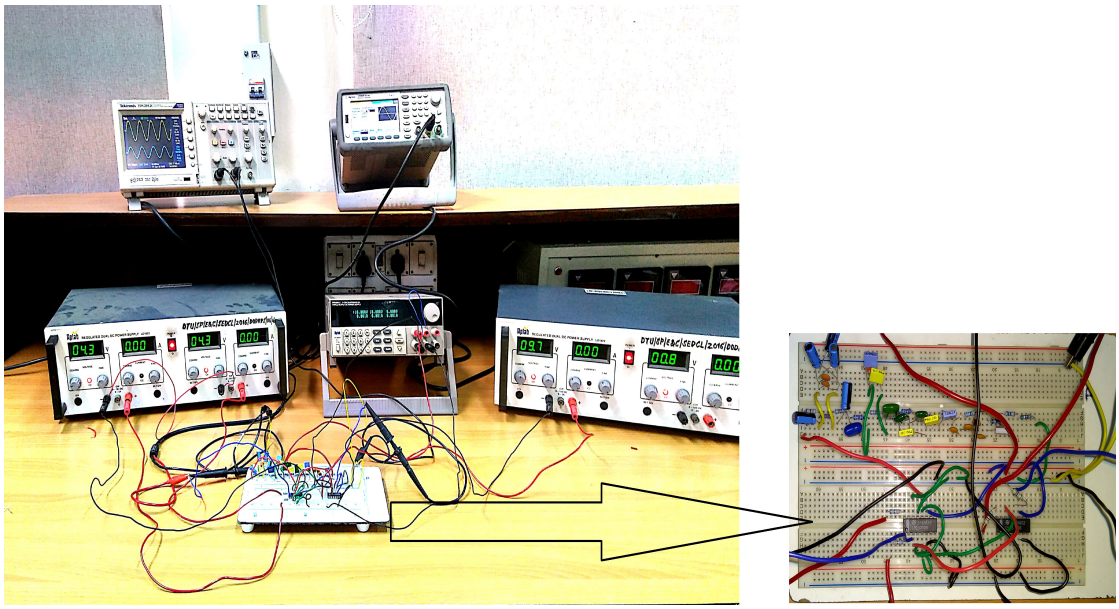

Figure 3.12: Hardware Setup

be observed from the results shown in Figs. 3.13 –3.15 that the experimental frequency responses for all the filter types are in close approximation to the theoretical responses. The transient response for FLPF demonstrates a phase difference of 177° as against the theoretical value of 174.6°. For the FHPF phase difference is recorded as 4.41° against the calculated value of 7.52°. For FAPF, phase at minima is observed to be 76.5° in contrast to the theoretical value of

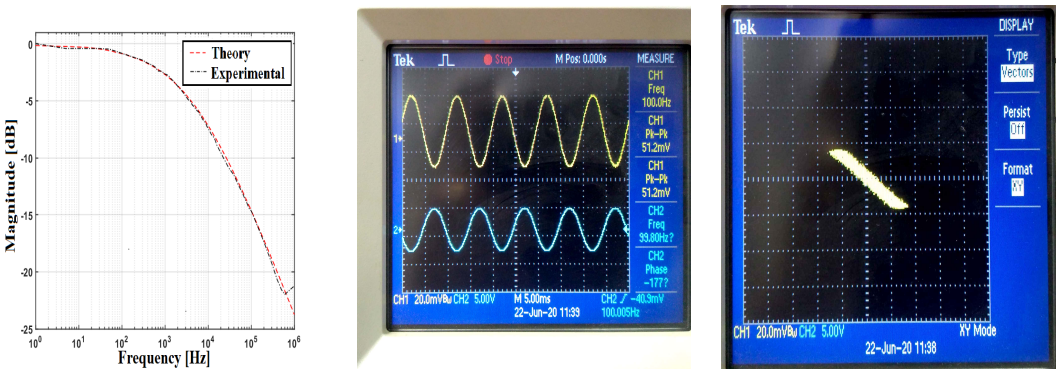

(a) (b) (c)

Figure 3.13: Experimental results for the proposed TAM FOF (FLPF) (a) Frequency Response (b) Transient Response (c) Lissajous pattern

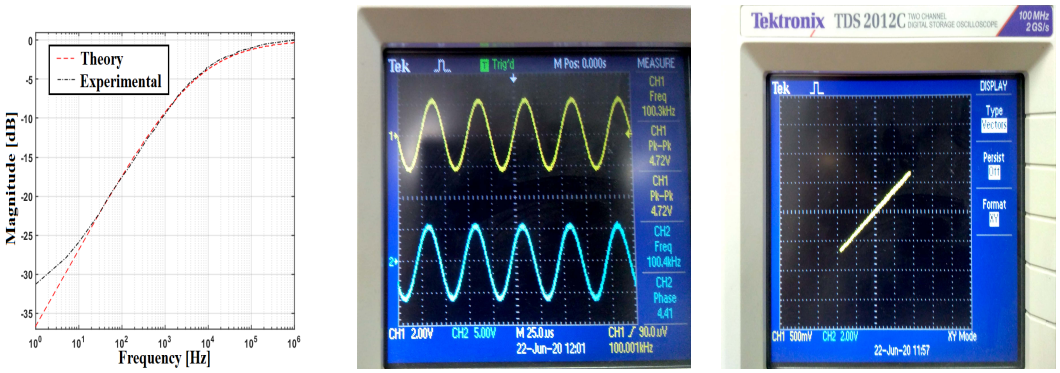

(a) (b) (c)

Figure 3.14: Experimental results for the proposed TAM FOF (FHPF) (a) Frequency Response (b) Transient Response (c) Lissajous pattern

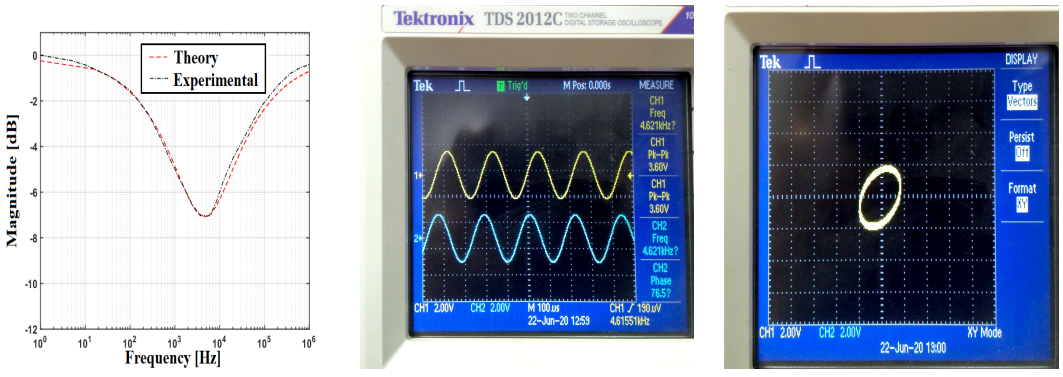

(a) (b) (c)

Figure 3.15: Experimental results for the proposed TAM FOF (FAPF) (a) Frequency Response (b) Transient Response (c) Lissajous pattern

90°. Minor deviations may be attributed to the components' tolerances used for realizing the FOC.

3.4 Conclusion

In this chapter an α-order multifunction TAM FOF is proposed for the very first time. The proposed TAM FOF offers FLPF, FHPF, and FAPF filter responses. The proposed structure's effectiveness has been verified through both SPICE simulations and experimental testing, and found that results fit in the theoretical predictions very well. Additionally, the electronic tunability of the pole frequency has been confirmed through SPICE simulations. The sensitivity of the proposed TAM FOF is analyzed using MATLAB, and the structure's robustness is verified through PVT and Monte-Carlo analysis. These findings suggest that the proposed TAM FOF can be a promising candidate for various applications in signal processing and communication systems.

Chapter 4

FOFs with Externally Tunable Design Parameters

This chapter presents the results and content of the following papers:

[1] **G. Varshney,** N. Pandey and R. Pandey, "Generalization of shadow filters in fractional domain," in International Journal of Circuit Theory and Applications, vol. 49, no. 10, pp. 3248-3265, 2021, doi: 10.1002/cta.3054. **(SCIE indexing, 2.378 IF)**

[2] **G. Varshney,** N. Pandey and R. Pandey, "Multi-Functional Fractional-Order Shadow Filter using OTA," in 2021 Innovations in Power and Advanced Computing Technologies (i-PACT), 2021, pp. 1-5, doi: 10.1109/i-PACT52855.2021.9696856.

4.1 Introduction

As outlined in the preceding chapter, filters are essential components of analog signal processing. Generally, filter parameters such as pole frequency (ω_0) and pole quality factor (Q) require tuning for various applications like audio equalizers, medical equipments, instrumentation, etc. [126]. This can be achieved by changing the passive components or through electronic tuning by varying transconductance /current/voltage gain of constituent active elements. In [127], Lakys and Fabre have introduced a new way of electronically tune the integer-order filter parameters. This method involves including an external amplifier within the feedback loop of the basic filter. By adjusting the gain of this external amplifier, the filter's parameters (ω_0 and Q) can be modified without affecting the active and passive components of the filter. These filters are called as shadow filters [127]. Various integer-order shadow filters are accessible in open literature, e.g. [128]–[132], and the sources cited therein.

In this chapter, the theory of integer-order shadow filters is generalized to fractional domain. The counterpart of integer-order shadow filters in fractional domain are called as shadow FOFs. Mathematical equations have been drafted to determine ω_0 and Q when different types of feedback signals, such as low-pass, high-pass, band-pass, or band-stop, are applied to the external amplifier in the feedback loop. The proposed theory has been demonstrated using MATLAB simulations. To verify the proposed theory, two active shadow FOFs are presented using a basic FOF and an externel amplifier with gain A in the feedback loop. Both the shadow FOFs are built around OTA. SPICE simulations are carried out to verify

the functionality of the proposed shadow FOFs using 180 nm CMOS technology model parameters.

4.2 Generalization of Second-Order Filters

This section reproduces the concept of generic 2α-order FOF described in [57]. The transfer function of a second-order filter in the integer domain is generally expressed as:

$$T(s) = \frac{Fs^2 + Es + G}{s^2 + 2ps + q} \tag{4.1}$$

Here coefficients p, q, F, E and G are constant terms. By selecting suitable values of F, E and G various filter responses such as low-pass (F=0, E=0, $G \neq 0$), high-pass ($F \neq 0, E$=0, G=0), band-pass (F=0, $E \neq 0, G$=0) or band-stop ($F \neq 0, E$=0, $G \neq 0$) may be realized.

The fractional domain generalization of (4.1), where integer-order capacitors are replaced with two FOCs of distinct fractional orders α and β respectively, the resulting FOF is of fractional order $(\alpha + \beta)$ and given as (4.2) [57].

$$T^{\alpha+\beta}(s) = \frac{Fs^{\alpha+\beta} + Es^{\alpha} + G}{s^{\alpha+\beta} + 2ps^{\alpha} + q} \tag{4.2}$$

By selecting suitable values of F, E and G, various FOF responses such as FLPF, FHPF, FBPF and FBSF may be realized, the conditions are summarized in Table 4.1. Assuming that α is equal to β, the $(\alpha + \beta)$-order FOF is modified

to 2α-order FOF and given by (4.3).

$$T^{2\alpha}(s) = \frac{Fs^{2\alpha} + Es^{\alpha} + G}{s^{2\alpha} + 2ps^{\alpha} + q} \tag{4.3}$$

Table 4.1: Conditions for the values of F, E, G and the corresponding FOFs

Values of F, E, G	Type of FOF
F=0, E=0, G≠0	FLPF
F=0, E≠0, G=0	FBPF
F≠0, E=0, G=0	FHPF
F≠0, E=0, G≠0	FBSF

Lets denote the denominator of (4.3) as D(s) which is also the characteristic equation of (4.3), the magnitude of D(s) can be derived as

$$|D(s)| = \sqrt{\omega^{4\alpha} + 4p\omega^{3\alpha}\cos(\alpha\pi/2) + (4p^2 + 2q\cos\alpha\pi)\omega^{2\alpha} + 4pq\omega^{\alpha}\cos(\alpha\pi/2) + q^2} \tag{4.4}$$

The stability of 2α-order FOF is determined by parameters p and q, Table 4.2 provides a summary of four possible cases of stability based on these parameters. The pole frequency (ω_0) and the pole quality factor (Q) of basic 2α-order FOF are also listed in Table 4.2 for each case of the stability [117].

Table 4.2: Stability conditions, pole frequency (ω_0) and pole quality factor (Q) for 2α-order FOF [117]

Stability Case	Relationship	Stability conditions and roots	ω_O, Q
Case-1	$p^2 \geq q$ & $p>0$ & $q>0$	$\alpha<2$ $r_{1,2}=-p\pm\sqrt{p^2-q}=g_{1,2}e^{j\pi}$	$\omega_{01,2}=g_{1,2}^{\frac{1}{\alpha}}$ $Q=\frac{-1}{2\cos\frac{\pi}{\alpha}}$
Case-2	$p^2<q$ & $p>0$ & $q>0$	$\alpha<\frac{2\delta}{\pi}$, $\delta=\cos^{-1}\frac{-p}{\sqrt{q}}>\frac{\pi}{2}$ $r_{1,2}=\sqrt{q}e^{\pm j\delta}$	$\omega_0=\sqrt{q}^{\frac{1}{\alpha}}$ $Q=\frac{-1}{2\cos\frac{\delta}{\alpha}}$
Case-3	$p^2<q$ & $p<0$ & $q>0$	$\alpha<\frac{2\delta}{\pi}$, $\delta=\cos^{-1}\frac{-p}{\sqrt{q}}<\frac{\pi}{2}$ $r_{1,2}=\sqrt{q}e^{\pm j\delta}$	$\omega_0=\sqrt{q}^{\frac{1}{\alpha}}$ $Q=\frac{-1}{2\cos\frac{\delta}{\alpha}}$
Case-4	$p^2 \geq q$ & $p<0$ or q<0	always unstable	- -

4.3 FOF with External Amplifier of Gain A (Shadowing Concept in Fractional Domain)

A shadow FOF employs a basic 2α-order FOF and an external amplifier with gain A in the feedback loop. Consider a basic 2α-order single-input multi-output FOF, where the two output responses are represented by $T(s)$ and $T_1(s)$ as shown in Fig. 4.1 (a). A shadow FOF may be designed by using any one or combinations of the outputs of the basic 2α-order FOF to drive the external amplifier in the feedback loop. The block diagram of the shadow FOF is depicted in Fig. 4.1 (b) in which output $T_1(s)$ is used to drive the external amplifier in the feedback loop. This arrangement modifies the transfer function from $T(s)=V_0/V_i$ to $T'(s)=V_0/V_{in}$, here V_i and V_{in} are the inputs to the filter before and after putting the external amplifier in the feedback loop, respectively. Now the modified transfer function $T'(s)$ holds the same filter response as $T(s)$ but with different characteristic equation.

Lets $T(s)$ is represented by (4.3) and $T_1(s)$ is given by (4.5). $T_1(s)$ may lead to

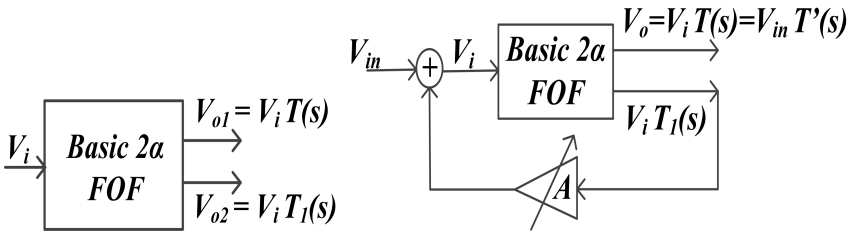

Figure 4.1: Block diagram of (a) Basic 2α-order cell with two outputs (b) Basic cell with external amplifier of gain A to constitute the shadow FOF

various filter responses through appropriate selection of coefficients H, B and L of the numerator polynomial (such as: FLPF, FHPF, FBPF and FBSF etc). Any of these responses may be used to drive the external amplifier. Then by routine network analysis of Fig. 4.1 (b) the modified transfer function $T'(s)$ is obtained and given in (4.6).

$$T_1(s) = \frac{Hs^{2\alpha} + Bs^{\alpha} + L}{s^{2\alpha} + 2ps^{\alpha} + q} \tag{4.5}$$

$$T'(s) = \frac{T(s)}{1 - AT_1(s)} \tag{4.6}$$

Combining (4.3), (4.5) and (4.6) gives $T'(s)$ that is expressed by (4.7). By examining equation (4.8), it is observed that the coefficients (X and Y) in the characteristic equation of $T'(s)$ involve the term A, representing the gain of the external amplifier. As a result, the pole frequency (ω_0') and the pole quality factor (Q') of the shadow FOF can be adjusted through the gain A of the external amplifier. This electronic tuning capability allows for the modification of the shadow FOF parameters without affecting its core components.

$$T'(s) = \frac{N'(s)}{D'(s)} = \frac{(F's^{2\alpha} + E's^{\alpha} + G')}{s^{2\alpha} + 2Xs^{\alpha} + Y} \tag{4.7}$$

Here:

$$(F', E', G') = \frac{(F, E, G)}{(1 - AH)} \tag{4.8a}$$

$$X = \frac{2p - AB}{2(1 - AH)} \tag{4.8b}$$

$$Y = \frac{q - AL}{1 - AH} \tag{4.8c}$$

4.4 Various Cases of Feedback Signals

The transfer function $T'(s)$ of shadow FOF represented by (4.7) is generic in nature, may result into four different instances depending upon the type of feedback signal $T_1(s)$, as $T_1(s)$ could be FLPF, FHPF, FBPF or FBSF. In the following subsections, the first three cases of stability are discussed (as the fourth case is always unstable, refer Table 4.2) related to the characteristic equation of $T'(s)$ for different instances based on the type of feedback signal $T_1(s)$.

For a shadow FOF, the pole frequency (ω_0') can be computed from the roots of the characteristic equation and the pole quality factor (Q') may be given as $-\frac{1}{2\cos\delta/\alpha}$ where δ is the angle of roots from the real axis [57]. For the FOF to be feasible the value of α must be less than $2\delta/\pi$ [57].

4.4.1 FLPF as Feedback Signal

For the case of FLPF feedback signal (H=0, B=0, $L \neq 0$), the characteristic equation of shadow FOF is given by:

$$s^{2\alpha} + 2ps^{\alpha} + (q - AL) = 0 \tag{4.9}$$

The constraint on A to make the shadow FOF feasible is $A < \frac{q}{L}$ for all the three cases. The three cases of stability for FLPF feedback signal are discussed below:

Case-1: $p^2 \geq (q - AL)$ & p>0 & q>AL

By finding the roots of the characteristic equation, ω_0' can be given as:

$\omega'_{01,2} = \left[-p \pm \sqrt{p^2 - (q - AL)}\right]^{1/\alpha}$.

The ω_0' varies with the external amplifier's gain A. For this case of stability the value of δ must be equal to π, and α must be less than 2. Thus, for a particular value of α the Q' is constant.

Case-2: p^2<$(q - AL)$ & p>0 & q>AL

The roots of characteristic equation give ω_0', and can be expressed as:

$\omega'_{01,2} = \left[\sqrt{q - AL}\right]^{1/\alpha}$.

The ω_0' varies with the external amplifier's gain A. For this case of stability the value of δ=$cos^{-1}\left[\frac{-p}{\sqrt{(q-AL)}}\right] > \frac{\pi}{2}$, which leads to variable Q' with external amplifier's gain A.

Case-3: p^2<$(q - AL)$ & p<0 & q>AL

By finding the roots of characteristic equation, ω_0' can be given as:

$\omega'_{01,2} = \left[\sqrt{q - AL}\right]^{1/\alpha}$.

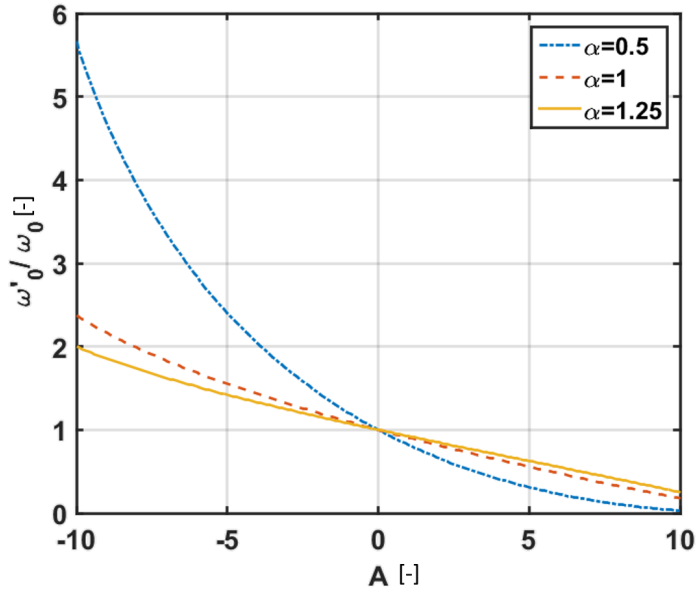

(a)

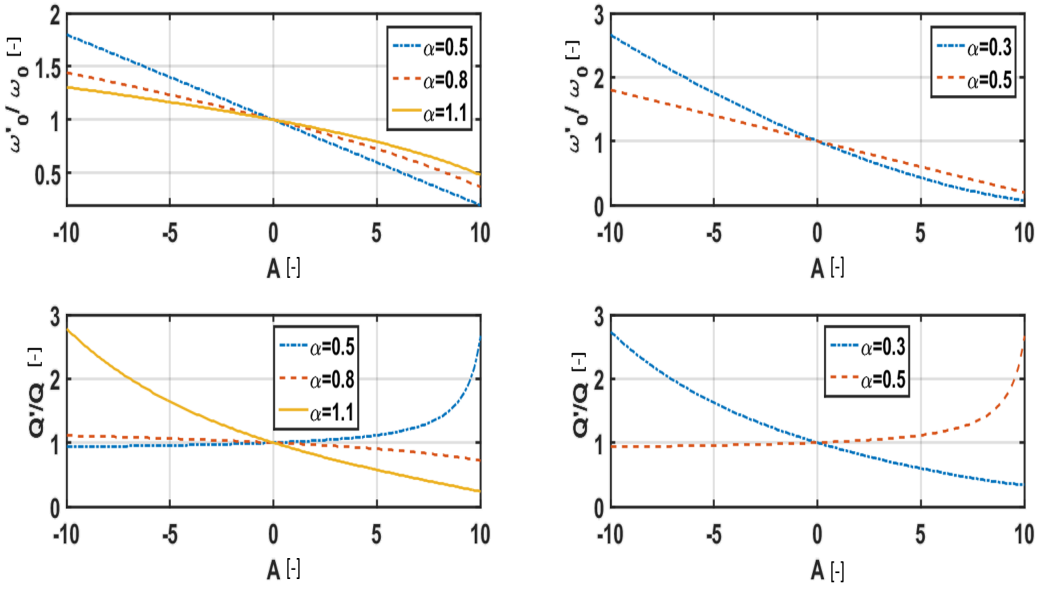

(b) (c)

Figure 4.2: Variation of ω_0'/ω_0 for case-1 and ω_0'/ω_0 & Q'/Q for case-2 and case-3 as a function of gain A for FLPF as feedback signal (a) Case-1 (b) Case-2 (c) Case-3

The ω_0' varies with the external amplifier's gain A. For this case of stability the value of $\delta = cos^{-1}\left[\frac{-p}{\sqrt{(q-AL)}}\right] < \frac{\pi}{2}$, which leads to variable Q' with external amplifier's gain A.

Figure 4.2 (a) shows variation of ω_0'/ω_0 as a function of external amplifier's gain A for three values of α for case-1 of stability with p, q and L are taken as 7, 25 and 2 respectively.

In Figs. 4.2 (b) and (c), the variation of ω_0'/ω_0 and Q'/Q with respect to external amplifier's gain A for case-2 and case-3 of stabilty are presented respectively. The respective values of q and L are taken as 25 and 2 with p=1.3 for case-2 and -1.3 for case-3. For these particular values of p, q and L, α<1.12 for case-2 of stabilty and α<0.6 for case-3 of stabilty to make shadow FOF stable.

For all the three cases of stability, the ω_0' is lower than ω_0 (pole frequency of basic 2α FOF) for positive values of A, while it will be greater than ω_0 for negative values of A.

The variation of Q' is different for various cases of stability. For case-1: Q' is fixed for a particular value of α. For case-2: for lower values of α, Q' is greater than Q for positive values of A, while the variation in Q' is very negligible for negative values A. As α approaches the maximum value for the stability of shadow FOF, the Q' becomes lower than Q for positive values of A and greater than Q for negative values of A. Further for case-3: for lower values of α, Q' is lower than Q for positive values of A, while it is greater than Q for negative values A. As α approaches the maximum value for the stability of shadow FOF, Q' is greater than Q for positive A, while the variation in Q' is very negligible for negative values A.

4.4.2 FHPF as Feedback Signal

In the case of a high-pass feedback signal ($H \neq 0,\ B{=}0,\ L{=}0$), the characteristic equation of $T'(s)$ is given by:

$$s^{2\alpha} + \frac{2p}{1-AH}s^{\alpha} + \frac{q}{1-AH} = 0 \tag{4.10}$$

The constraint on A to make the shadow FOF feasible is $A{<}\frac{1}{H}$ for all the three cases. The three cases of stability for FHPF feedback signal are discussed below:

Case-1: $p^2 \geq q(1-AH)$ & $p{>}0$ & $q{>}0$

By finding the roots of characteristic equation, ω_0' can be given as:

$\omega'_{01,2} = \left[\frac{1}{(1-AH)}\left(-p \pm \sqrt{p^2 - q(1-AH)}\right)\right]^{1/\alpha}$.

The ω_0' varies with the external amplifier's gain A. For this case of stability the value of δ must be equal to π, and α must be less than 2. Thus, for a particular value of α the Q' is constant.

Case-2: $p^2{<}q(1-AH)$ & $p{>}0$ & $q{>}0$

The roots of characteristic equation give ω_0', and can be expressed as:

$\omega'_{01,2} = \left[\sqrt{\frac{q}{1-AH}}\right]^{1/\alpha}$.

The ω_0' varies with the external amplifier's gain A. For this case of stability the value of $\delta{=}cos^{-1}\left[\frac{-p}{\sqrt{q(1-AH)}}\right] {>} \frac{\pi}{2}$, which leads to variable Q' with external amplifier's gain A.

Case-3: $4p^2{<}q(1-AH)$ & $p{<}0$ & $q{>}0$

By finding the roots of characteristic equation, ω_0' can be given as:

$\omega'_{01,2} = \left[\sqrt{\frac{q}{1-AH}}\right]^{1/\alpha}$.

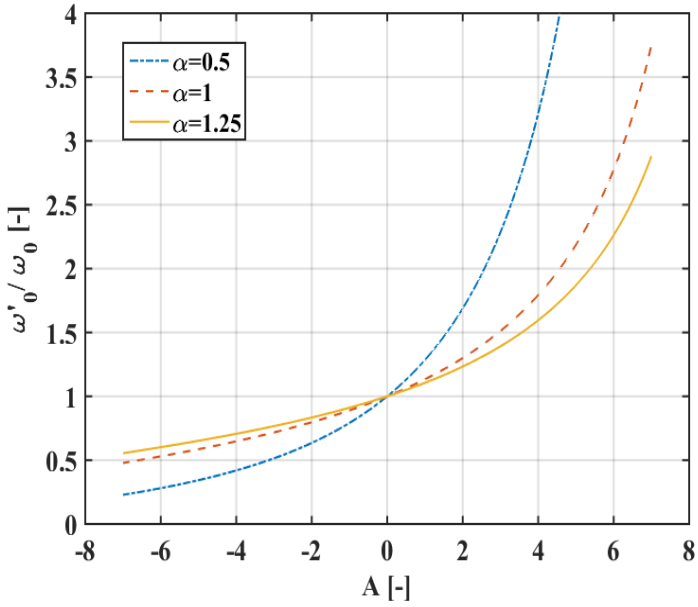

(a)

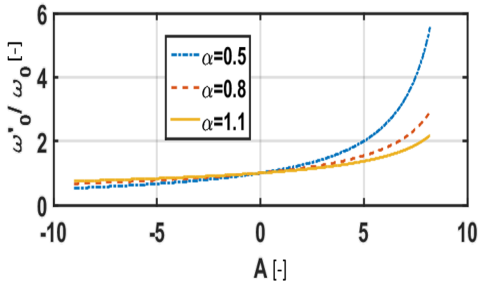

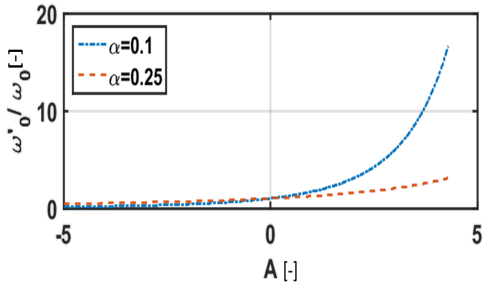

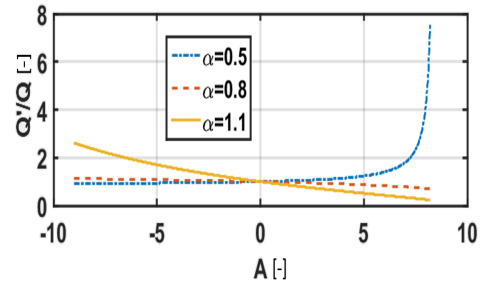

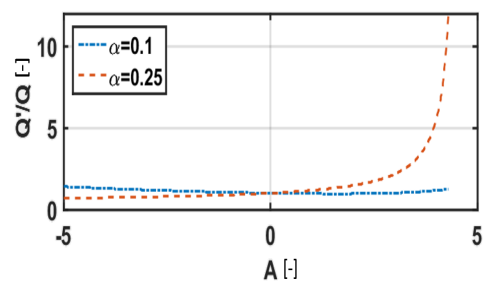

(b) (c)

Figure 4.3: Variation of ω_0'/ω_0 for case-1 and ω_0'/ω_0 & Q'/Q for case-2 and case-3 as a function of gain A for FHPF as feedback signal (a) Case-1 (b) Case-2 (c) Case-3

The ω_0' varies with the external amplifier's gain A. For this case of stability the value of $\delta = cos^{-1}\left[\frac{-p}{\sqrt{q(1-AH)}}\right] < \frac{\pi}{2}$, which leads to variable Q' with external amplifier's gain A.

Figure 4.3 (a) shows variation of ω_0'/ω_0 as a function of external amplifier's gain A for case-1 of stability for three values of α. Values of p, q and H are taken as 2, 2 and 0.1 respectively.

In Figs. 4.3 (b) and (c), the variation of ω_0'/ω_0 and Q'/Q with respect to external amplifier's gain A for case-2 and case-3 of stabilty are presented, respectively. The respective values of q and H are taken as 2 and 0.1 with p=0.4 for case-2 of stability and -0.4 for case-3 of stability. For these particular values of p, q and H, to make shadow FOF stable, α<1.13 for case-2 of stabilty and α<0.29 for case-3 of stabilty. For all the three cases of stability, the ω_0' is lower than ω_0 for negative values of A, while it will be greater than ω_0 for positive values of A.

The variation of Q' is different for various cases of stability. For case-1: Q' is fixed for a particular value of α. For case-2: for lower values of α, the value of Q' is close to Q for negative values A, while Q' is greater than Q for positive values of A. As α approaches the maximum value for the stability of shadow FOF, the Q' becomes lower than Q for positive values of A and greater than Q for negative values of A. Further for case-3: As α approaches the minimum value for the stability of shadow FOF, the Q' becomes greater than Q for positive values of A and lower than Q for negative values of A, while for higher values of α, the variation of Q' is reversed i.e., Q' becomes lower than Q for positive values of A and greater than Q for negative values of A.

4.4.3 FBPF as Feedback Signal

In the case of a band-pass feedback signal (H=0, $B \neq 0$, L=0), the characteristic equation of $T'(s)$ is given by:

$$s^{2\alpha} + (2p - AB)s^{\alpha} + q = 0 \tag{4.11}$$

The three cases of stability for FBPF feedback signal are discussed below:

Case-1: $(2p - AB)^2 \geq 4q$ & $p > \frac{AB}{2}$ & $q > 0$

By finding the roots of characteristic equation, ω_0' can be given as:

$\omega'_{01,2} = \left[\left(\frac{2p-AB}{2}\right)\left(-1 \pm \sqrt{1 - \frac{4q}{(2p-AB)^2}}\right)\right]^{1/\alpha}$.

The ω_0' varies with the external amplifier's gain A. For this case of stability the value of δ must be equal to π, and α must be less than 2. Thus, for a particular value of α the Q' is constant.

Case-2: $(2p - AB)^2 < 4q$ & $p > \frac{AB}{2}$ & $q > 0$

The roots of characteristic equation give ω_0', and can be expressed as:

$\omega'_{01,2} = \left(\sqrt{q}\right)^{1/\alpha}$.

The ω_0' varies with the external amplifier's gain A. For this case of stability the value of $\delta = \arccos\left[\frac{-(2p-AB)}{2\sqrt{q}}\right] > \frac{\pi}{2}$, which leads to variable Q' with external amplifier's gain A.

Case-3: $(2p - AB)^2 < 4q$ & $p < \frac{AB}{2}$ & $q > 0$

By finding the roots of characteristic equation, ω_0' can be given as:

$\omega'_{01,2} = \left(\sqrt{q}\right)^{1/\alpha}$.

The ω_0' varies with the external amplifier's gain A. For this case of stability

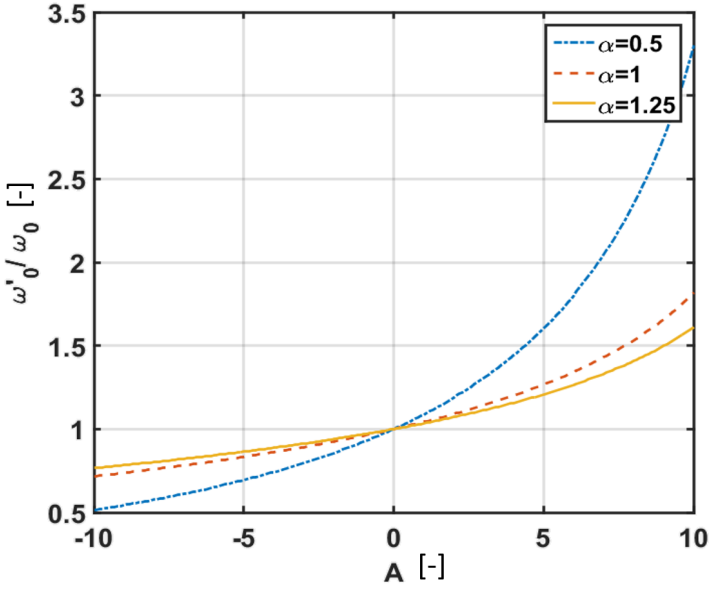

(a)

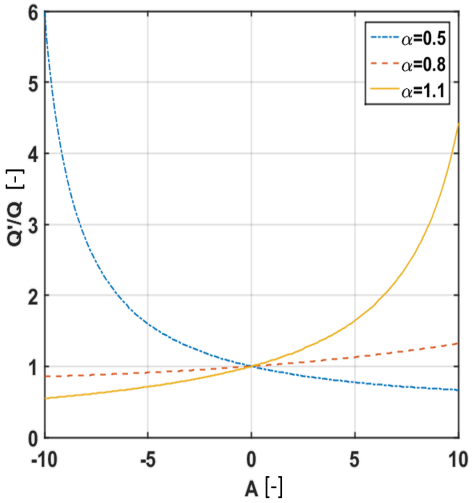

(b)

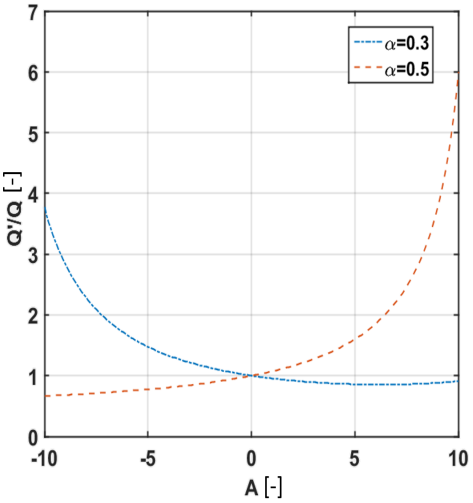

(c)

Figure 4.4: Variation of ω_0'/ω_0 for case-1 and Q'/Q for case-2 and case-3 as a function of gain A for FBPF as feedback signal (a) Case-1 (b) Case-2 (c) Case-3

the value of $\delta = \arccos\left[\frac{-(2p-AB)}{2\sqrt{q}}\right] < \frac{\pi}{2}$, which leads to variable Q' with external amplifier's gain A.

Figure 4.4 (a) shows variation of ω_0'/ω_0 as a function of external amplifier's gain A for case-1 of stability for three values of α. Values of p, q and B are taken

as 3, 3 and 0.2 respectively.

In Figs. 4.4 (b) and (c), the variation of ω_0'/ω_0 with respect to external amplifier's gain A for case-2 and case-3 of stabilty are presented, respectively. The respective values of q and B are taken as 20 and 0.2 with p=2 for case-2 of stability and -2 for case-3 of stability. For these particular values of p, q and B, to make shadow FOF stable, α<1.29 for case-2 of stabilty and α<0.53 for case-3 of stabilty.

For cases-1 of stability, ω_0' is lower than ω_0 for negative values of A, while it will be greater than ω_0 for positive values of A. For case-2 and case-3 of stability, the ω_0' is fixed for a particular value of α.

The variation of Q' is different for various cases of stability. For case-1: Q' is fixed for a particular value of α. While for case-2 and case-3 of stability, for lower values of α the value of Q' is lower than Q for positive values of A and it is greater than Q for negative values of A, as the maximum value of α is approached this trend is reversed, now Q' is greater than Q for positive values of A and it is lower than Q for negative values of A.

4.4.4 FBSF as Feedback Signal

In the case of a band-stop feedback signal ($H \neq 0,\ B$=0, $\ L \neq 0$), the characteristic equation of $T'(s)$ is given by:

$$s^{2\alpha} + \frac{2p}{1-AH}s^{\alpha} + \frac{q-AL}{1-AH} = 0 \tag{4.12}$$

The three cases of stability for FBSF feedback signal are discussed below:

Case-1: $p^2 \geq (q - AL)(1 - AH)$ & $p>0$ & $q>AL$

By finding the roots of characteristic equation, ω_0' can be given as:

$\omega'_{01,2} = \left[\frac{1}{(1-AH)}\left(-p \pm \sqrt{p^2 - (q - AL)(1 - AH)}\right)\right]^{1/\alpha}$.

The ω_0' varies with the external amplifier's gain A. For this case of stability the value of δ must be equal to π, and α must be less than 2. Thus, for a particular value of α the Q' is constant.

Case-2: $p^2<(q - AL)(1 - AH)$ & $p>0$ & $q>AL$

The roots of characteristic equation give ω_0', and can be expressed as:

$\omega'_{01,2} = \left[\sqrt{\frac{q-AL}{1-AH}}\right]^{1/\alpha}$.

The ω_0' varies with the external amplifier's gain A. For this case of stability the value of $\delta = \arccos\left[\frac{-p}{\sqrt{(q-AL)(1-AH)}}\right] > \frac{\pi}{2}$, which leads to variable Q' with external amplifier's gain A.

Case-3: $p^2<(q - AL)(1 - AH)$ & $p<0$ & $q>AL$

By finding the roots of characteristic equation, ω_0' can be given as:

$\omega'_{01,2} = \left[\sqrt{\frac{q-AL}{1-AH}}\right]^{1/\alpha}$.

The ω_0' varies with the external amplifier's gain A. For this case of stability the value of $\delta = \arccos\left[\frac{-p}{\sqrt{(q-AL)(1-AH)}}\right] < \frac{\pi}{2}$, which leads to variable Q' with external amplifier's gain A.

Figure 4.5 (a) shows variation of ω_0'/ω_0 as a function of external amplifier's gain A for case-1 of stability for three values of α. Values of p, q, L and H are taken as 20, 20, 2 and 0.1 respectively.

In Figs. 4.5 (b) and (c), the variation of ω_0'/ω_0 and Q'/Q with respect to external

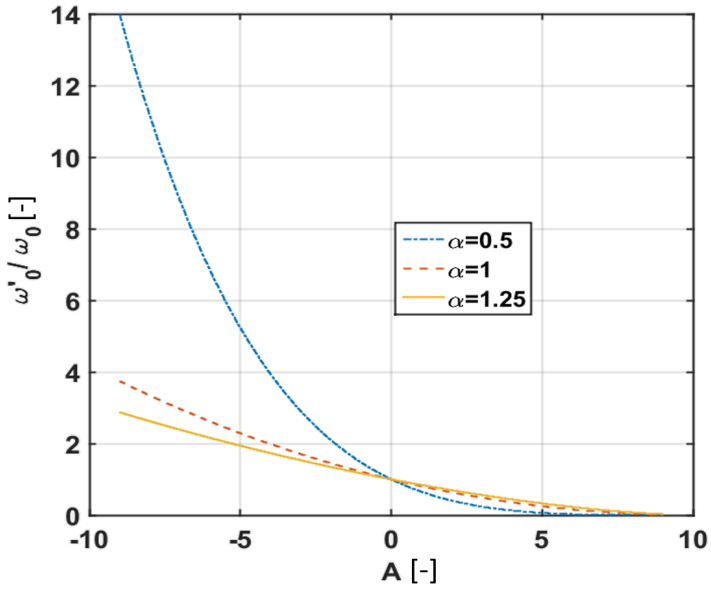

(a)

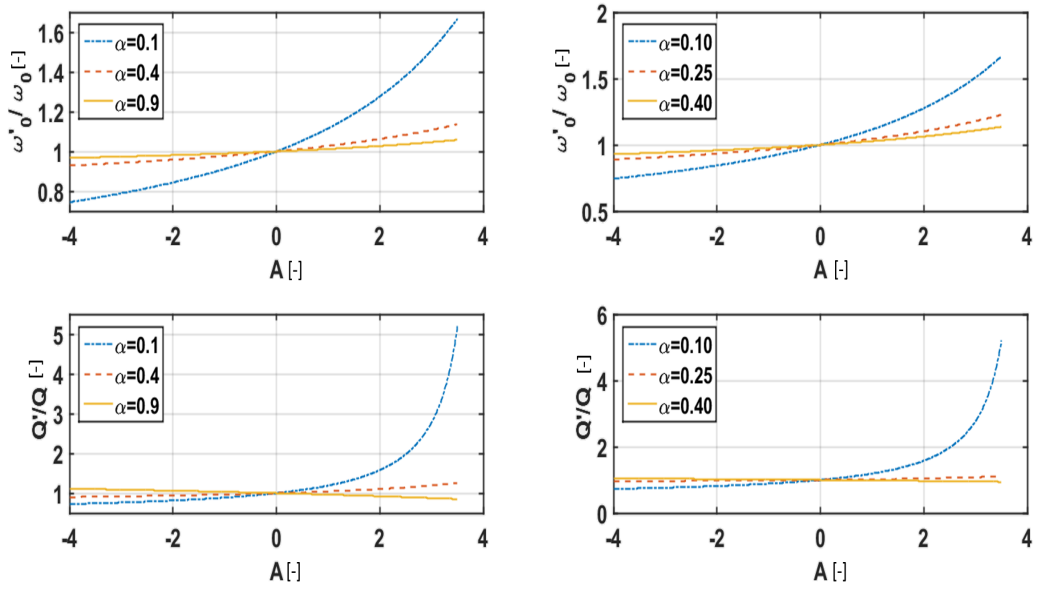

(b) (c)

Figure 4.5: Variation of ω_0'/ω_0 for case-1 and ω_0'/ω_0 & Q'/Q for case-2 and case-3 as a function of gain A for FBSF as feedback signal (a) Case-1 (b) Case-2 (c) Case-3

amplifier's gain A for case-2 and case-3 of stabilty are presented, respectively. The respective values of q, L and H are taken as 25, 2 and 0.1 with p=0.5 for case-2 of stability and -0.5 for case-3 of stability. For these particular values of p, q, L and

H, to make shadow FOF stable, α<1 for case-2 of stabilty and α<0.49 for case-3 of stabilty.

For case-1 of stabillity, ω_0' is lower than ω_0 for positive values of A and it is greater than ω_0 for negative values of A. Although for case-2 and case-3 of stability the variation in ω_0' is reversed, i.e., it is greater than ω_0 for positive values of A and it is lower than ω_0 for negative values of A.

The variation of Q' is different for various cases of stability. For case-1: Q' is fixed for a particular value of α. For case-2 and case-3 of stability: for lower values of α with positive values of A the variation is more but as α approaches its maximum value for the stability of shadow FOF, the variation in Q' is very negligible. Further, for negative values of A, the variation in Q' is very negligible for all values of α.

The various cases of stability are summarized in Table 4.3 based on each case of feedback signal. Table 4.3 also enlistes the gain (E', F' or G'), pole frequency ω_0' and pole quality factor $\left[Q' = -\frac{1}{2\cos\delta/\alpha}\right]$.

4.5 Verification of Proposed Theory

The proposed theory of shadow filters in fractional domain has been verified using two active 2α-order FOFs. Both circuits are discussed in the following subsections.

Table 4.3: Different cases of stability for $T'(s)$ for various feedback signals

Feedback Signal ($T_1(s)$)	Gain (E', F' or G')	Case-1 ($X^2 \geq$ Y, X>0, Y>0)	Case-2 ($X^2 <$Y, X>0, Y>0)	Case-3 ($X^2 <$Y, X<0, Y>0)
FLPF	$E,\ F$ *or* G	$\omega'_{01,2}=\left[-p \pm \sqrt{p^2-(q-AL)}\right]^{1/\alpha}$ $\delta=\pi, \alpha<2$	$\omega'_{01,2}=\left[\sqrt{q-AL}\right]^{1/\alpha}$ $\delta=\arccos\left[\frac{-p}{\sqrt{(q-AL)}}\right]>\frac{\pi}{2}$	$\omega'_{01,2}=\left[\sqrt{q-AL}\right]^{1/\alpha}$ $\delta=\arccos\left[\frac{-p}{\sqrt{(q-AL)}}\right]<\frac{\pi}{2}$
FHPF	$\frac{E,\ F\ or\ G}{(1-AH)}$	$\omega'_{01,2}=\left[\frac{1}{(1-AH)}\left(-p \pm \sqrt{p^2-q(1-AH)}\right)\right]^{1/\alpha}$ $\delta=\pi, \alpha<2$	$\omega'_{01,2}=\left[\sqrt{\frac{q}{1-AH}}\right]^{1/\alpha}$ $\delta=\arccos\left[\frac{-p}{\sqrt{q(1-AH)}}\right]>\frac{\pi}{2}$	$\omega'_{01,2}=\left[\sqrt{\frac{q}{1-AH}}\right]^{1/\alpha}$ $\delta=\arccos\left[\frac{-p}{\sqrt{q(1-AH)}}\right]<\frac{\pi}{2}$
FBPF	$E,\ F$ *or* G	$\omega'_{01,2}=\left[\left(\frac{2p-AB}{2}\right)\left(-1 \pm \sqrt{1-\frac{4q}{(2p-AB)^2}}\right)\right]^{1/\alpha}$ $\delta=\pi, \alpha<2$	$\omega'_{01,2}=\left(\sqrt{q}\right)^{1/\alpha}$ $\delta=\arccos\left[\frac{-(2p-AB)}{2\sqrt{q}}\right]>\frac{\pi}{2}$	$\omega'_{01,2}=\left(\sqrt{q}\right)^{1/\alpha}$ $\delta=\arccos\left[\frac{-(2p-AB)}{2\sqrt{q}}\right]<\frac{\pi}{2}$
FBSF	$\frac{E,\ F\ or\ G}{(1-AH)}$	$\omega'_{01,2}=\left[\frac{1}{(1-AH)}\left(-p \pm \sqrt{p^2-(q-AL)(1-AH)}\right)\right]^{1/\alpha}$ $\delta=\pi, \alpha<2$	$\omega'_{01,2}=\left[\sqrt{\frac{q-AL}{1-AH}}\right]^{1/\alpha}$ $\delta=\arccos\left[\frac{-p}{\sqrt{(q-AL)(1-AH)}}\right]>\frac{\pi}{2}$	$\omega'_{01,2}=\left[\sqrt{\frac{q-AL}{1-AH}}\right]^{1/\alpha}$ $\delta=\arccos\left[\frac{-p}{\sqrt{(q-AL)(1-AH)}}\right]<\frac{\pi}{2}$

4.5.1 Proposed Shadow FOF Circuit I

The proposed shadow FOF circuit I consists of $OTA_1 - OTA_4$ (basic 2α-order FOF) and $OTA_5 - OTA_7$ (external amplifier with gain A) is shown in Fig. 4.6. The basic 2α-order FOF contains three outputs, such as: FHPF, FLPF and FBPF. The transfer function of the basic 2α-order FOF is given by (4.13).

$$\frac{V(s)_{HP}}{V_i(s)} = \frac{s^{2\alpha}}{s^{2\alpha} + s^{\alpha}\frac{g_{m1}}{C_{\alpha1}} + \frac{g_{m1}g_{m2}}{C_{\alpha1}C_{\alpha2}}} \tag{4.13a}$$

$$\frac{V(s)_{LP}}{V_i(s)} = \frac{\frac{-g_{m1}g_{m2}}{C_{\alpha1}C_{\alpha2}}}{s^{2\alpha} + s^{\alpha}\frac{g_{m1}}{C_{\alpha1}} + \frac{g_{m1}g_{m2}}{C_{\alpha1}C_{\alpha2}}} \tag{4.13b}$$

$$\frac{V(s)_{BP}}{V_i(s)} = \frac{s^{\alpha}\frac{g_{m1}}{C_{\alpha1}}}{s^{2\alpha} + s^{\alpha}\frac{g_{m1}}{C_{\alpha1}} + \frac{g_{m1}g_{m2}}{C_{\alpha1}C_{\alpha2}}} \tag{4.13c}$$

Any of the available outputs can drive the external amplifier. As per the type of feedback signal given to the external amplifier (i.e., FHPF, FLPF or FBPF), there will be three types of output responses of shadow FOF. The FHPF, FLPF and FBPF output responses of shadow FOF for FHPF, FLPF and FBPF feedback signals are given in (4.14), (4.15) and (4.16) respectively, here A is the gain of the external amplifier. When the feedback signal is given at the $'p'$ terminal of the OTA_5, the gain A is equal to $\frac{g_{mb}}{g_{ma}}$; to achieve negative polarity of gain A the feedback signal must be given at the $'n'$ terminal of the OTA_5.

$$T(s)_{HP\_HP} = \frac{V(s)_{HP\_HP}}{V_{in}(s)} = \frac{s^{2\alpha}}{s^{2\alpha} + s^{\alpha}\frac{g_{m1}}{(1-A)C_{\alpha1}} + \frac{g_{m1}g_{m2}}{(1-A)C_{\alpha1}C_{\alpha2}}} \tag{4.14a}$$

$$T(s)_{LP\_HP} = \frac{V(s)_{LP\_HP}}{V_{in}(s)} = \frac{\frac{-g_{m1}g_{m2}}{C_{\alpha1}C_{\alpha2}}}{s^{2\alpha} + s^{\alpha}\frac{g_{m1}}{(1-A)C_{\alpha1}} + \frac{g_{m1}g_{m2}}{(1-A)C_{\alpha1}C_{\alpha2}}} \tag{4.14b}$$

$$T(s)_{BP\_HP} = \frac{V(s)_{BP\_HP}}{V_{in}(s)} = \frac{s^{\alpha}\frac{g_{m1}}{C_{\alpha1}}}{s^{2\alpha} + s^{\alpha}\frac{g_{m1}}{(1-A)C_{\alpha1}} + \frac{g_{m1}g_{m2}}{(1-A)C_{\alpha1}C_{\alpha2}}} \tag{4.14c}$$

$$T(s)_{HP\_LP} = \frac{V(s)_{HP\_LP}}{V_{in}(s)} = \frac{s^{2\alpha}}{s^{2\alpha} + s^{\alpha}\frac{g_{m1}}{C_{\alpha1}} + \frac{(1-A)g_{m1}g_{m2}}{C_{\alpha1}C_{\alpha2}}} \tag{4.15a}$$

$$T(s)_{LP\_LP} = \frac{V(s)_{LP\_LP}}{V_{in}(s)} = \frac{\frac{-g_{m1}g_{m2}}{C_{\alpha1}C_{\alpha2}}}{s^{2\alpha} + s^{\alpha}\frac{g_{m1}}{C_{\alpha1}} + \frac{(1-A)g_{m1}g_{m2}}{C_{\alpha1}C_{\alpha2}}} \tag{4.15b}$$

$$T(s)_{BP\_LP} = \frac{V(s)_{BP\_LP}}{V_{in}(s)} = \frac{s^{\alpha}\frac{g_{m1}}{C_{\alpha1}}}{s^{2\alpha} + s^{\alpha}\frac{g_{m1}}{C_{\alpha1}} + \frac{(1-A)g_{m1}g_{m2}}{C_{\alpha1}C_{\alpha2}}} \tag{4.15c}$$

$$T(s)_{HP\_BP} = \frac{V(s)_{HP\_BP}}{V_{in}(s)} = \frac{s^{2\alpha}}{s^{2\alpha} + s^{\alpha}\frac{(1-A)g_{m1}}{C_{\alpha1}} + \frac{g_{m1}g_{m2}}{C_{\alpha1}C_{\alpha2}}} \tag{4.16a}$$

$$T(s)_{LP\_BP} = \frac{V(s)_{LP\_BP}}{V_{in}(s)} = \frac{\frac{-g_{m1}g_{m2}}{C_{\alpha1}C_{\alpha2}}}{s^{2\alpha} + s^{\alpha}\frac{(1-A)g_{m1}}{C_{\alpha1}} + \frac{g_{m1}g_{m2}}{C_{\alpha1}C_{\alpha2}}} \tag{4.16b}$$

$$T(s)_{BP\_BP} = \frac{V(s)_{BP\_BP}}{V_{in}(s)} = \frac{s^{\alpha}\frac{g_{m1}}{C_{\alpha1}}}{s^{2\alpha} + s^{\alpha}\frac{(1-A)g_{m1}}{C_{\alpha1}} + \frac{g_{m1}g_{m2}}{C_{\alpha1}C_{\alpha2}}} \tag{4.16c}$$

There can be total nine possible combinations for different feedback signals and the cases of stability, such as case-1, 2 and 3 of stability for FHPF feedback signal; case-1, 2 and 3 of stability for FLPF feedback signal and case-1, 2 and 3 of stability for FBPF feedback signal. Three cases are chosen to present here; case-1 for FHPF feedback signal (Variable ω_0', fixed Q'), case-2 for FLPF feedback signal (Variable ω_0', variable Q') and case-3 for FBPF feedback (Fixed ω_0', variable Q'). By using the method outlined for stability constraints for various feedback signals in Sect. 4.4, the values of g_{m1}, g_{m2} and A are calculated. The constraint on g_ms and A,

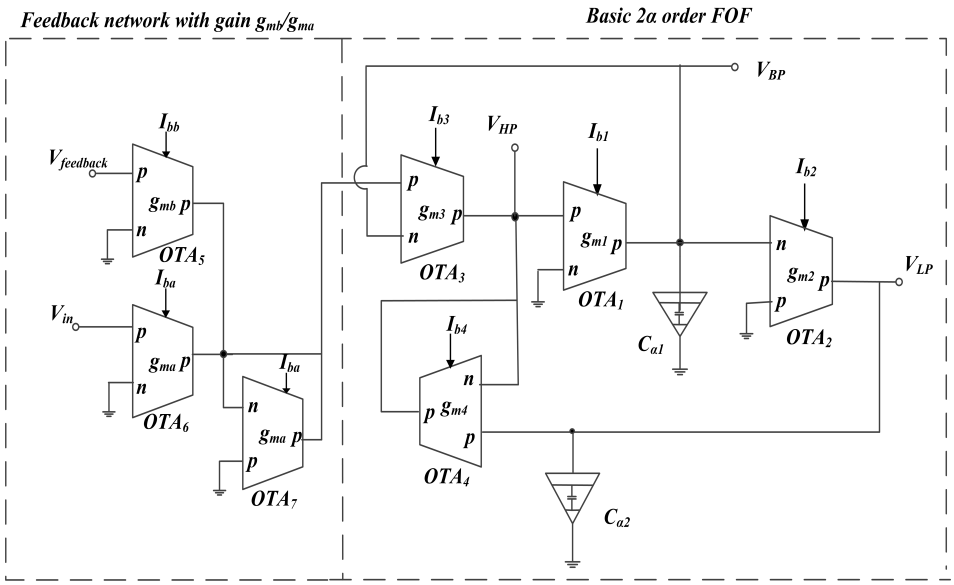

Figure 4.6: Circuit diagram of proposed shadow FOF circuit I

and the effect on ω_0' and Q' for various cases are given in Table 4.4.

Table 4.4: Constraints on g_m & A and effect on ω_0' & Q' for different cases of stability

Feedback signal	Stability case	Constraint on g_m	Constraint on A	Effect on ω_0' and Q'
FHPF	Case-1	$g_{m1} \geq 4(1-A)g_{m2}$	$A < 1$	Variable ω_0', fixed Q'
FLPF	Case-2	$g_{m1} < 4(1-A)g_{m2}$	$A < 1$	Variable ω_0', variable Q'
FBPF	Case-3	$(1-A)^2 g_{m1} < 4g_{m2}$	$A > 1$	Fixed ω_0', variable Q'

4.5.1.1 Simulation results

To illustrate the functionality of the proposed shadow FOF circuit I, SPICE simulations have been performed with 180 nm CMOS technology model parameters. Section 2.4 provides the details of the transistors used in OTA, and its corresponding CMOS schematic is illustrated in Fig. 2.8 (b). The proposed shadow FOF circuit I uses FOC, which is approximated via 12^{th} order R-C ladder network based on

CFE approximation [35]. The schematic of the R-C ladder network is depicted in Fig. 4.7. The values of $C_{\alpha 1}$ and $C_{\alpha 2}$, for all the three cases, are taken same and equal to 3.75 $\mu\mho sec^{\alpha}$ with α=0.5. The values of R_0, R_i and C_i (i=1, 2, ...11) to emulate FOC with α=0.5 and C_{α}=3.75 $\mu\mho sec^{\alpha}$ can be referred from Sect. 3.3.1. The FBPF output response of proposed shadow FOF circuit I has been considered to verify the effect of each feedback signal on ω_0' and Q'.

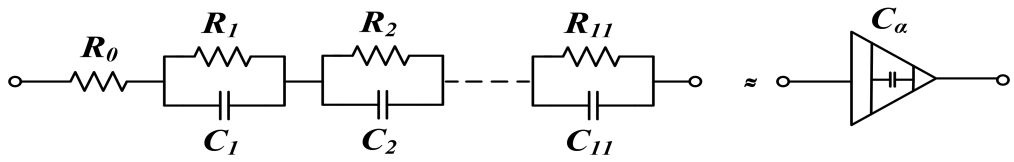

Figure 4.7: 12^{th} order R-C ladder network (based on CFE approximation) realizing FOC

To realize case-1 for FHPF feedback signal, the values of g_{m1} and g_{m2} are taken as 534 $\mu A/V$ and 55 $\mu A/V$ respectively, while the values of g_{m3} and g_{m4} are taken same and equal to 272 $\mu A/V$. The gain A of the external amplifier is set as -0.64, -1, and -1.62 by adjusting the values of g_{ma} and g_{mb}. The magnitude response of $T(s)_{BP\_HP}$ is shown in Fig. 4.8 (a) and it is observed that the value of Q' is fixed at 0.085 for all the three values of A while the ω_0' is variable with A.

Further, to realize case-2 of FLPF feedback signal and case-3 of FBPF feedback signal, the values of g_{m1} and g_{m2} are as 376.50 $\mu A/V$ and the values of g_{m3} and g_{m4} are taken as 272 $\mu A/V$. The gain A of the external amplifier is set as -1.16, -2, -3.76, and -6.21 for the case-2 of FLPF feedback signal, while for case-3 of FBPF feedback signal, it is set as 1.62, 2, 2.12, and 2.45. The magnitude responses of $T(s)_{BP\_LP}$ and $T(s)_{BP\_BP}$ are shown in Figs. 4.8 (b) and (c) respectively. It is observed from the figures that for case-2 of FLPF feedback signal, ω_0' and Q' both

are variable with A, while for case-3 of FBPF feedback signal the ω_0' is constant at 1.50 kHz for all the four values of A while Q' is variable with A.

Table 4.5 consists of the values of pole frequency in Hertz (f_0'=$\omega_0'/2\pi$) and Q' with respect to the external amplifier's gain A, for each case of feedback signal. It is observed from the Table 4.5 and above discussion that for case-1 of FHPF feedback signal the ω_0' is variable with fixed Q' while for case-2 of FLPF feedback signal the ω_0' and Q' both are variable. For case-3 of FBPF feedback signal the ω_0' is fixed with variable Q' which corroborates with the theory proposed in Sect. 4.3.

Table 4.5: Summarized simulation results for proposed shadow FOF circuit I

FHPF feedback signal (case-1)			FLPF feedback signal (case-2)			FBPF feedback signal (case-3)		
A	Q'	f_0'	A	Q'	f_0'	A	Q'	f_0'
-0.64	0.085	116.4 Hz	-1.16	0.22	2.75 kHz	1.62	0.36	1.50 kHz
-1.00	0.085	89.1 Hz	-2.00	0.23	3.45 kHz	2.00	0.69	1.50 kHz
-1.62	0.085	71.3 Hz	-3.76	0.25	5.45 kHz	2.12	1.39	1.50 kHz
-	-	-	-6.21	0.29	8.80 kHz	2.45	2.18	1.50 kHz

In addition, to analyse the linearity of proposed shadow FOF circuit I, total harmonic distortion (THD) has been simulated for $A=-1.62$ for FHPF feedback signal (case-1), $A=-2$ for FLPF feedback signal (case-2) and A=2 for FBPF feedback signal (case-3) using same simulation settings. The variation in THD (in %) as a function of input signal amplitude is plotted in Fig. 4.9. For this a sinusoidal signal V_{in} with varying magnitude is applied at the input of the proposed shadow FOF circuit I for all the three cases. It is observed that for input signal $< 60mV$ the maximum THD remains under 3.5% for FHPF feedback case while it remains under 2% for FLPF and FBPF feedback cases.

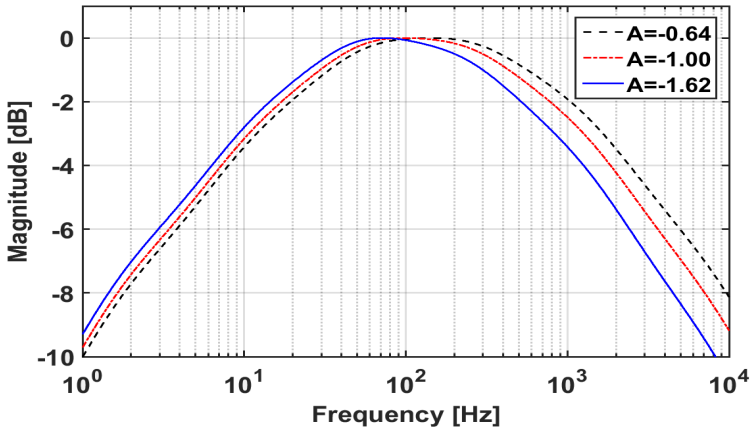

(a)

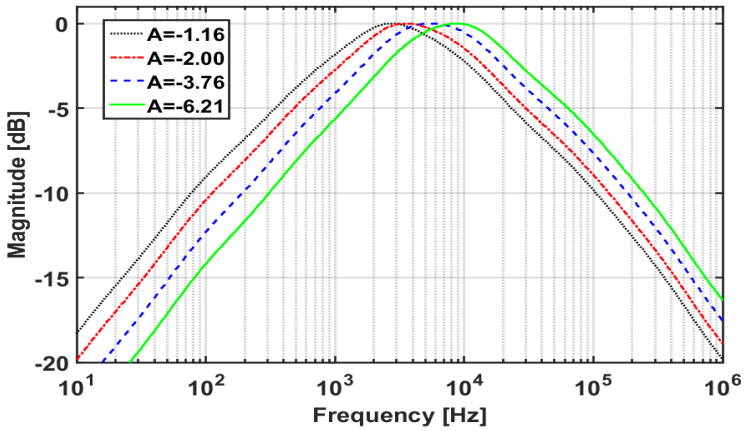

(b)

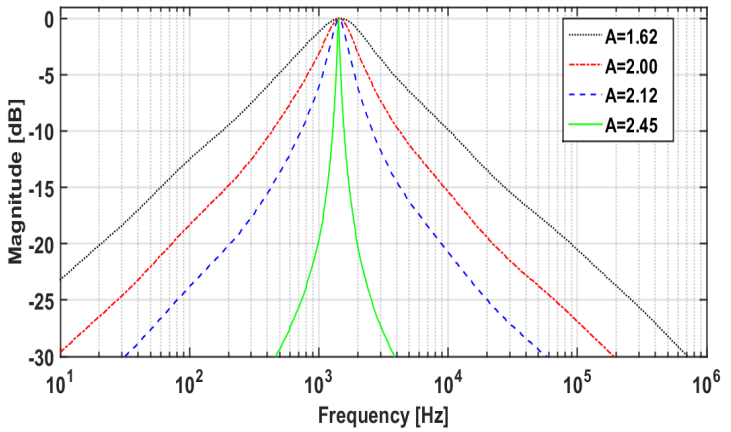

(c)

Figure 4.8: Proposed shadow FOF circuit I; FBPF Magnitude response for various A and feedback signal as (a) FHPF (case-1) (b) FLPF (case-2) (c) FBPF (case-3)

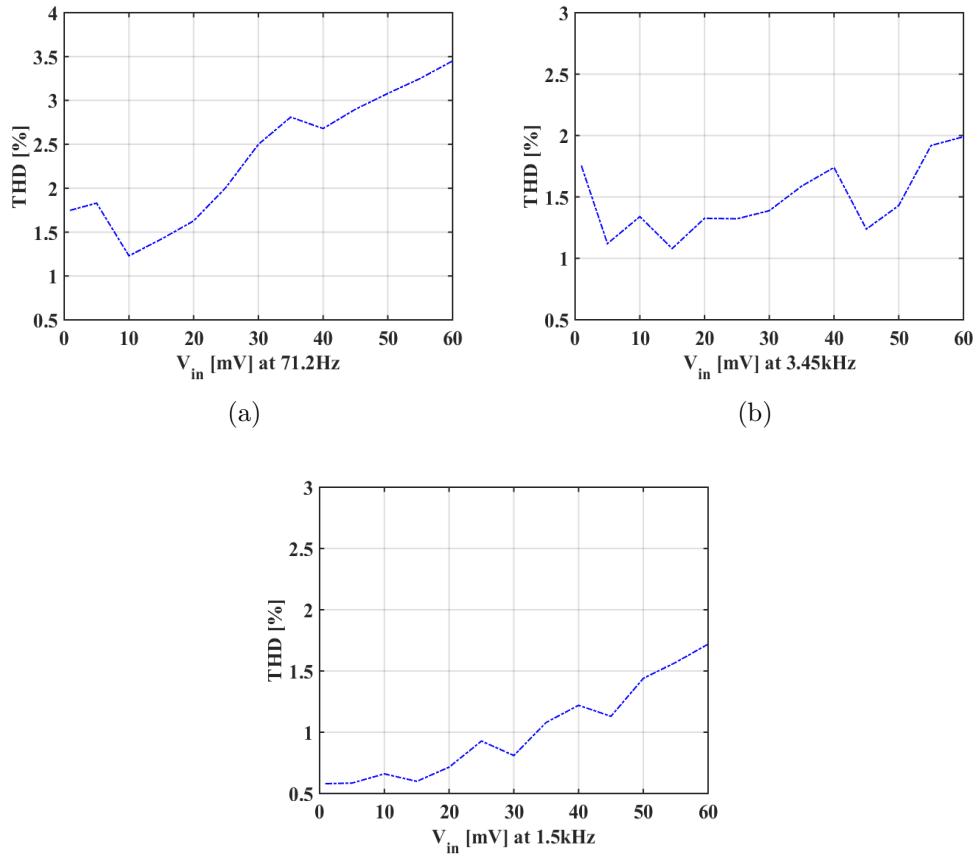

Figure 4.9: THD vs V_{in} for shadow FOF for proposed Shadow FOF circuit I; for feedback signals as (a) FHPF (case-1, $A = -1.62$) (b) FLPF (case-2, $A = -2$) (c) FBPF (case-3, A=2)

4.5.1.2 Robustness

To examine the robustness of the proposed shadow FOF circuit I, corner analysis and Monte-Carlo analysis are done. The results of these analyses are discussed below.

Corner analysis

The outputs of the circuit may fluctuate due to random variations in process variables around their nominal values during the fabrication process. To evaluate the sensitivity of the output of the proposed shadow FOF circuit I to the random

variations that may occur during fabrication, the proposed circuit is examined at the five process corners i.e. FF, FS, TT, SF and SS for $A = -1.62$ for FHPF feedback signal (case-1), $A = -2$ for FLPF feedback signal (case-2) and A=2 for FBPF feedback signal (case-3)using same simulation settings. The magnitude response of FBPF is shown in Figs. 4.10 (a), (b) and (c) for FHPF feedback case-1 ($A = -1.62$), FLPF feedback case-2 ($A = -2$) and FBPF feedback case-3 (A=2) respectively for all the five corners. The absence of any sudden changes in the response confirms the reliability and stability of the proposed shadow FOF circuit I.

Monte-Carlo analysis

To get additional perception on the sensitivity of the proposed shadow FOF circuit I with respect to C_α, Monte-Carlo analysis is performed with uniform Gaussian distribution of passive components used to realize C_α with ±5% resistance and capacitance tolerances, on 500 random samples. The same simulation settings are taken with $A = -1.62$ for FHPF feedback signal (case-1), $A = -2$ for FLPF feedback signal (case-2) and A=2 for FBPF feedback signal (case-3). The distribution of ω_0' of FBPF response for 500 samples is shown in Figs. 4.11 (a), (b) and (c) for FHPF feedback case-1 ($A = -1.62$), FLPF feedback case-2 ($A = -2$) and FBPF feedback case-3 (A=2) respectively. The ω_0' for all the samples lies within a small range and the mean for all the three cases matched with the corresponding ω_0' within 3% error, this shows the validity of proposed shadow FOF's for the random variation in $C_\alpha's$ value.

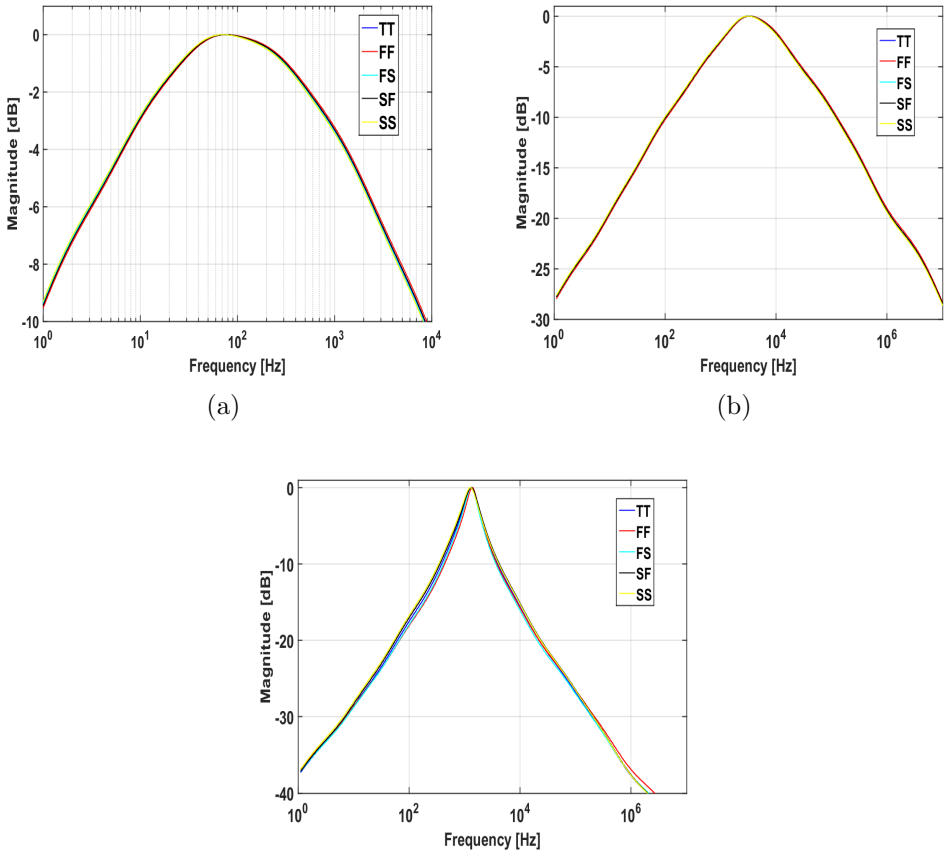

Figure 4.10: Corner analysis for proposed shadow FOF circuit I; FBPF response, for feedback signal as (a) FHPF (case-1, $A = -1.62$) (b) FLPF (case-2, $A = -2$) (c) FBPF (case-3, A=2)

4.5.2 Proposed Shadow FOF Circuit II

The proposed shadow FOF circuit II consists of $OTA_1 - OTA_3$ (basic 2α-order FOF) and $OTA_4 - OTA_6$ (external amplifier with gain A) is shown in Fig. 4.12. The basic 2α-order FOF contains two outputs, such as: FBPF and FLPF. The transfer function of the basic 2α-order FOF is given by (4.17).

$$\frac{V(s)_{LP}}{V_i(s)} = \frac{\frac{-g_{m1}g_{m3}}{C_{\alpha1}C_{\alpha2}}}{s^{2\alpha} + s^{\alpha}\frac{g_{m2}}{C_{\alpha1}} + \frac{g_{m2}g_{m3}}{C_{\alpha1}C_{\alpha2}}} \tag{4.17a}$$

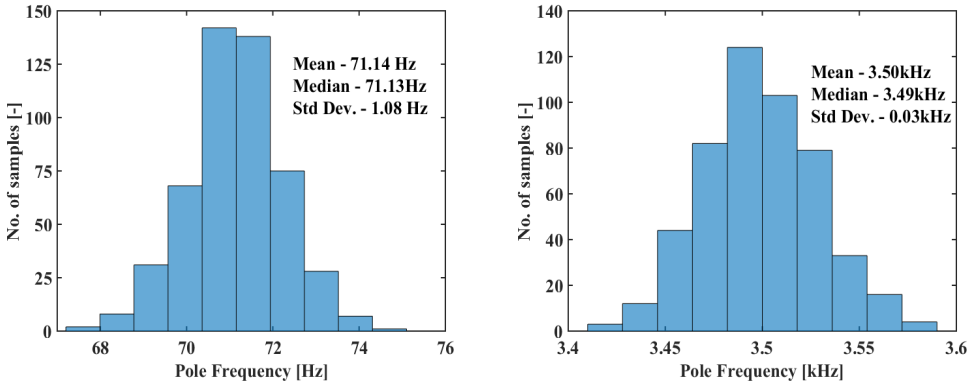

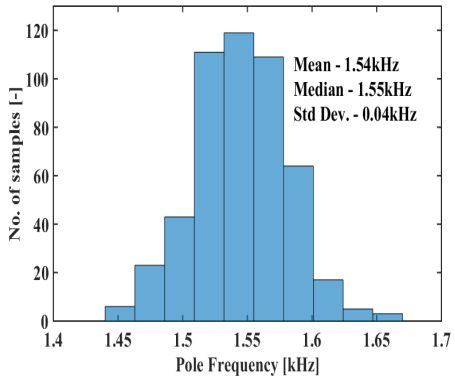

Figure 4.11: Monte Carlo Analysis for proposed shadow FOF circuit I for the random variations in C_α; for feedback signal as (a) FHPF (case-1, $A=-1.62$) (b) FLPF (case-2, $A=-2$) (c) FBPF (case-3, A=2)

$$\frac{V(s)_{BP}}{V_i(s)} = \frac{s^\alpha \frac{g_{m1}}{C_{\alpha1}}}{s^{2\alpha} + s^\alpha \frac{g_{m2}}{C_{\alpha1}} + \frac{g_{m2}g_{m3}}{C_{\alpha1}C_{\alpha2}}} \tag{4.17b}$$

Any of the available outputs can drive the external amplifier. As per the type of feedback signal (i.e. FLPF or FBPF), there will be two types of output responses of shadow FOF. The FLPF and FBPF output responses of the proposed shadow FOF circuit II for FLPF and FBPF feedback signals are given in (4.18) and (4.19), respectively, here A is the gain of the external amplifier. When the feedback signal is given at the $'p'$ terminal of the OTA_5, the gain A is equal to $\frac{g_{mb}}{g_{ma}}$; to achieve negative polarity of gain A the feedback signal must be given at the $'n'$ terminal

of the OTA_5.

$$T(s)_{LP\_LP} = \frac{V(s)_{LP\_LP}}{V_{in}(s)} = \frac{\frac{-g_{m1}g_{m3}}{C_{\alpha1}C_{\alpha2}}}{s^{2\alpha} + s^{\alpha}.\frac{g_{m2}}{C_{\alpha1}} + \frac{g_{m3}}{C_{\alpha1}C_{\alpha2}}(g_{m2} - A.g_{m1})} \tag{4.18a}$$

$$T(s)_{BP\_LP} = \frac{V(s)_{BP\_LP}}{V_{in}(s)} = \frac{s^{\alpha}.\frac{g_{m1}}{C_{\alpha1}}}{s^{2\alpha} + s^{\alpha}.\frac{g_{m2}}{C_{\alpha1}} + \frac{g_{m3}}{C_{\alpha1}C_{\alpha2}}(g_{m2} - A.g_{m1})} \tag{4.18b}$$

$$T(s)_{(LP)\_BP} = \frac{V(s)_{(LP)\_BP}}{V_{in}(s)} = \frac{\frac{-g_{m1}g_{m3}}{C_{\alpha1}C_{\alpha2}}}{s^{2\alpha} + s^{\alpha}.\frac{g_{m2} - A.g_{m1}}{C_{\alpha1}} + \frac{g_{m2}g_{m3}}{C_{\alpha1}C_{\alpha2}}} \tag{4.19a}$$

$$T(s)_{(BP)\_BP} = \frac{V(s)_{(BP)\_BP}}{V_{in}(s)} = \frac{s^{\alpha}.\frac{g_{m1}}{C_{\alpha1}}}{s^{2\alpha} + s^{\alpha}.\frac{g_{m2} - A.g_{m1}}{C_{\alpha1}} + \frac{g_{m2}g_{m3}}{C_{\alpha1}C_{\alpha2}}} \tag{4.19b}$$

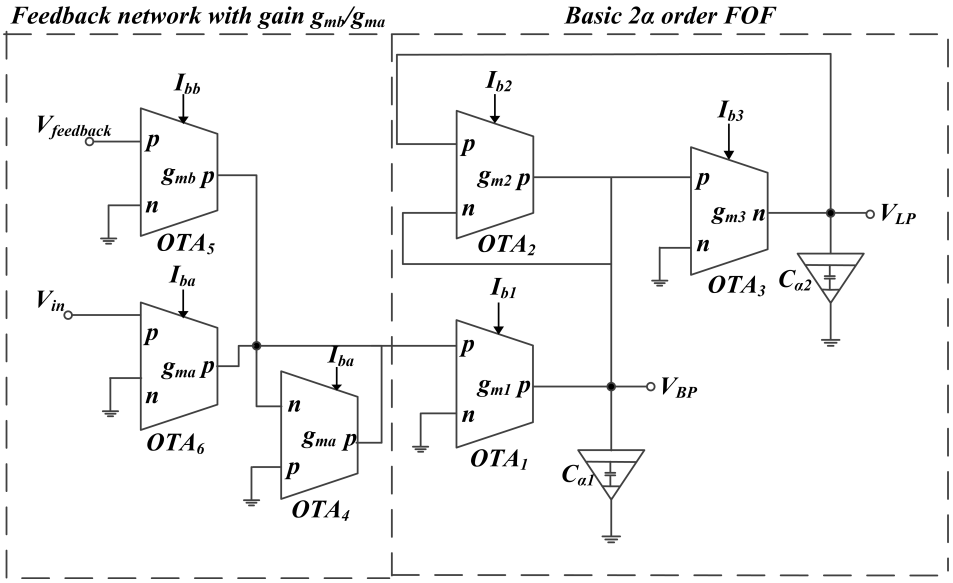

Figure 4.12: Circuit diagram of proposed shadow FOF circuit II

There can be total six combinations for different feedback signals and the cases of stability, such as case-1, 2 and 3 of stability for FLPF feedback signal and case-1, 2 and 3 of stability for FBPF feedback signal. Two cases are chosen to present here; case-2 for FLPF feedback signal (Variable ω_0', variable Q') and case-2 for

FBPF feedback (Fixed ω_0', variable Q'). By using the method outlined for stability constraints for various feedback signals in Sect. 4.4, the values of g_{m1}, g_{m2} and A are calculated. The constraint on A & g_ms and the effect on ω_0' and Q' for both the cases are given in Table 4.6.

Table 4.6: Constraints on g_m & A and effect on ω_0' & Q' for both the cases

Feedback signal	Stability case	Constraint on g_m ($C_{\alpha1}$=$C_{\alpha2}$)	Constraint on A	Effect on ω_0' and Q'
FLPF	Case-2	$g_{m2}^2 < 4g_{m3}(g_{m2} - Ag_{m1})$	$A < 1$	Variable ω_0', variable Q'
FBPF	Case-2	$(g_{m2} - Ag_{m1})^2 < 4g_{m2}g_{m3}$	$A < 1$	Fixed ω_0', variable Q'

4.5.2.1 Simulation results

To verify the functionality of the proposed shadow FOF circuit II, SPICE simulations have been carried out with 180 nm CMOS technology model parameters. Section 2.4 provides the detais of the transistors used in OTA, and its corresponding CMOS schematic is illustrated in Fig. 2.8 (b). The proposed shadow FOF uses FOC, which is approximated via 12^{th}-order R-C ladder network based on CFE approximation [35]. The schematic of the R-C ladder network is depicted in Fig. 4.7. The values of $C_{\alpha1}$ and $C_{\alpha2}$, for all the three cases, are taken same and equal to 3.75 $\mu\mho sec^{\alpha}$ with α=0.5. The values for R_0, R_i and C_i (i=1, 2, ...11) to emulate FOC with α=0.5 and C_{α}=3.75 $\mu\mho sec^{\alpha}$ can be referred from Sect. 3.3.1. The FBPF output response of the proposed shadow FOF circuit II has been considered to verify the effect of each feedback signal on ω_0' and Q'.

To realize case-2 of FLPF feedback signal, the values of g_{m2} and g_{m3} are taken same and equal to 534 $\mu A/V$ and g_{m1} is set as 377 $\mu A/V$. The external amplifier's

gain A is realized as -1, -2, -3.76 and -10 by adjusting the values of g_{ma} and g_{mb}.

The magnitude response of $T(s)_{BP\_LP}$ (case-2) is shown in Fig. 4.13 (a). It is clear that ω_0' and Q' both are variable with respect to external amplifier's gain A, but the dependency of Q' on gain A is negligible for negative values of A, which corroborates with the theory proposed in Sect. 4.3.

Further, case-2 of FBPF feedback signal is realized and the value of g_{m1} is taken as 55 $\mu A/V$ while g_{m2} and g_{m3} are taken same and equal to 534 $\mu A/V$. The magnitude response of $T(s)_{BP\_LP}$ (case-2) is shown in Fig. 4.13 (b). It is observed from the figure that for a fixed ω_0', Q' is variable with respect to external amplifier's gain A, same has been derived in theory as well.

Table 4.7 consists of the values of pole frequency in Hertz (f_0'=$\omega_0'/2\pi$) and Q' with respect to the external amplifier's gain A, for each case of feedback signal. It is clear from the Table 4.7, as the external amplifier's gain A becomes more negative, f_0' increases for case-2 of FLPF feedback signal, while it remains constant for FBPF feedback signal case-2. The Q' for both the cases is variable, which corroborates with theoretical predictions. Further, to analyse the linearity of shadow FOF circuit II, total harmonic distortion (THD) has been simulated for $A=-2$ for

Table 4.7: Summaized simulation results for proposed shadow FOF circuit II

A	FLPF feedback signal (case-2)		FBPF feedback signal (case-2)	
	Q'	f_0'	Q'	f_0'
-1	0.20	3.44 kHz	0.15	2.22 kHz
-2	0.23	5.16 kHz	0.12	2.22 kHz
-3.76	0.26	7.71 kHz	0.08	2.22 kHz
-10	0.28	13.77 kHz	0.04	2.22 kHz

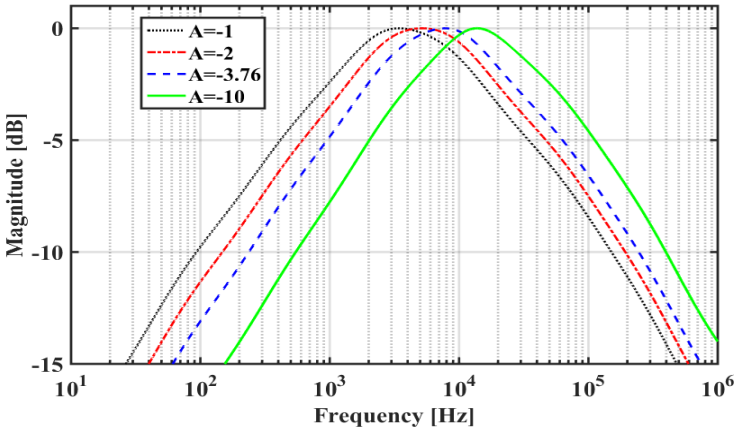

(a)

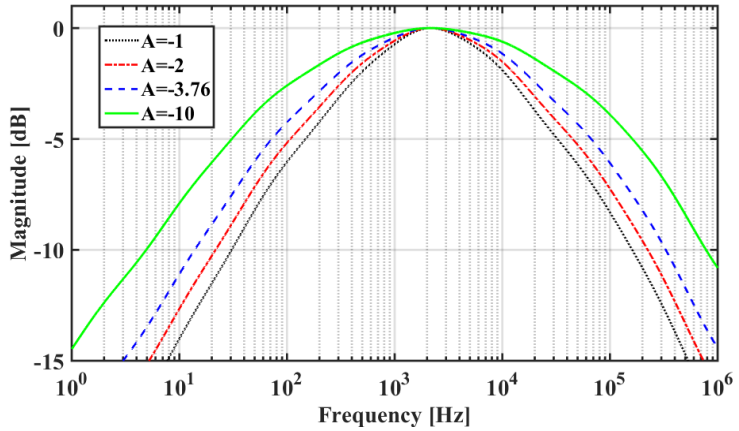

(b)

Figure 4.13: Proposed Shadow FOF circuit II; FBPF Magnitude response for various A and feedback signal as (a) FLPF (case-2) (b) FBPF (case-2)

FLPF feedback signal (case-2) and $A = -2$ for FBPF feedback signal (case-2) using the same simulation settings. For this a sinusoidal signal V_{in} with varying magnitude is applied at the input of the proposed shadow FOF circuit II for both the cases. The measured THD is shown in Figs. 4.14 (a) and (b) for FLPF feedback case-2 ($A = -2$) and FBPF feedback case-2 ($A = -2$) respectively. It is found that for input signal $< 60mV$ the maximum THD remains under 3% for both the cases.

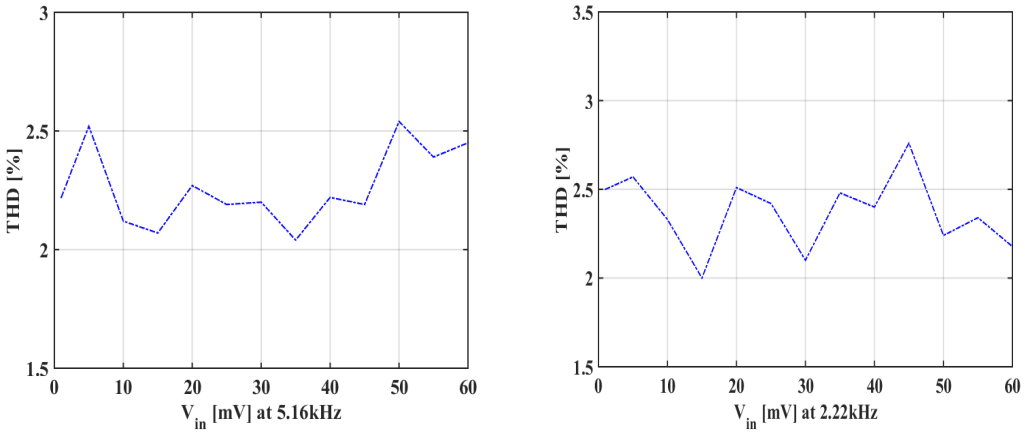

(a) (b)

Figure 4.14: THD vs V_{in} for proposed Shadow FOF circuit II; for feedback signal as (a) FLPF (case-2, $A = -2$) (b) FBPF (case-2, $A = -2$)

4.5.2.2 Robustness

The robustness of the proposed Shadow FOF Circuit II was evaluated through two types of analyses: corner analysis and Monte-Carlo analysis. The results of these analyses are discussed below.

Corner analysis

To evaluate the sensitivity of the output of the proposed shadow FOF circuit II to the random variations that may occur during fabrication, the proposed circuit is examined at the five process corners i.e. FF, FS, TT, SF and SS for the same simulation settings with $A = -10$ for FLPF feedback signal (case-2) and $A = -10$ for FBPF feedback signal (case-2). The magnitude responses of FBPF for both the cases i.e., FLPF feedback (case-2, $A = -10$) and FBPF feedback (case-2, $A = -10$) are shown in Figs. 4.15 (a) and (b), respectively for all the five corners FF, FS, TT, SF and SS. The absence of any sudden changes in the response confirms the reliability and stability of the proposed shadow FOF circuit II.

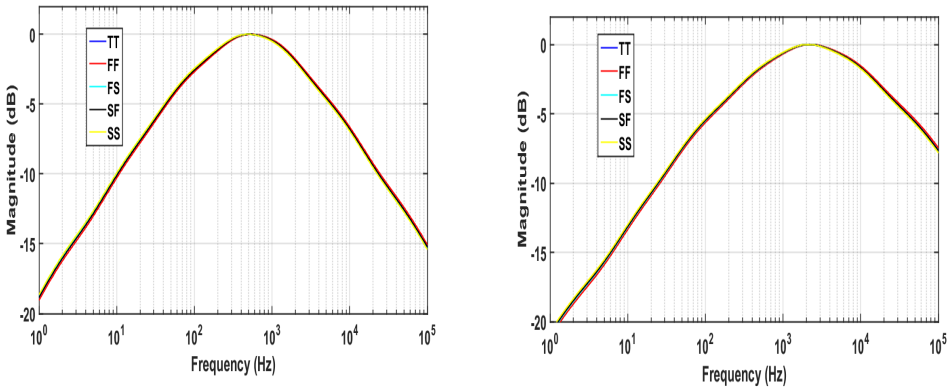

(a) (b)

Figure 4.15: Corner analysis for proposed shadow FOF circuit II; FBPF response, for feedback signal as (a) FLPF (Case-2, $A = -10$) (b) FBPF as feedback signal (Case-2, $A = -10$)

Monte-Carlo analysis

To get further insight on sensitivity of the proposed shadow FOF circuit II with respect to random variations in C_α, Monte Carlo analysis is performed on 500 random samples. The samples were generated using a uniform Gaussian distribution with a $\pm 5\%$ tolerance for the passive components that were used to realize C_α. The distribution of the ω_0' of FBPF for FLPF feedback case-2 signal and FBPF feedback signal case-2 with $A = -2$ is illustrated in Figs. 4.16 (a) and (b) respectively. The ω_0' for all the samples lies within a small range and the mean for both the cases matched with the corresponding ω_0' within 1% error, this shows the validity of proposed shadow FOF's for the random variation in $C_\alpha' s$ value.

4.6 Conclusion

In this chapter, the theory of integer-order shadow filters is generalized to fractional domain. Mathematical equations have been drafted to determine the pole frequency

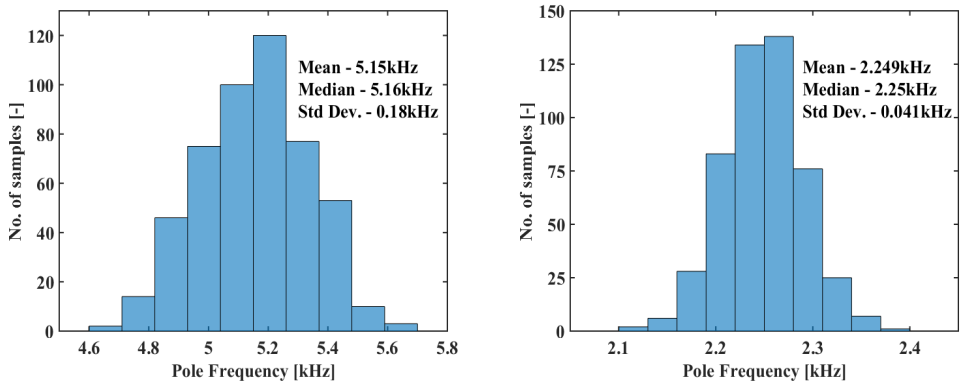

(a) (b)

Figure 4.16: Monte Carlo Analysis for proposed shadow FOF circuit II for the variations in C_α; for feedback signal as (a) FLPF (Case-2, $A = -2$) (b) FBPF (Case-2. $A = -2$)

and pole quality factor when different types of feedback signals, such as low-pass, high-pass, band-pass, or band-stop, are applied to the external amplifier in the feedback loop and demonstrated using MATLAB simulations. The proposed theory is verified through SPICE simulations using two active FOFs and found that results fit in the theoretical predictions very well. The shadow FOF's parameters such as ω_0' and Q' are tuned with the help of external amplifier's gain, without changing the active or passive components of the basic FOF. For both of the shadow FOF circuits the THD is found to be below 4%. Further, corner and Monte-Carlo analysis have been performed to verify the robustness of the shadow FOF circuits.

Chapter 5

Electronically Tunable Fractional-Order Oscillators

This chapter presents the results and content of the following papers:

[1] **G. Varshney,** N. Pandey and R. Pandey, "Electronically tunable fractional-order multivibrator using OTA and its application as versatile modulator," in AEU - International Journal of Electronics and Communications, vol. 141, pp. 153956, 2021, doi: 10.1016/j.aeue.2021.153956. **(SCI indexing, 3.169 IF)**

[2] **G. Varshney,** N. Pandey and R. Pandey, "Design and implementation of OTA based fractional-order oscillator," in Analog Integrated Circuits and Signal Processing, vol. 113, no. 1, pp. 93-103, 2022, doi: 10.1007/s10470-022-02069-0. **(SCI indexing, 1.321IF)**

[3] **G. Varshney,** N. Pandey and R. Pandey, "OTA Based Fractional-Order Oscillator with Controlled Phase Difference," 2022 IEEE International Symposium

on Circuits and Systems (ISCAS 2022), doi: 10.1109/iscas48785.2022.9937515.

5.1 Introduction

Oscillators are extensively employed for signal generation in a wide range of applications such as waveform generation, signal transmission, reception, and jamming [133]. There are two broad categories in which oscillators can be classified: sinusoidal oscillators and relaxation oscillators (multivibrator). Recently, there has been growing interest in the design of fractional-order oscillators (FOOs), which incorporate the fractional-order concepts in oscillator designing.

The FOOs are generalized version of integer-order oscillators that offer a broader range of frequency of oscillation and allow for controlled phase shift through α. This feature of FOOs make them suitable for a wide range of applications. For instance, the ability to generate very low frequencies makes them ideal for use in biomedical applications, while the capability to generate very high frequencies makes them well-suited for communication systems. Further, oscillators with controlled phase shift have a wide range of applications, including PSK modulation-demodulation schemes, Alzheimer's disease diagnosis, and music synthesizing, etc., [134], [135].

This chapter presents three new sinusoidal FOOs and one fractional-order multivibrator based on OTA. The first two circuits of the sinusoidal FOO are designed using the trans-admittance mode FAPF with a trans-impedance mode integrator/differentiator topology. Additionally, the third circuit of the sinusoidal FOO features a unique design that enables independent control of the phase difference between its two output voltages. Further, an electronically tunable fractional-order multivibrator based on OTA has been generalized to fractional domain. The mathematical formula for the time period has been derived using Reimann-Liouville fractional

integral.

5.2 Proposed Sinusoidal FOO Circuit I & Circuit II

Two circuits to construct sinusoidal FOO are presented in this section. The circuit I consists of a trans-admittance mode FAPF connected with a trans-impedance mode integrator, whereas the circuit II contains a trans-admittance mode FAPF connected with a trans-impedance mode differentiator. Both circuits are discussed in the following subsections.

5.2.1 Proposed Sinusoidal FOO Circuit I

The proposed FOO circuit I consists of a trans-admittance mode FAPF comprised of two OTAs (OTA_1 and OTA_2) along with a FOC (C_α), and a trans-impedance mode integrator comprised of a FOC (C_β), is shown in Fig. 5.1. It provides one output V_{O1}. By performing routine network analysis, characteristic equation of the proposed FOO circuit I is obtained and given below:

$$s^{\alpha+\beta} - \frac{g_{m2}}{C_\beta}s^\alpha + \frac{g_{m2}}{C_\alpha}s^\beta + \frac{g_{m1}g_{m2}}{C_\alpha C_\beta} = 0 \tag{5.1}$$

The Barkhausen criterion is necessary but not sufficient condition for the sustained oscillations in a fractional-order oscillatory system [136]. In order to ensure the presence of imaginary conjugate poles at $\pm j\omega$ axis, it is assumed that the imaginary conjugate poles are already on $\pm j\omega$ axis. It is also necessary for these poles

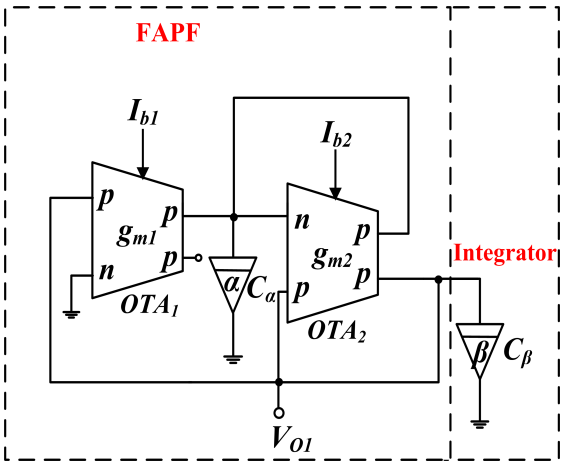

Figure 5.1: Proposed sinusoidal FOO circuit I (FAPF followed by integrator)

to satisfy the characteristic equation of the oscillator for a specific oscillation frequency (ω_0). Hence putting $+j\omega_0$ and $-j\omega_0$ in the characteristic equation of the proposed FOO circuit I gives (5.2).

$$\omega_0^{\alpha+\beta}\cos\frac{(\alpha+\beta)\pi}{2}-\omega_0{}^{\alpha}\frac{g_{m2}}{C_\beta}\cos\frac{\alpha\pi}{2}+\omega_0{}^{\beta}\frac{g_{m2}}{C_\alpha}\cos\frac{\beta\pi}{2}+\frac{g_{m1}g_{m2}}{C_\alpha C_\beta}=0 \tag{5.2a}$$

$$\omega_0^{\beta}\sin\frac{(\alpha+\beta)\pi}{2}+\omega_0{}^{\beta-\alpha}\frac{g_{m2}}{C_\alpha}\sin\frac{\beta\pi}{2}-\frac{g_{m2}}{C_\beta}\sin\frac{\alpha\pi}{2}=0 \tag{5.2b}$$

By solving (5.2a) and (5.2b), the frequency of oscillation (FO) and condition of oscillation (CO) are determined. For various cases of α and β, FO and CO are given in Table 5.1.

To design the proposed FOO circuit I, first of all, the FO is set to the desired value. By using FO's equation for a particular case of α and β (given in Table 5.1) the values of C_α, C_β and g_{m2} are chosen. Now using CO equation the remaining parameter i.e., g_{m1} is calculated.

5.2.2 Proposed Sinusoidal FOO Circuit II

The proposed FOO circuit II consists of a trans-admittance mode FAPF comprised of two OTAs (OTA_1 and OTA_2) along with a FOC (C_α), and a trans-impedance mode integrator comprised of another two OTAs (OTA_3 and OTA_4) along with a FOC (C_β), is shown in Fig. 5.2. It provides one output V_{O1}. By performing routine network analysis, the characteristic equation of the proposed FOO circuit II is obtained and given below:

$$s^{\alpha+\beta} + \frac{g_{m3}g_{m4}}{g_{m2}C_\beta}s^\alpha - \frac{g_{m1}}{C_\alpha}s^\beta + \frac{g_{m3}g_{m4}}{C_\alpha C_\beta} = 0 \tag{5.3}$$

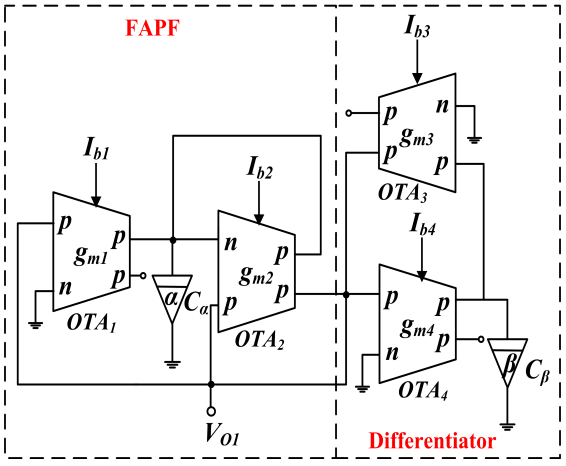

Figure 5.2: Proposed sinusoidal FOO circuit II (FAPF followed by differentiator)

By using the method outlined in Sect. 5.2.1 to calculate FO and CO; lets consider the poles of characteristic equation of proposed FOOO circuit II are $\pm j\omega_0$. Hence putting $+j\omega_0$ and $-j\omega_0$ in the characteristic equation of the proposed FOO circuit II

gives (5.4).

$$\omega_0^{\alpha+\beta}\cos\frac{(\alpha+\beta)\pi}{2}+{\omega_0}^{\alpha}\frac{g_{m3}g_{m4}}{g_{m2}C_\beta}\cos\frac{\alpha\pi}{2}-{\omega_0}^{\beta}\frac{g_{m1}}{C_\alpha}\cos\frac{\beta\pi}{2}+\frac{g_{m3}g_{m4}}{C_\alpha C_\beta}=0 \quad (5.4a)$$

$$\omega_0^{\beta}\sin\frac{(\alpha+\beta)\pi}{2}-{\omega_0}^{\beta-\alpha}\frac{g_{m1}}{C_\alpha}\sin\frac{\beta\pi}{2}+\frac{g_{m3}g_{m4}}{g_{m2}C_\beta}\sin\frac{\alpha\pi}{2}=0 \quad (5.4b)$$

On solving (5.4), the expression for FO and CO are obtained. For various cases of α and β, FO and CO are given in Table 5.1.

To design the proposed FOO circuit II, first of all, the FO is set to the desired value. By using FO's equation for a particular case of α and β (given in Table 5.1) the values of C_α, C_β, g_{m2}, g_{m3} and g_{m4} for $(\alpha=\beta\neq 1)$ and $(\alpha\neq 1,\ \beta=1)$ case are chosen and C_α, C_β, g_{m1}, g_{m3} and g_{m4} for $(\alpha=1,\ \beta\neq 1)$ case are chosen. Now using CO equation the remaining parameter i.e., g_{m1} for $(\alpha=\beta\neq 1)$ and $(\alpha\neq 1,\ \beta=1)$ case, and g_{m2} for $(\alpha=1,\ \beta\neq 1)$ case is calculated.

5.2.3 Functional Verification

To demonstrate the functionality of proposed FOO circuit I and circuit II, SPICE simulations have been carried out with 180 nm CMOS technology model parameters. The supply voltages are taken as $\pm 1.5\ V$. Section 2.4 provides the details of the transistors used in OTA, and its corresponding CMOS schematic is illustrated in Fig. 2.8 (b). The FOC utilized in the proposed FOO structures is realized using the R-C ladder network based on 7^{th} order Valsa's algorithm [116] shown in Fig. 5.12. The passive components' values to emulate FOCs of magnitude 1 $\mu\mho sec^{\alpha}$

Table 5.1: CO and FO for various cases of α and β

Circuit	Case	FO	CO
Proposed FOO	$\alpha=\beta\neq 1$	$\omega_0=\left[\frac{(g_{m2}/C_\beta)-(g_{m2}/C_\alpha)}{2cos\frac{\alpha\pi}{2}}\right]^{1/\alpha}$	$g_{m1}=\frac{g_{m2}}{C_\alpha\ C_\beta}\left[\frac{C_\alpha-C_\beta}{2cos\frac{\alpha\pi}{2}}\right]^2$
Circuit I	$\alpha=1;\beta\neq 1$	$\omega_0^\beta cos\frac{\beta\pi}{2}+\frac{g_{m2}}{C_\alpha}\omega_0^{\beta-1}sin\frac{\beta\pi}{2}-\frac{g_{m2}}{C_\beta}=0$	$g_{m1}=\frac{C_\alpha\ C_\beta}{g_{m2}}\left[\omega_0^{1+\beta}sin\frac{\beta\pi}{2}-\frac{g_{m2}}{C_\alpha}\omega_0^\beta cos\frac{\beta\pi}{2}\right]$
	$\alpha\neq 1;\beta=1$	$\omega_0\ cos\frac{\alpha\pi}{2}+\frac{g_{m2}}{C_\alpha}\omega_0^{1-\alpha}-\frac{g_{m2}}{C_\beta}sin\frac{\alpha\pi}{2}=0$	$g_{m1}=\frac{C_\alpha\ C_\beta}{g_{m2}}\left[\omega_0^{1+\alpha}sin\frac{\alpha\pi}{2}+\frac{g_{m2}}{C_\alpha}\omega_0^\alpha cos\frac{\alpha\pi}{2}\right]$
Proposed FOO	$\alpha=\beta\neq 1$	$\omega_0=\left[\frac{(g_{m1}/C_\alpha)-(g_{m3}g_{m4}/g_{m2}C_\beta)}{2cos\frac{\alpha\pi}{2}}\right]^{1/\alpha}$	$g_{m1}=C_\alpha\left[\left(2cos\frac{\alpha\pi}{2}\sqrt{\frac{g_{m3}g_{m4}}{C_\alpha C\beta}}\right)+\frac{g_{m3}g_{m4}}{g_{m2}C_\beta}\right]$
Circuit II	$\alpha=1;\beta\neq 1$	$\omega_0^\beta cos\frac{\beta\pi}{2}-\frac{g_{m1}}{C_\alpha}\omega_0^{\beta-1}sin\frac{\beta\pi}{2}+\frac{g_{m3}g_{m4}}{C_\alpha C_\beta}=0$	$g_{m2}=\frac{g_{m3}g_{m4}}{C_\beta}\left[1/(\omega_0^{1+\beta}sin\frac{\beta\pi}{2}+\frac{g_{m1}}{C_\alpha}\omega_0^\beta cos\frac{\beta\pi}{2})\right]$
	$\alpha\neq 1;\beta=1$	$\omega_0^{1+\alpha}sin\frac{\alpha\pi}{2}-\frac{g_{m3}g_{m4}}{g_{m2}C_\beta}\omega_0^\alpha cos\frac{\alpha\pi}{2}-\frac{g_{m3}g_{m4}}{C_\alpha C_\beta}=0$	$g_{m1}=\frac{C_\alpha}{\omega_0^{1-\alpha}}\left[\omega_0 cos\frac{\alpha\pi}{2}+\frac{g_{m3}g_{m4}}{g_{m2}C_\beta}\right]$

and 2 $\mu\mho sec^{\alpha}$ with fractional-orders 0.5 are given in Table 5.2.

Table 5.2: Specifications for passive components used to construct approximated FOC based on Valsa's algorithm

C_{α} (α)	R_p C_p	R_1 C_1	R_2 C_2	R_3 C_3	R_4 C_4	R_5 C_5	R_6 C_6	R_7 C_7
1 $\mu\mho sec^{\alpha}$ (0.5)	259.5 $k\Omega$ 157.84 pF	173.01 $k\Omega$ 57.8 nF	69.5 $k\Omega$ 23.12 nF	27.68 $k\Omega$ 9.248 nF	11.07 $k\Omega$ 3.69 nF	4.34 $k\Omega$ 1.48 nF	1.77 $k\Omega$ 592 pF	708.63 Ω 236.8 pF
2 $\mu\mho sec^{\alpha}$ (0.5)	129.75 $k\Omega$ 315.68 pF	86.51 $k\Omega$ 115.6 nF	34.75 $k\Omega$ 46.24 nF	13.84 $k\Omega$ 18.496 nF	5.535 $k\Omega$ 7.38 nF	2.17 $k\Omega$ 2.96 nF	0.885 $k\Omega$ 1.184 nF	354.315 Ω 473.6 pF

The transient response and frequency spectrum for the proposed FOO circuit I is shown in Fig. 5.3 and for the proposed FOO circuit II, it is shown in Fig. 5.4, for different cases of α and β. The simulation settings for the perticular case of α and β are given in Table 5.3. Table 5.3 provides a summary of the theoretical and simulated frequencies of oscillations in Hertz for all the mentioned cases. The error between simulated and theoretical values of frequency of oscillation lies within 9% for both the topologies which corroborates with the theoretical predictions.

Moreover, to show the electronic tuning of frequency of oscillation for the proposed circuits of FOO, graphs between f_0 (f_0=$\omega_0/2\pi$), g_{m1} and g_{m2} are plotted and shown in Fig. 5.5, taking the values of C_{α}, C_{β}, g_{m3} and g_{m4} from Table 5.3 for α=β=0.5 case. By analyzing the information presented in Fig. 5.5, it can be concluded that the frequency of oscillation can be modified through the electronic adjustment of g_{m1} and/or g_{m2}.

The study is extended to investigate the usability of proposed FOO circuit

Table 5.3: Simulation settings for proposed fractional-order oscillators

Circuit	Case	g_{m1} $[\mu A/V]$	g_{m2} $[\mu A/V]$	g_{m3} $[\mu A/V]$	g_{m4} $[\mu A/V]$	C_α	C_β	Theoretical oscillation frequency in $[Hz]$	Simulated oscillation frequency in $[Hz]$
Proposed FOO	α=β=0.5	25	100	-	-	2 $\mu\mho sec^\alpha$	1 $\mu\mho sec^\beta$	198.1	180.8
Circuit I	α=1, β=0.5	160.51	10	-	-	1 $\mu\mho sec^\alpha$	1 $\mu\mho sec^\beta$	28.5	27.3
Proposed FOO	α=β=0.5	241.42	100	100	100	1 $\mu\mho sec^\alpha$	1 $\mu\mho sec^\beta$	1.55k	1.41k
Circuit II	α=0.5, β=1	21.99	100	100	100	1 $\mu\mho sec^\alpha$	1 $\mu\mho sec^\beta$	103.9	96.5

I for generating very low frequencies. The proposed FOO circuit I is designed to generate a sinusoidal waveform of 5 Hz. The values of C_α and C_β are kept constant at 2 $\mu\mho sec^\alpha$ and 1 $\mu\mho sec^\beta$ respectively, with α=β=0.5. To achieve the desired frequency of 5Hz, g_{m1} and g_{m2} are chosen as 3.96 $\mu A/V$ and 15.85 $\mu A/V$, respectively. However, the generated waveform had a frequency of 4.9 Hz, slightly lower than the designed value with a percentage error of 1%. The transient

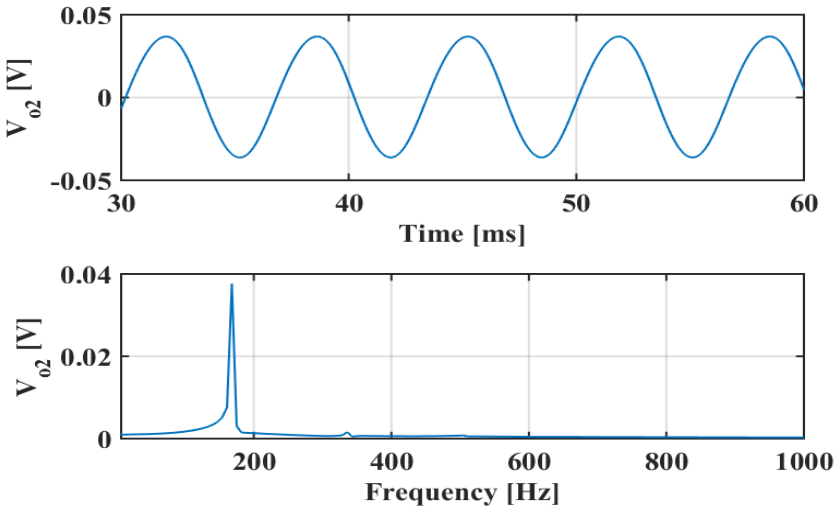

(a)

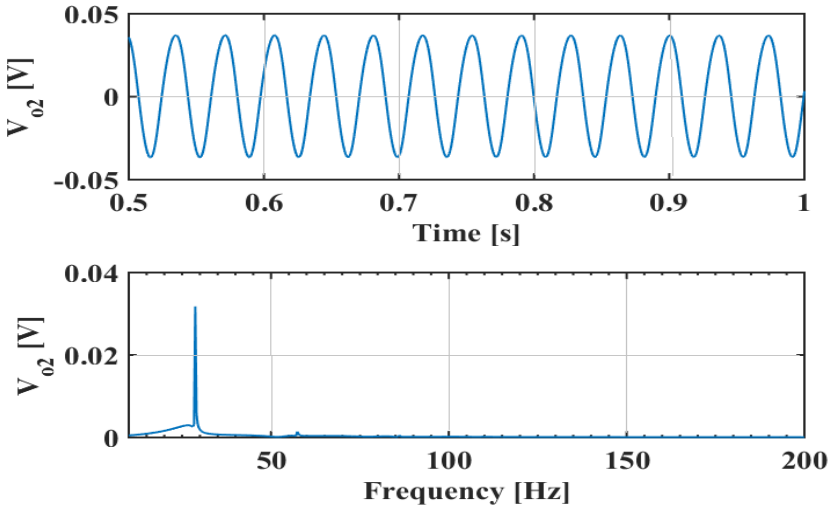

(b)

Figure 5.3: Transient response and frequency spectrum of proposed FOO circuit I (a) α=β=0.5 (b) α=1 & β=0.5

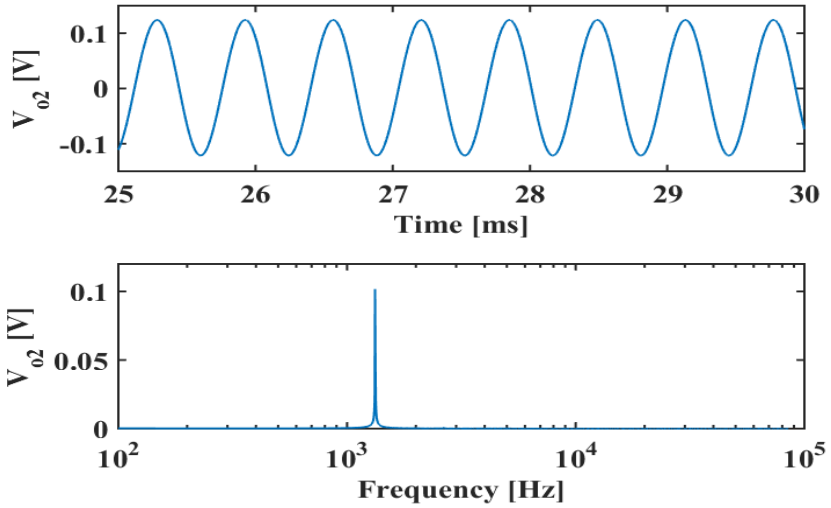

(a)

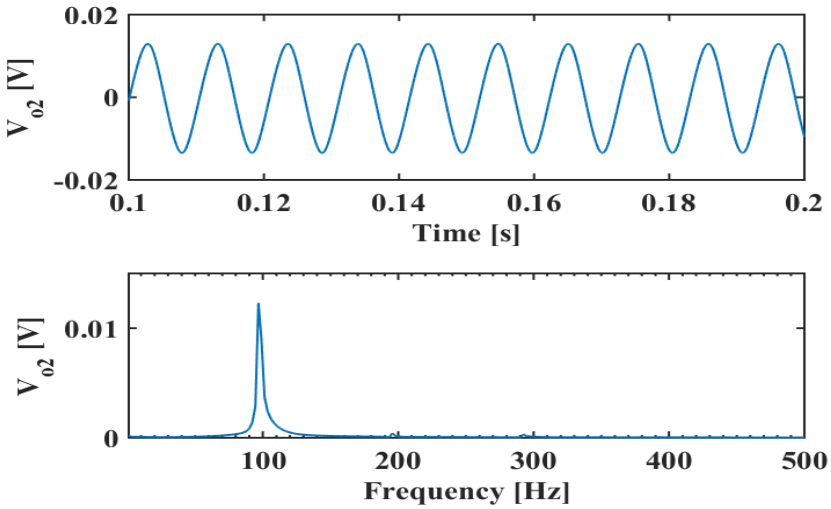

(b)

Figure 5.4: Transient response and frequency spectrum of proposed FOO circuit II (a) α=β=0.5 (b) α=0.5 & β=1

response and frequency spectrum are illustrated in Fig. 5.6.

5.2.4 Stability Analysis

The stability of the proposed FOO circuits I and circuit II has been verified using root locus method for linear fractional-order system outlined in section 2.3 [117].

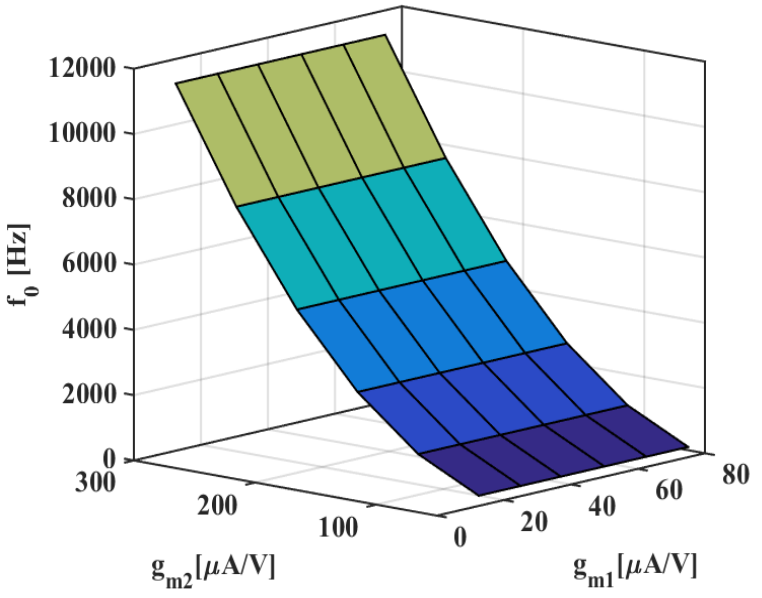

(a)

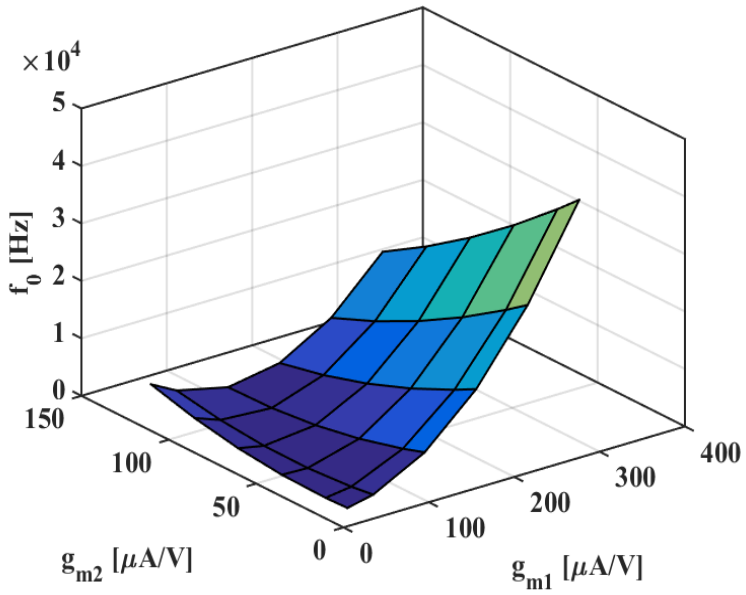

(b)

Figure 5.5: Electronic tuning of f_0 with g_{m1} and g_{m2} (a) FOO circuit I (b) FOO circuit II

The pole plots for the characteristic equation of the proposed FOO circuit I and circuit II are acquired through *forlocus* function of MATLAB [122] for α=β=0.5 case (p=1 and q=2; as α=$\frac{p}{q}$=0.5) with the same simulation settings specified in

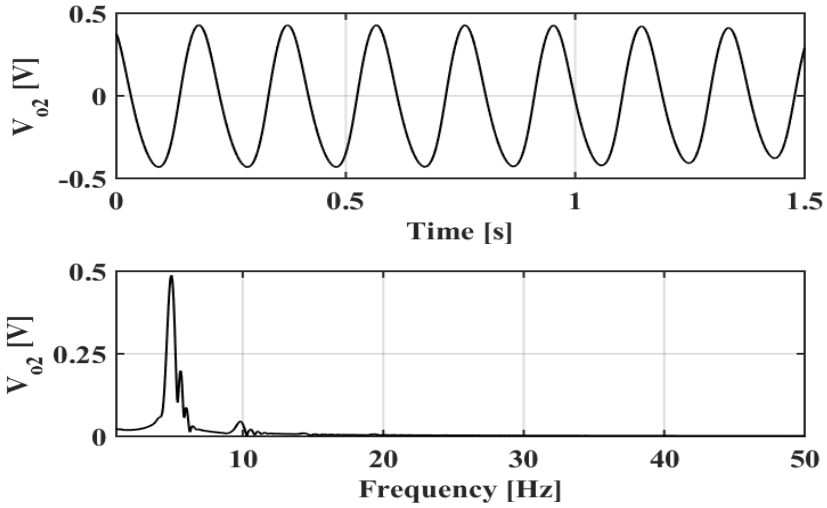

Figure 5.6: Transient response and frequency spectrum of the proposed FOO circuit I in VLF mode

Table 5.3 for the specified case and shown in Figs. 5.7 (a) and (b) respectively. The boundaries for stable and unstable regions are separated by $\pm\frac{\pi}{2q}$ (i.e., $\pm\frac{\pi}{4}$) and shown as dotted dash lines. As it may be witnessed from Figs. 5.7 (a) and (b) that both the roots lie on the line $\pm\frac{\pi}{4}$, hence proposed structures oscillate and none of the roots are in unstable region so the proposed FOO circuits I and circuit II do not show unstable behaviour.

5.2.5 Sensitivity Analysis

The sensitivity analysis is one of the most important analysis to study the performance of a circuit. Thus, the sensitivity analysis for the frequency of oscillation of the proposed FOO circuits I and circuit II with respect to various circuit components (i.e., C_α, C_β, g_{m1}, g_{m2}, g_{m3} and g_{m4}) has been derived mathematically and given in Table 5.4. Based on the information presented in Table 5.4, it can be observed

(a)

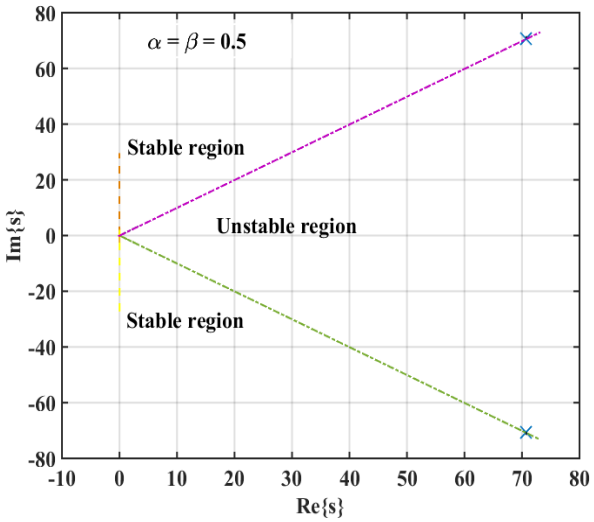

(b)

Figure 5.7: Pole plots for α=β=0.5 for (a) proposed FOO circuit I (b) proposed FOO circuit II

that the frequency of oscillation of the proposed FOOs is more sensitive to lower values of the fractional-order α. As the value of fractional-order α approaches unity the sensitivity reduces.

Table 5.4: Sensitivity with respect to various parameters for Proposed FOO circuit I and circuit II

$\lvert S_Y^{\omega_0} \rvert$	Proposed FOO circuit I	Proposed FOO circuit II
$\lvert S_{g_{m1}}^{\omega_0} \rvert$	0	$\frac{1}{\alpha}\left[1-\frac{g_{m3}g_{m4}C_\alpha}{g_{m1}g_{m2}C_\beta}\right]$
$\lvert S_{g_{m2}}^{\omega_0} \rvert$	$\frac{1}{\alpha}$	$\frac{1}{\alpha}\left[1-\frac{g_{m1}g_{m2}C_\beta}{g_{m3}g_{m4}C_\alpha}\right]$
$\lvert S_{g_{m3}}^{\omega_0} \rvert$	-	$\lvert S_{g_{m2}}^{\omega_0} \rvert$
$\lvert S_{g_{m4}}^{\omega_0} \rvert$	-	$\lvert S_{g_{m2}}^{\omega_0} \rvert$
$\lvert S_{C_\alpha}^{\omega_0} \rvert$	$\frac{C_\beta}{\alpha(C_\alpha - C_\beta)}$	$\lvert S_{g_{m1}}^{\omega_0} \rvert$
$\lvert S_{C_\beta}^{\omega_0} \rvert$	$\frac{C_\alpha}{\alpha(C_\alpha - C_\beta)}$	$\lvert S_{g_{m2}}^{\omega_0} \rvert$

5.2.6 Robustness

To verify the robustness of the proposed sinusoidal FOO circuits, PVT and Monte-Carlo analysis are performed. The results of these analyses for α=β=0.5 case are discussed below.

5.2.6.1 PVT analysis

The PVT analysis of the proposed FOOs has been carried out to examine the robustness. Both of the proposed FOO circuits are simulated at different process corners, supply voltage variations and temperature variations.

The proposed FOO circuit I and circuit II are examined at five process corners i.e. FF, FS, TT, SF and SS for α=β=0.5 case with simulation settings specified in Sect. 5.3.1 for this case. The values of frequency of oscillation in Hetrz ($f_0 = \omega_0/2\pi$) and percentage error from TT corner point for all the remaining four corner points (i.e., FF, FS, SF, SS) are observed and enlisted in Table 5.5. It is clear from the results that the percentage error in frequency of oscillation lies within 5% for various corners.

Figures 5.8 and 5.9 depict the transient response in presence of supply voltage variations (1.5 V and 1.5 V±3%) and temperature variations (0°, 27° and 70°) respectively, for both of the proposed FOO circuits. No abrupt changes have been observed in the transient response of the proposed FOO circuits in the presence of supply voltage and temperature variations. The results of PVT analysis suggest that both of the FOO circuits are able to perform consistently under a wide range

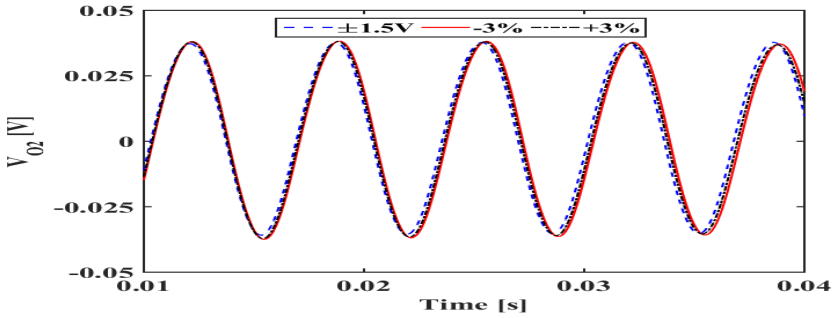

(a)

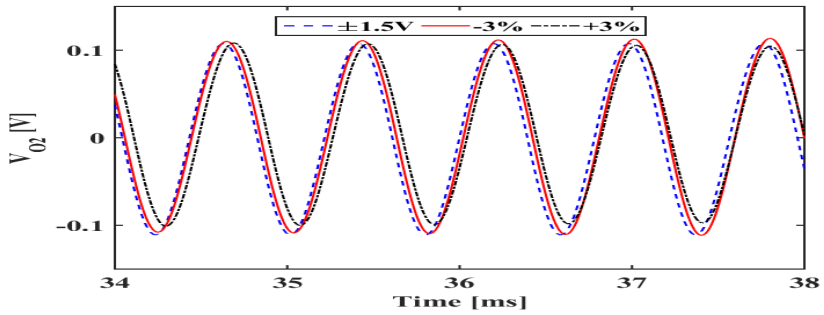

(b)

Figure 5.8: Transient response for supply voltage variations for proposed FOO (a) circuit I (b) circuit II

of operating conditions.

5.2.6.2 Monte-Carlo analysis

To draw further attention on sensitivity of the proposed FOO circuits I and circuit II with respect to random variations in FOC i.e. C_α and C_β, Monte-Carlo simulation is done on 250 random samples. The values of passive components, used for FOC realization, are randomly varied in uniform Gaussian distribution with a tolerance of ±5%. The distribution of the frequency of oscillation for the proposed FOO circuit I and circuit II is shown in Fig. 5.10 (a) and (b) respectively, for α=β=0.5 case. The simulation settings are specified in Table 5.3. The frequency

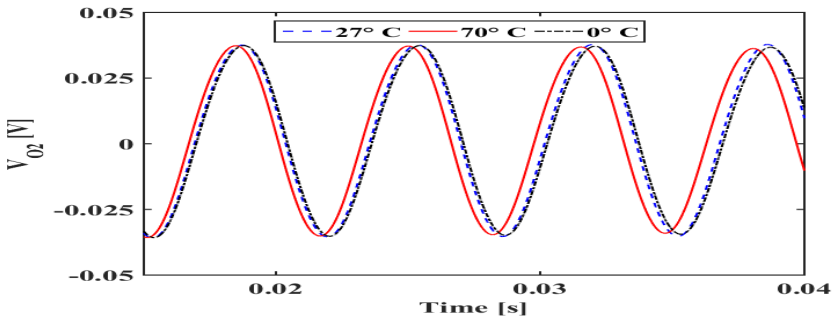

(a)

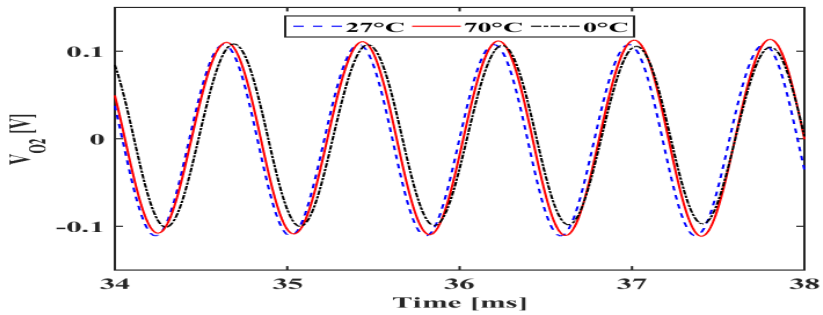

(b)

Figure 5.9: Transient response for temperature variations for proposed FOO (a) circuit I (b) circuit II

Table 5.5: Oscillation frequency of Proposed FOO circuit I and circuit II for all five process corners for $\alpha = \beta = 0.5$

Process corner	Oscillation Frequency (Hz)	% error from TT corner	Circuit
FF	188.93	4.50%	
FS	183.75	1.63%	
TT	180.93	-	Proposed FOO
SF	183.13	1.29%	Circuit I
SS	172.88	4.38%	
FF	$1.38k$	2.29%	
FS	$1.36k$	3.82%	
TT	$1.41k$	-	Proposed FOO
SF	$1.36k$	3.82%	Circuit II
SS	$1.35k$	4.58%	

of oscillation for all the samples lies within a small range and the mean for both the cases matched with the corresponding frequency of oscillation within ±0.5% error, this shows the validity of proposed FOO circuit I and circuit II for the random variation in C_α's value.

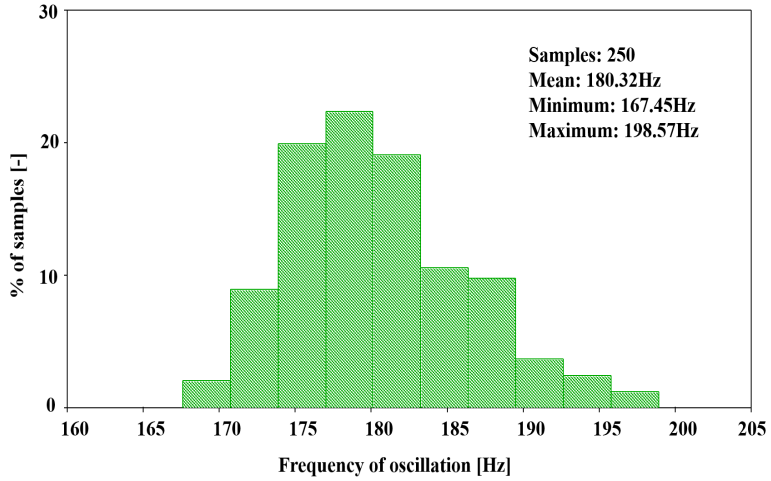

(a)

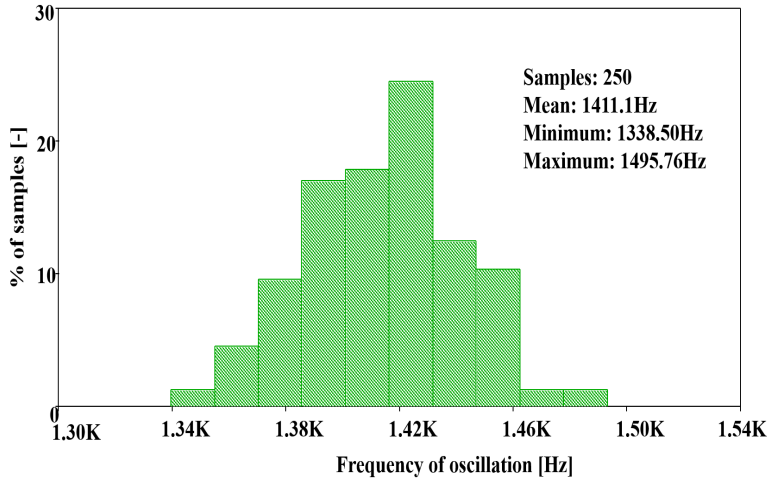

(b)

Figure 5.10: Monte Carlo analysis for random variations in C_α of (a) proposed FOO circuit I (b) proposed FOO circuit II

5.3 Proposed Sinusoidal FOO Circuit III

The proposed FOO circuit III, employs two OTAs (OTA_1 and OTA_2) and two FOCs (C_α and C_β) with fractional-order α and β respectively, is shown in Fig. 5.11. The circuit provides two outputs as V_{O1} and V_{O2}. Using routine network analysis, the characteristic equation of the proposed FOO circuit III is given by as:

$$s^{\alpha+\beta} - s^{\beta}\frac{g_{m1}}{C_\alpha} + \frac{g_{m1}g_{m2}}{C_\alpha C_\beta} = 0 \tag{5.5}$$

The method to obtain FO and CO of the FOO has already been disccussed in

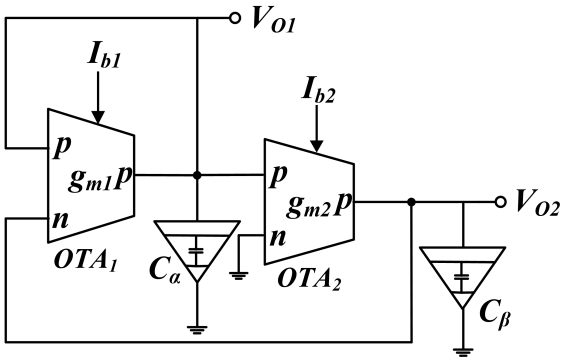

Figure 5.11: Proposed sinusoidal FOO circuit III

Sect. 5.2.1. By using the same method, lets consider the poles of the characteristic equation of the proposed FOO circuit III are $\pm j\omega_0$. Hence putting $+j\omega_0$ and $-j\omega_0$ in (5.5) and by separating its real and imaginary parts (5.6) is obtained.

$$\omega_0^{\alpha+\beta}\ cos\frac{(\alpha+\beta)\pi}{2} - \frac{g_{m1}}{C_\alpha}\omega_0^{\beta}\ cos\frac{\beta\pi}{2} + \frac{g_{m1}g_{m2}}{C_\alpha C_\beta} = 0 \tag{5.6a}$$

$$\omega_0^{\alpha+\beta}\ sin\frac{(\alpha+\beta)\pi}{2} - \frac{g_{m1}}{C_\alpha}\omega_0^{\beta}\ sin\frac{\beta\pi}{2} = 0 \tag{5.6b}$$

By solving (5.6b), the FO is calculated as:

$$\textbf{FO}: \qquad \omega_0 = \left[\frac{g_{m1}\ sin\frac{\beta\pi}{2}}{C_\alpha\ sin\frac{(\alpha+\beta)\pi}{2}}\right]^{\frac{1}{\alpha}} \tag{5.7}$$

The CO may be obtained by putting the value of ω_0 from (5.7) into (5.6a) and given as below:

$$\textbf{CO}: \qquad g_{m1} = \left[\frac{C_\alpha\ sin\frac{(\alpha+\beta)\pi}{2}}{sin\frac{\beta\pi}{2}}\right]\left[\frac{g_{m2}}{C_\beta\left(cos\frac{\beta\pi}{2} - \frac{sin\frac{\beta\pi}{2}}{tan\frac{\alpha+\beta\pi}{2}}\right)}\right]^{\frac{\alpha}{\beta}} \tag{5.8}$$

Further, the output terminals' voltage (V_{O1} and V_{O2}) of the proposed FOO circuit III are linked as $\frac{V_{O1}}{V_{O2}}=\frac{s^\beta C_\beta}{g_{m2}}$, which suggests that the phase difference between two voltages ($\Delta\phi=\angle V_{O1}$-$\angle V_{O2}$) is equal to $\frac{\beta\pi}{2}$, i.e. $\Delta\phi$ depends only upon the FOC's order and can be controlled independently.

5.3.1 Functional Verification

To demonstrate the functionality of the proposed FOO circuit III, SPICE simulations with 180 nm CMOS technology model parameters have been conducted. The supply voltages are used as $\pm 1.5\ V$. Section 2.4 provides the details of the transistors used in OTA, and its corresponding CMOS schematic is illustrated in Fig. 2.8 (b). The FOC utilized in the proposed FOO circuit III is realized using the R-C ladder network based on 7^{th} order Valsa's algorithm [116] shown in Fig. 5.12. The passive components' values to emulate FOCs of magnitude 1 $\mu\mho sec^\alpha$ and 2 $\mu\mho sec^\alpha$ with fractional-orders 0.5 are given in Table 5.2 and FOCs of magnitude

1 $\mu\mho sec^{\alpha}$ with fractional-order 0.8 is given in Table 5.6.

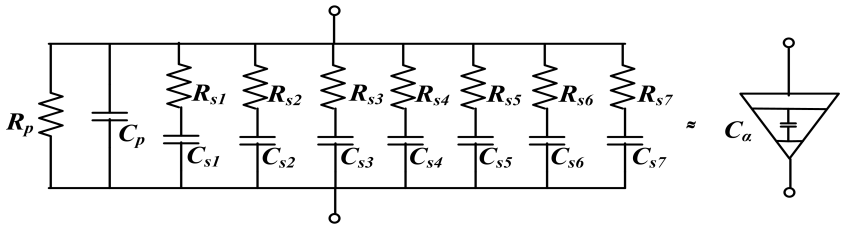

Figure 5.12: 7^{th} order R-C network to emulate FOC's behaviour based on Valsa'a algorithm

Table 5.6: Specifications for passive components used to construct approximated FOC based on Valsa's algorithm

C_α (α)	R_p C_p	R_1 C_1	R_2 C_2	R_3 C_3	R_4 C_4	R_5 C_5	R_6 C_6	R_7 C_7
1 $\mu\mho sec^{\alpha}$ (0.8)	254.43 $k\Omega$ 34 nF	73.66 $k\Omega$ 135.77 nF	17 $k\Omega$ 94.11 nF	3.92 $k\Omega$ 65.23 nF	906 Ω 45.21 nF	209 Ω 31.34 nF	48.27 Ω 21.72 nF	11.14 Ω 15.06 nF

First of all, β is chosen as per the required phase difference ($\Delta\phi$) between V_{O1} and V_{O2}, here β is chosen as 0.5 to make $\Delta\phi = 45°$ and 0.8 to make $\Delta\phi = 72°$. For α=β=0.5, by choosing C_α=1 $\mu\mho sec^{\alpha}$, C_β=2 $\mu\mho sec^{\beta}$ and g_{m2}=100 μA/V, to satisfy CO the value of g_{m1} is calculated as 100 μA/V. While for α=β=0.8, choosing C_α=C_β=1 $\mu\mho sec^{\alpha}$ and g_{m2}=406.42 μA/V gives the value of g_{m1} is obtained as 155.26 μA/V, to satisfy condition of oscillations.

The transient response and frequency spectrum for both the cases i.e., α=β=0.5 and α=β=0.8 of the proposed FOO circuit III are shown in Figs. 5.13 (a) and (b) respectively. The simulated and theoretical frequency of oscillation are 727.08 Hz and 795.7 Hz respectively for α=β=0.5 whereas the same are 154.4 Hz and 159.15 Hz respectively for α=β=0.8. The error between simulated and theoretical values of

frequency of oscillation lies within 9%. The transient response of V_{O1} and V_{O2} is shown in Fig. 5.14, which verifies the phase difference between the two voltages is 46° for α=β=0.5 and 71.2° for α=β=0.8 with an error of 2.22% and 1.15% respectively from the theoretical phase difference.

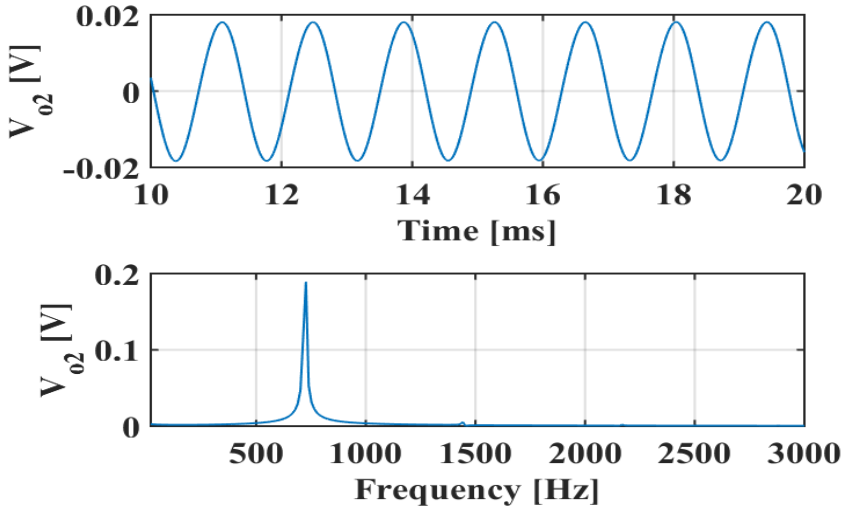

(a)

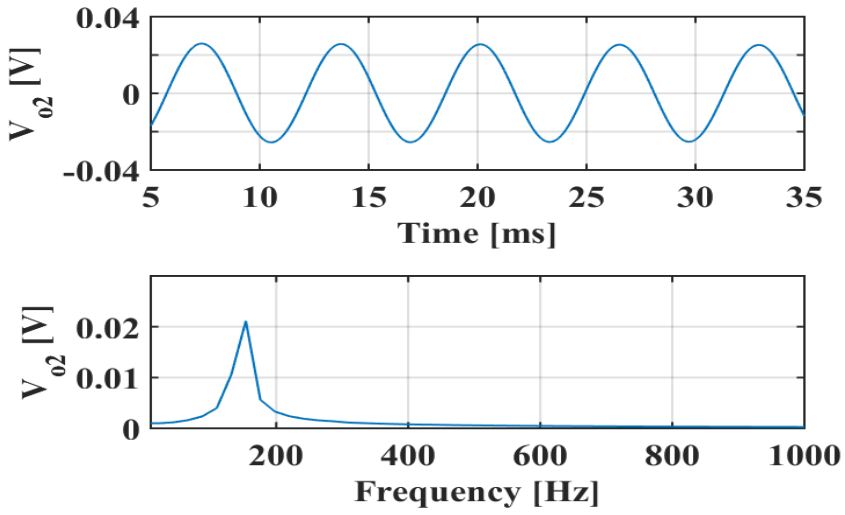

(b)

Figure 5.13: Transient response and frequency spectrum of the proposed FOO circuit III for (a) α=β=0.5 (b) α=β=0.8

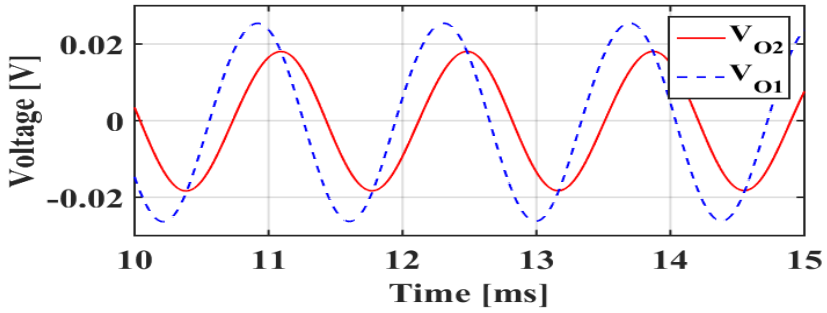

(a)

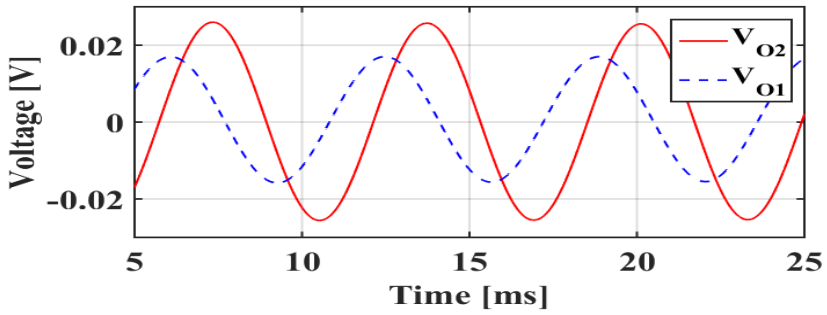

(b)

Figure 5.14: Transient response of V_{O1} and V_{O2} (a) α=β=0.5 (b) α=β=0.8

5.3.2 Stability Analysis

The stability of the proposed FOO circuit III has been verified using root locus method for linear fractional-order system outlined in section 2.3 [117]. The pole plot is obtained through *forlocus* function of MATLAB [122] for α=β=0.5 case (p=1 and q=2; as α=$\frac{p}{q}$=0.5) with simulation settings specified in Sect. 5.3.1 and shown in Fig. 5.15. The boundaries for stable and unstable regions are separated by $\pm\frac{\pi}{2q}$ (i.e., $\pm\frac{\pi}{4}$) and shown as dotted dash lines. As it is observed from Fig. 5.15, the roots lie on the line $\pm\frac{\pi}{4}$ and none of the roots are in unstable region, so the proposed FOO circuit III does not show unstable behavior.

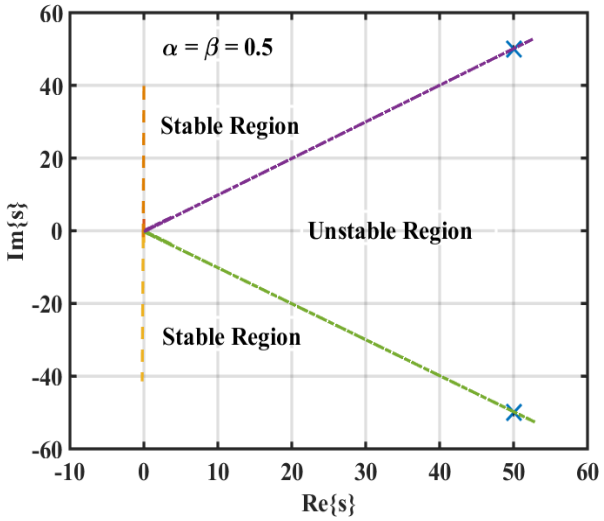

Figure 5.15: Proposed FOO circuit III's pole plot for $\alpha = \beta = 0.5$

5.3.3 Sensitivity Analysis

To examine the sensitivity of the frequency of oscillation of proposed FOO circuit III with respect to various circuit components (i.e. C_α, C_β, g_{m1} and g_{m2}), the mathematical formulas have been derived and given below:

$$|S_{g_{m1}}^{\omega_0}| = |S_{C_\alpha}^{\omega_0}| = \frac{1}{\alpha} \tag{5.9a}$$

$$|S_{g_{m2}}^{\omega_0}| = |S_{C_\beta}^{\omega_0}| = 0 \tag{5.9b}$$

From the above equations of sensitivities, it is clear that the frequency of oscillation of the proposed FOO circuit III is more sensitive for g_{m1} and C_α variations and the sensitivity is higher for lower values of the fractional-order α. As the value of fractional-order α approaches unity the sensitivity also becomes one. Further, the frequency of oscillation of the proposed FOO circuit III does not show any variations towards g_{m2} and C_β.

5.3.4 Robustness

To examine the robustness of the proposed FOO circuit III, corner analysis and Monte-Carlo analysis are done. The results of these analyses are discussed below.

5.3.4.1 Corner analysis

The proposed FOO circuit III is examined at five process corners i.e. FF, FS, TT, SF and SS for α=β=0.5 case with same simulation settings specified in Sect. 5.3.1 for this case. Table 5.7 contains frequency of oscillation in Hertz ($f_0 = \omega_0/2\pi$) and % error for all five corner points from TT corner point and it appears that the % error lies within 5%, which corroborates robustness of the proposed FOO circuit III for given corners.

Table 5.7: Oscillation frequency of Proposed FOO circuit III for all five process corners for $\alpha = \beta = 0.5$

	FF	FS	TT	SF	SS
f_0 $[Hz]$	760.33	717.29	727.08	721.18	698.25
% error from TT corner	4.60%	1.35%	–	0.81%	3.96%

5.3.4.2 Monte-Carlo analysis

To get further impression on the sensitivity of the proposed FOO circuit III with respect to random variations in FOC i.e. C_α and C_β, Monte-Carlo analysis is carried out on 250 random samples. The values of passive components used for FOC realization are randomly varied in uniform Gaussian distribution with a

tolerance of ±5%. The distribution of frequency of oscillation in Hertz (f_0=$\omega_0/2\pi$) is shown in Fig. 5.16 for α=β=0.5 case with same simulation settings specified in Sect. 5.3.1. The entire data range lies in a small range and the mean is matched with the corresponding f_0 within 0.5% error, this shows the robustness of proposed FOO circuit III for the random variations in FOC's value.

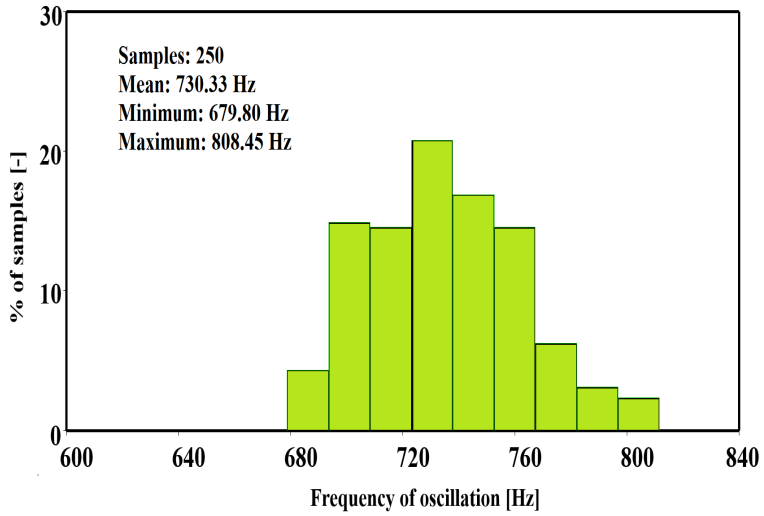

Figure 5.16: Monte Carlo analysis of proposed FOO circuit III for random variations in C_α

5.4 Fractional-Order Multivibrator

In sections 5.2 and 5.3, three sinusoidal FOOs are presented. In this section, a multivibrator, built around three OTAs [137], is generalized in fractional domain, this generalized multivibrator is called fractional-order multivibrator. The mathematical formula for the time period of the proposed fractional-order multivibrator is derived. The proposed fractional-order multivibrator employs a Schmitt Trigger and a fractional-order integrator. The Schmitt Trigger, comprises of two voltage amplifiers

interconnected in regenerative feedback manner, the first amplifier utilizes OTA_1 and R_1, while the other amplifier is formed using OTA_2 and R_2. The fractional-order integrator, composed of OTA_3 and FOC (C_α), is incorporated into the regenerative feedback path, as depicted in Fig. 5.17 (a) [137].

The saturation levels ($L_\pm$) at the output node V_{O1} of the proposed fractional-order multivibrator depend upon bias current of OTA_1 (I_{b1}), the values are given as ($L_\pm = \pm I_{b1}R_1$), while the lower threshold voltage (V_{TL}) and higher threshold voltage (V_{TH}) depend upon bias current of OTA_2 (I_{b2}), as they are decided by the comparison voltage V_{O2}, the values are given as ($V_{TL} = -I_{b2}R_2$) and ($V_{TH} = I_{b2}R_2$) respectively. The time constant of the integrator is directly proportional to the bias current of OTA_3 (I_{b3}).

Assume, initially the output V_{O1} of the proposed fractional-order multivibrator be at one of its two possible levels, say L_+ (i.e., positive saturation level), which makes OTA_3 saturate. Thus, a bias current I_{b3} starts to flow through the C_α and C_α starts charging towards this level. As soon as the voltage at C_α (V_{O3}) reaches a level called higher threshold voltage (V_{TH}), equal to the voltage at the positive terminal of OTA_1, the output V_{O1} switches its state to negative saturation voltage L_-. Now the negative saturation voltage at V_{O1} reverses the direction of the output current of OTA_3, leads to discharging of C_α, which will continue untill the lower threshold voltage (V_{TL}) is reached. At this point, OTA_1 again changes its state and output V_{O1} becomes L_+ and the direction of output current of OTA_3 is reversed, hence, voltage on C_α (i.e., V_{O3}) starts to increase again, and the new cycle of oscillation starts. This procedure is shown in Fig. 5.17 (b), with the dotted line as the voltage across C_α and the solid line as voltage at the output

node V_{O1}.

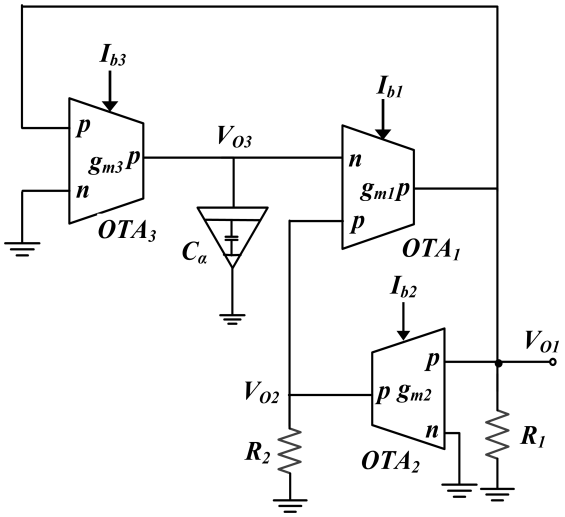

(a)

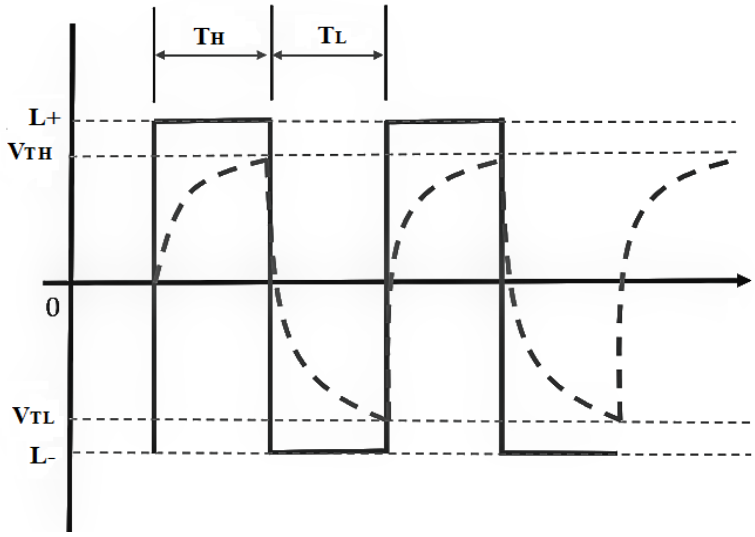

(b)

Figure 5.17: Fractional-order multivibrator (a) Circuit diagram (b) waveforms, dotted line is voltage across C_α, solid line is square wave output at node V_{O1}

5.4.1 Oscillation Frequency

From the above discussion of proposed fractional-order multivibrator, it is clear that the time period is defined as the total time taken to charge and discharge the C_α via bias current I_{b3}. Equation (5.10) represents voltage across C_α (V_{O3}), which

is equal to fractional integral of order α of $\frac{I_{B3}}{C_\alpha}$ and is given as below:

$$V_{O3} = {}_{t_1}I^{\alpha}_{t_2}\left[\frac{I_{b3}}{C_\alpha}\right] \tag{5.10}$$

Where ${}_{t_1}I^{\alpha}_{t_2}[f(t)]$ is the fractional integral of order α of function $f(t)$ within the time limits of t_1 and t_2, it can also be denoted as ${}_{t_1}D^{-\alpha}_{t_2}[f(t)]$ [15].

The Riemann-Liouville fractional integral of a constant may be calculated by using (6) of [15] and is given below:

$${}_{t_1}I^{\alpha}_{t_2}\left[Kt^0\right] = \frac{K(t_2-t_1)^{\alpha}}{\Gamma(1+\alpha)} \tag{5.11}$$

Here $\Gamma(.)$ is the Gamma function.

For the charging duration T_H (i.e., $[t_2 - t_1] = T_H$) in Fig. 5.17 (b), by using (5.11), (5.10) can be solved as:

$$V_{TH} - V_{TL} = \frac{T_H^{\alpha}}{\Gamma(1+\alpha)}\frac{I_{b3}}{C_\alpha} \tag{5.12}$$

Substituting the values of V_{TH} and V_{TL} as $I_{b2}R_2$ and $-I_{b2}R_2$ respectively in (5.12), T_H is obtaine as:

$$T_H = \left[\frac{2I_{b2}R_2C_\alpha\Gamma(1+\alpha)}{I_{b3}}\right]^{\frac{1}{\alpha}} \tag{5.13}$$

Similarly, for the discharging duration T_L, the current I_{b3} is reversed and by referring to Fig. 5.17 (b), (5.10) can be solved as:

$$V_{TL} - V_{TH} = \frac{T_L^{\alpha}}{\Gamma(1+\alpha)}\frac{-I_{b3}}{C_\alpha} \tag{5.14}$$

Substituting the values of V_{TH} and V_{TL} as $I_{b2}R_2$ and $-I_{b2}R_2$ respectively in (5.14), T_L is obtained as:

$$T_L = \left[\frac{2I_{b2}R_2C_\alpha\Gamma(1+\alpha)}{I_{b3}}\right]^{\frac{1}{\alpha}} \tag{5.15}$$

Total time period of oscillation (T_α) can be obtained by adding T_H and T_L. The frequency of oscillation (f_α) is the reciprocal of (T_α).

$$T_\alpha = T_H + T_L = 2\left[\frac{2I_{b2}R_2C_\alpha\Gamma(1+\alpha)}{I_{b3}}\right]^{\frac{1}{\alpha}}, \quad f_\alpha = \frac{1}{T_\alpha} \tag{5.16}$$

Due to the fact that the magnitude of charging and discharging currents are same, the duty cycle of the generated waveforms is 50%. The amplitude of the square wave at the output node V_{O1} is $L_\pm$ and equals to $\pm I_{b1}R_1$, can be controlled electronically with the help of bias current of OTA_1 (I_{b1}). Further, T_α can be electronically controlled using the bias current of OTA_3 (I_{b3}), thus one can say that the amplitude of the square wave and T_α can be tuned independently. From (5.16), it is clear that T_α can also be controlled using fractional-order α. Hence α provides an extra degree of freedom.

For the case of integer-order capacitor, 1 is placed as the value of α in (5.16) and the time period and frequency of oscillation of integer-order multivibrator is obtained as below:

$$T = \frac{4I_{b2}R_2C}{I_{b3}}, \quad f = \frac{1}{T} \tag{5.17}$$

5.4.2 Functional Verification

To prove the concept of the proposed fractional-order multivibrator, SPICE simulations have been carried out with 180 nm CMOS technology model parameters. The supply voltages are taken as $\pm 1.8\ V$. The values of R_1 and R_2 are taken the same and equal to 50 $k\Omega$. Section 2.4 provides the details of the transistors used in OTA, and its corresponding CMOS schematic is illustrated in Fig. 2.8 (b). The FOC utilized in the proposed fractional-order multivibrator is realized using the R-C ladder network based on 7^{th} order Valsa's algorithm and shown in Fig. 2.5 [116]. The values of passive components to realize FOC with $\alpha = 0.5$, 0.8 and $C_\alpha = 1\ \mu\mho sec^\alpha$ are given in Table 2.3.

Figure 5.18 shows the waveforms at the output terminals V_{O1} and V_{O3} for two different values of α (i.e., 0.5 and 0.8). The bias currents I_{b1}, I_{b2} and I_{b3} are taken as 25 μA, 25 μA and 100 μA respectively, while C_α is taken as 1 $\mu\mho sec^\alpha$ for both the values of α.

Simulation results for the time period of the proposed fractional-order multivibrator for α=0.5, 0.8 and 1 with I_{b3} swept from 20 μA to 120 μA are listed in Table 5.8. The values of I_{b1} and I_{b2} are taken same and equal to 25 μA. It can be interpreted from Table 5.8 that the proposed fractional-order multivibrator has lower time period and hence higher frequency than integer-order multivibrator for the same value of I_{b3}. For example, for $I_{b3} = 120\ \mu A$, the frequency of the proposed fractional-order multivibrator is about 125 times higher than that of integer-order multivibrator. The graph between time period and I_{b3} for $\alpha = 0.5$ and 0.8 is shown in Fig. 5.19. It may be observed from (5.16), as α increases, the term $(1/\alpha)$ in the

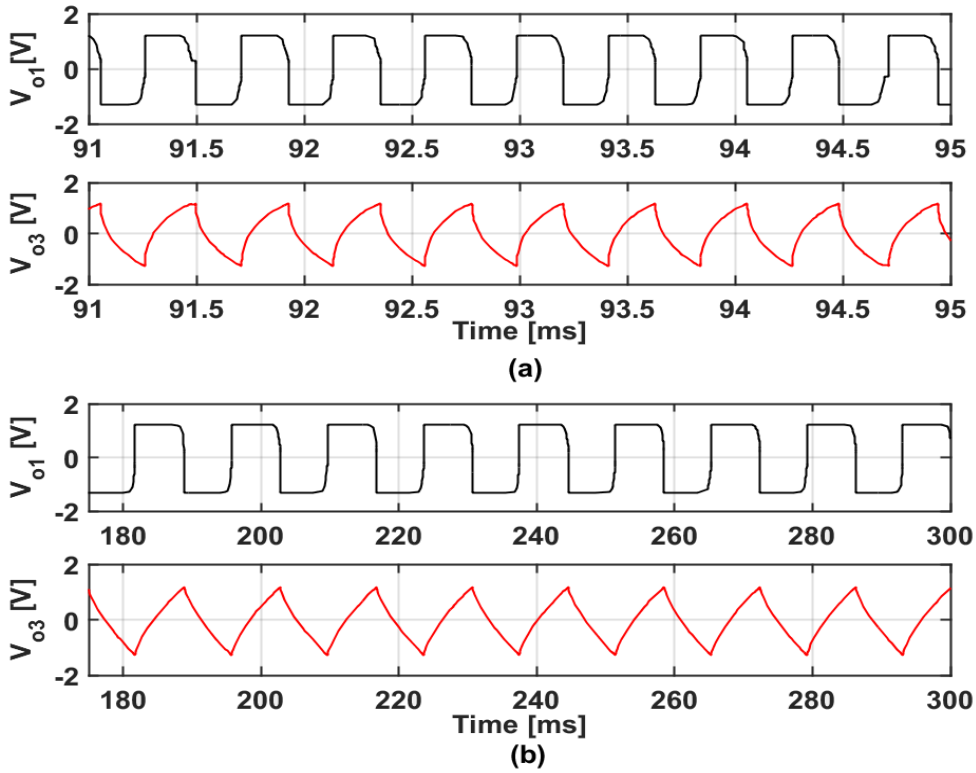

Figure 5.18: The time domain responses for I_{b1}=I_{b2}=25 μA and I_{b3}=100 μA (a) α=0.5 (b) α=0.8

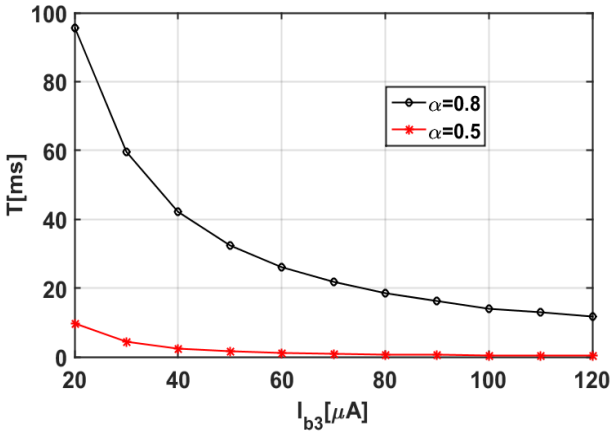

Figure 5.19: Time period with respect to bias current I_{b3} with I_{b1}=I_{b2}=25 μA

exponent decreases, which causes the curve to approach its asymptotic limit more quickly.

Further, to examine electronic tuning of T_α of the proposed fractional-order multivibrator, the output V_{O1} are shown in Fig. 5.20 for four different values of

Table 5.8: Variation of simulated time period with bias current I_{b3}

Bias current $I_{b3}(\mu A)$	Time period (ms)		
	α=0.5	α=0.8	α=1 Integer-order capacitor
20	9.42	95.17	228.60
30	5.20	58.81	154.29
40	2.40	41.44	116.87
50	1.60	31.62	94.27
60	1.13	25.44	79.05
70	0.84	21.22	68.18
80	0.65	18.16	60.00
90	0.53	15.85	53.63
100	0.47	14.04	48.51
110	0.37	12.59	44.38
120	0.33	11.40	40.88

I_{b3} i.e., 40 μA, 60 μA, 80 μA and 100 μA. The values of I_{b1} and I_{b2} are taken same and equal to 25 μA with α=0.5 and C_α=1 $\mu\mho sec^\alpha$. The T_α decreases as I_{b3} increases but the amplitude of the square wave remains unchanged.

To test independent electronic control over the amplitude of square wave V_{O1}, I_{b1} is swept form 8 μA to 26 μA and the bias currents I_{b2} and I_{b3} are taken as 25 μA and 100 μA respectively. The graph between amplitude of V_{O1} and I_{b1} is shown in Fig. 5.21 for α=0.5 and 0.8. It is clear from the graph that the amplitude of square wave is directly proportional to I_{b1} and does not depend upon the value of α.

The T_α of the proposed fractional-order multivibrator can also be controlled using R_2 while R_1 determines the amplitude of the waveform. Figure 5.22 shows the waveform at output V_{O1} for three different values of R_1 and R_2 (i.e., (a) R_1=R_2=5 $k\Omega$ (b) R_1=R_2=15 $k\Omega$ (c) R_1=R_2=25 $k\Omega$). It is clear from Fig. 5.22, amplitude of the square waveform shows an upward trend with increasing R_1 and

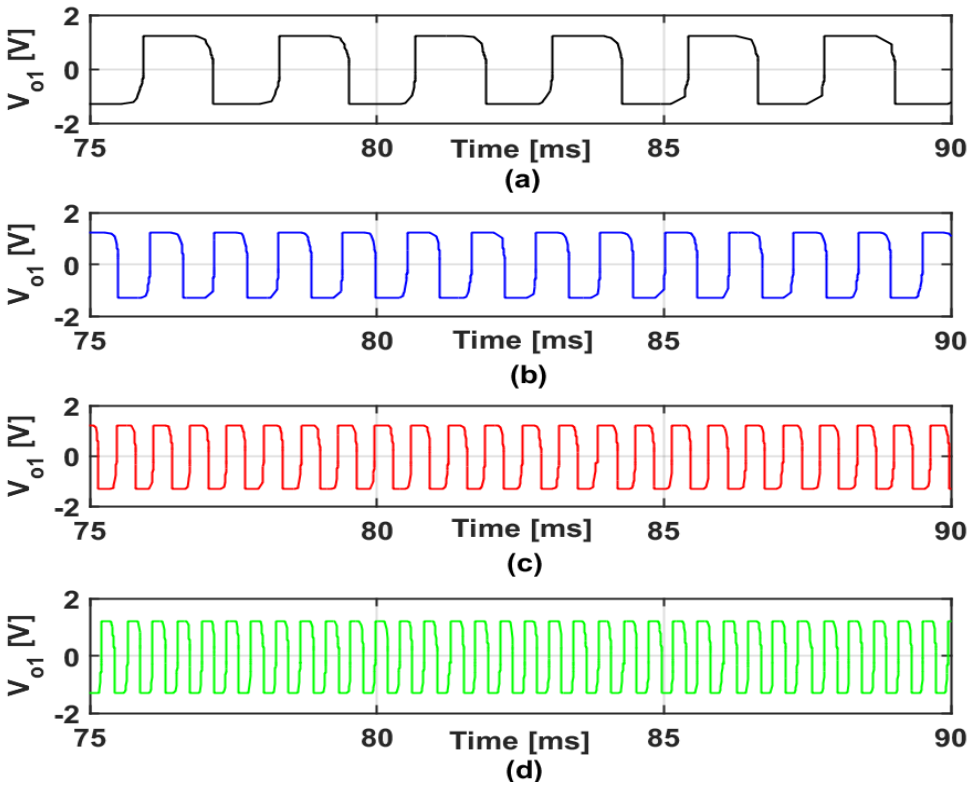

Figure 5.20: The time domain responses for I_{b1}=I_{b2}=25 μA and α=0.5 (a) I_{b3}=40 μA (b) I_{b3}=60 μA (c) I_{b3}=80 μA (d) I_{b3}=100 μA

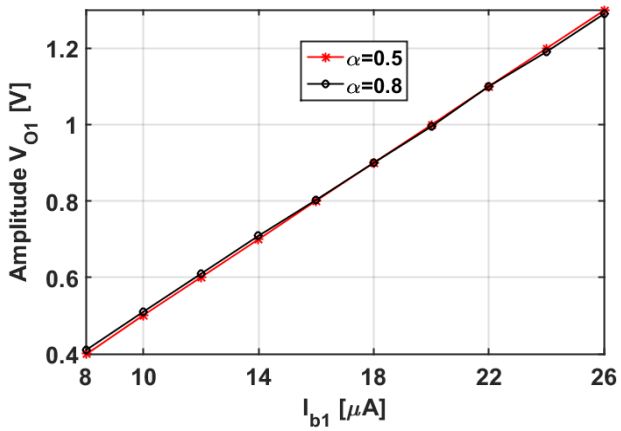

Figure 5.21: Square wave amplitude (V_{O1}) against bias current I_{b1} with I_{b2}=25 μA, I_{b3}=100 μA

time period also rises with increase in R_2.

The simulation has also been carried out to find out minimum and maximum frequencies of the proposed fractional-order multivibrator. To determine the minimum frequency of the proposed fractional-order multivibrator (i.e., maximum time period),

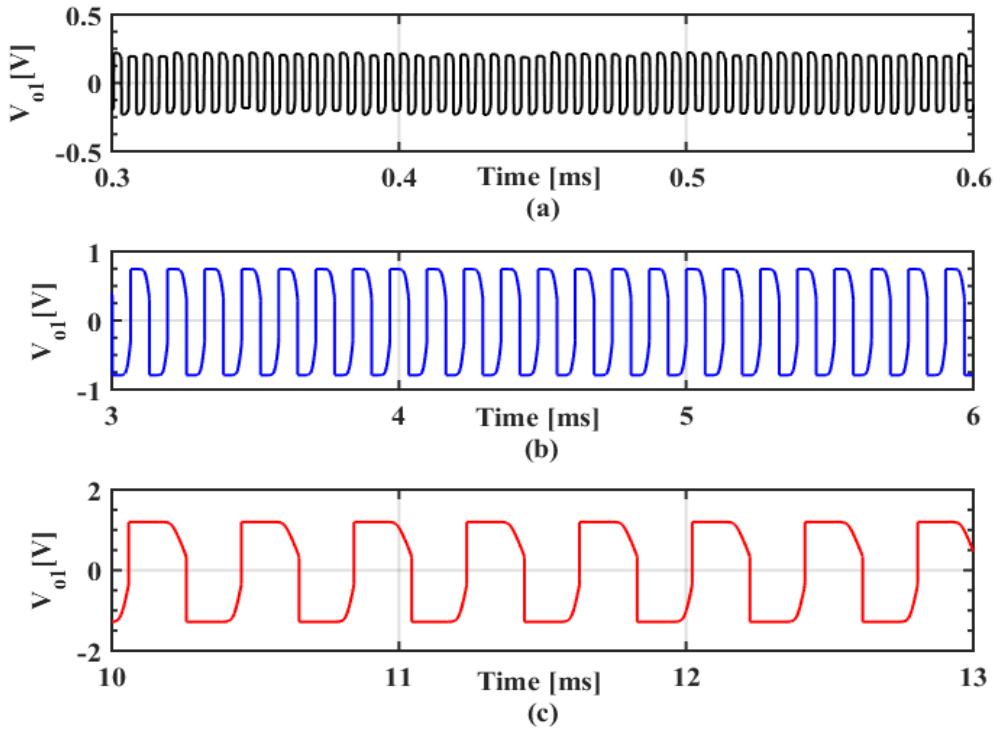

Figure 5.22: The time domain responses for I_{b1}=I_{b2}=50 μA, I_{b3}=100 μA and α=0.5 (a) R_1=R_2=5 $k\Omega$ (b) R_1=R_2=15 $k\Omega$ (c) R_1=R_2=25 $k\Omega$

the charging current of C_α (i.e., I_{b3}) must be minimized but should be large enough to saturate OTA_1. Whereas the comparison voltage V_{O2} must be maximize so that the time taken by C_α to charge the node V_{O3} upto voltage V_{O2} will be high.

In the same way, to determine the maximum frequency of the oscillator (i.e., minimum time period), C_α should be charged fast i.e., I_{b3} must be increased (considering the maximum current sourcing/sinking capability of OTA) and to minimize the time taken by C_α to charge, comparison voltage V_{O2} must be minimum but large enough to saturate OTA_1. The simulation settings to calculate the same are listed down in Table 5.9. The minimum and maximum frequencies of the proposed fractional-order multivibrator are found to be approximately 10 Hz and 750 kHz respectively.

Table 5.9: Simulation settings for calculating minimum and maximum frequencies

	I_{B1}, R_1	I_{B2}, R_2	I_{B3}	C_α,α
Minimum Frequency	25 μA, 20 $k\Omega$	90 μA, 20 $k\Omega$	8 μA	1 μF, 0.5
Maximum Frequency	25 μA, 20 $k\Omega$	10 μA, 10 $k\Omega$	200 μA	1 μF, 0.5

5.4.3 Robustness

To examine the robustness of the proposed fractional-order multivibrator, corner analysis and Monte-Carlo analysis are done, the same are discussed below.

5.4.3.1 Corner analysis

The performance of the proposed fractional-order multivibrator is analysed at all process corners (i.e.,FF, FS, TT, SF and SS) for I_{b1}=I_{b2}=25 μA, I_{b3}=100 μA, α=0.5 and C_α=1 $\mu\mho sec^\alpha$. The values of time periods and percentage error from TT corner point, for the remaining four corner points are listed in Table 5.10. It is clear from the Table 5.10 that the percentage error lies within 0.15%, which verifies the robustness of the circuit against various corners.

Table 5.10: Time period of square wave at node (V_{O1}) and % error from TT corner for all five process corners

	FF	FS	TT	SF	SS
Time period (μs)	469.25	468.06	468.67	469.34	468.74
% error from TT corner	0.123%	0.131%	–	0.142%	0.015%

5.4.3.2 Monte-Carlo analysis

To get an insight on sensitivity of the proposed fractional-order multivibrator with respect to C_α, uniform Gaussian distribution and $\pm 5\%$ tolerance in resistances and capacitances values used for C_α realization is considered and Monte-Carlo analysis is performed on 500 random samples. The distribution of time period of V_{O1} for all the samples is shown in Fig. 5.23. The mean and standard deviation is found to be 0.466 ms and 0.0426 ms respectively. It is observed from the above analysis that the spread in time period of oscillation is within a small range and the mean is matched with the corresponding time period of oscillation (i.e. 0.4687 ms) within 0.6% error, which verify the smaller component sensitivity of the proposed fractional-order multivibrator.

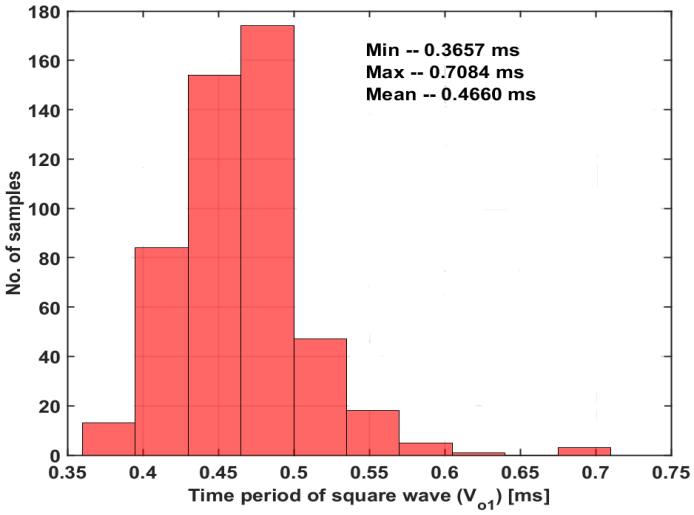

Figure 5.23: Monte Carlo Analysis of proposed fractional-order multivibrator for random variations in C_α

5.4.4 Applications

As discussed in Section 5.4.2, that the proposed fractional-order multivibrator may be a good choice over integer-order multivibrator for high frequency oscillation requirement. In modulation process, a high frequency carrier signal is required to modulate the message signal. Therefore, the proposed fractional-order multivibrator can play a crucial role in generating high-frequency oscillation signals for modulation purposes. Hence, this subsection explores the application of the proposed fractional-order multivibrator to implement various modulation circuits such as amplitude modulators (AM), frequency modulators (FM), delta modulators (DM), and sigma-delta modulators (SDM), as presented in [138]. Additionally, the electronic tuning feature of the proposed fractional-order multivibrator is also examined to adjust the modulation index of analog modulators, such as amplitude modulator and frequency modulator.

5.4.4.1 Amplitude modulator

In amplitude modulation, the information signal is encoded in a carrier wave by varying its instantaneous amplitude. From Section 5.4.2, it is observed that the amplitude of output V_{O1} of the proposed fractional-order multivibrator can be electronically controlled by bias current of OTA_1 (I_{b1}). If the information signal ($I_{m(t)}$) is applied as I_{b1}, superimposed on a DC offset current (I_{offset}) such that $(I_{offset}) \geq |(I_{m(t)})|_{min}$, then the proposed fractional-order multivibrator works as amplitude modulator.

To verify the working of the proposed fractional-order multivibrator as an amplitude

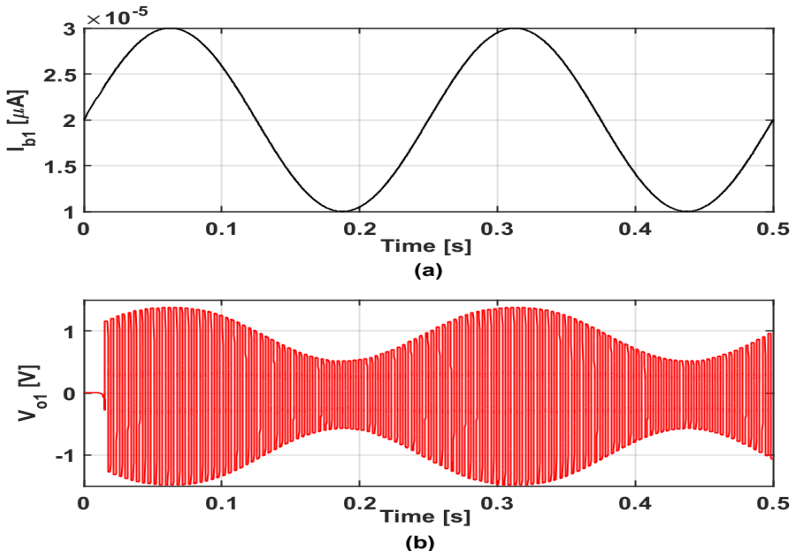

Figure 5.24: Square wave amplitude modulation with I_{b2}=25 μA, I_{b3}=50 μA and α=0.5 (a) Information signal (b) AM signal

modulator, a sinusoidal information signal, peak to peak amplitude of 10 μA and frequency of 4 Hz, with a DC offset current equals to 20 μA is applied as the bias current of OTA_1 (I_{b1}). The values of I_{b2}, I_{b3}, C_α and α are taken as 25 μA, 50 μA, 1 $\mu\mho sec^\alpha$ and 0.5 respectively. The information signal I_{b1} and amplitude modulated signal V_{O1} are shown in Fig. 5.24 and it is observed that the amplitude of modulated signal is varying according to the amplitude of information signal.

For a special case of single-frequency sinusoidal information signal $I_{m(t)} = I_m cos(\omega_m t)$, the relative proportion of information signal's magnitude ($|I_{m(t)}|$) and carrier signal's magnitude ($|I_{offset}|$) is defined as modulation index (m) of AM waveform. The modulation index can be tuned to a desired value by setting I_{offset}. The variation of AM modulation index m with respect to I_{offset} for $|I_{m(t)}|$ = 5 μA, C_α=1 $\mu\mho sec^\alpha$ and α=0.5 is shown in Fig. 5.25.

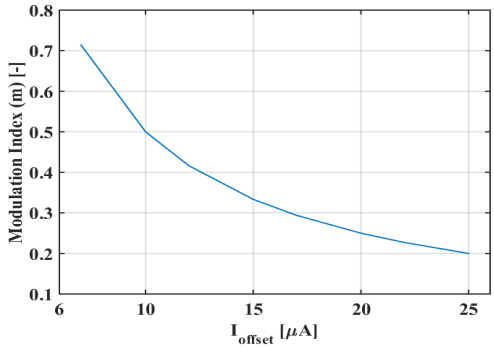

Figure 5.25: AM modulation index (m) Vs I_{offset} for $|Im(t)|$=5 μA

5.4.4.2 Frequency modulator

In frequency modulation, the information signal is encoded in a carrier wave by varying its instantaneous frequency. As derived in Section 5.4.2, the frequency of oscillation of the proposed fractional-order multivibrator can be electronically controlled by using I_{b2} and/or I_{b3}. If the sinusoidal information signal ($I_m(t)$) superimposed on a DC offset signal (I_{offset}) is applied as the bias current of OTA_3, then the proposed fractional-order multivibrator works as frequency modulator. The instantaneous frequency of frequency modulator circuit is given as:

$$f_\alpha(t) = \frac{1}{2}\left[\frac{I_m(t)}{2I_{b2}R_2C_\alpha\Gamma(1+\alpha)}\right]^{\frac{1}{\alpha}} \tag{5.18}$$

The changing ratio of the output frequency to the information signal is defined as the modulation sensitivity (k_f) and given by (5.19).

$$k_f = \frac{\Delta f}{\Delta I_{m(t)}} = \frac{1}{2\alpha}\left[\frac{(2f_\alpha)^{(1-\alpha)}}{2I_{b2}R_2C_\alpha\Gamma(1+\alpha)}\right] \tag{5.19}$$

For a special case of single-frequency sinusoidal information signal $I_{m(t)} = I_m cos(\omega_m t)$, the modulation index β of frequency modulator is defined as:

$$\beta = (k_f I_m)/f_m \tag{5.20}$$

Where f_m is the frequency of the information signal in Hertz ($f_m = \omega_m/2\pi$). In order to get frequency modulated signal, a sinusoidal information signal of peak to peak amplitude 20 μA, superimposed on a DC offset of 50 μA is applied as the bias current of OTA_3 (I_{b3}). The values of I_{b1} and I_{b2} are taken as same and equal to 25 μA while the value of α is taken as 0.5. Figure 5.26 shows the information signal I_{b3} and frequency modulated signal V_{O1}. It is clear from Fig. 5.26 that as the amplitude of information signal is increased the frequency of modulated signal is increased and for minimum amplitude of information signal the frequency of modulated signal is also minimum.

It is clear from (5.19), that k_f depends on I_{b2} and α, and modulation index β is directly proportional to k_f. The variation of FM modulation index β with respect to I_{b2} and α is shown in Fig. 5.27 (a) and (b) respectively for $|I_{m(t)}|$=20 μA and C_α=1 $\mu \mho sec^\alpha$.

5.4.4.3 Delta modulator

Pulse code modulation (PCM) is the fundamental technique for digital modulation, but data redundancy in encoding digital signal is the key shortcoming of PCM.

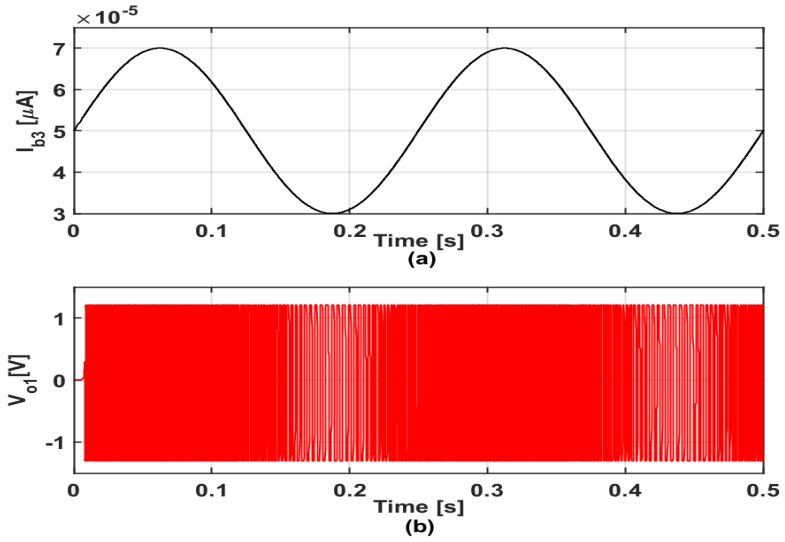

Figure 5.26: Square wave frequency modulation with I_{b1}=I_{b2}=25 μA and α=0.5 (a) Information signal (b) FM signal

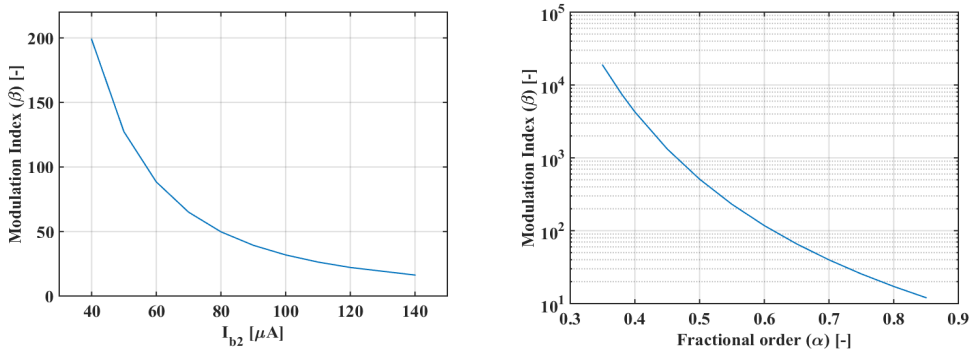

(a) (b)

Figure 5.27: FM modulation index (β) for $|I_{m(t)}|$=20 μA (a) with respect to I_{b2} (α=0.5) (b) with respect to α

To recover this problem, the difference between current sample and its predicted value is encoded rather than the absolute value. This technique is acknowledged as differential pulse code modulation (DPCM). Delta modulation (DM) is a special case of DPCM that produces a one-bit encoded output. Its block diagram is illustrated in Fig. 5.28.

To achieve delta modulator functionality from the proposed fractional-order multivibrator, the terminal of resistance R_2 should not be grounded, rather than an information

signal is fed to this terminal. Now, the OTA_3 and C_α construct the integrator and the information signal is compared with the output voltage of integrator (V_{O2}). The rest of the circuit constructs limiter (OTA_1 and R_1) and sampler (OTA_2) blocks. In order to get delta modulated signal, a sinusoidal signal with 4 frequency and peak to peak amplitude of $1V$ is applied as the information signal. The values of I_{b1} and I_{b2} are taken same and equal to 25 μA while the value of I_{b2} and α is taken as 50 μA and 0.5 respectively. The information signal and delta modulated signal V_{O1} are shown in Fig. 5.29.

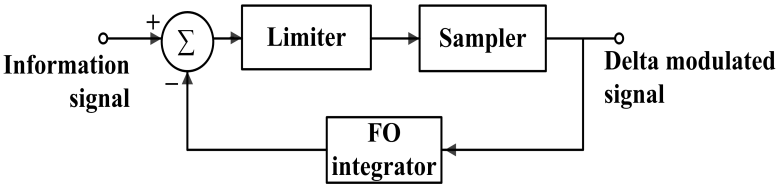

Figure 5.28: Delta modulator block diagram

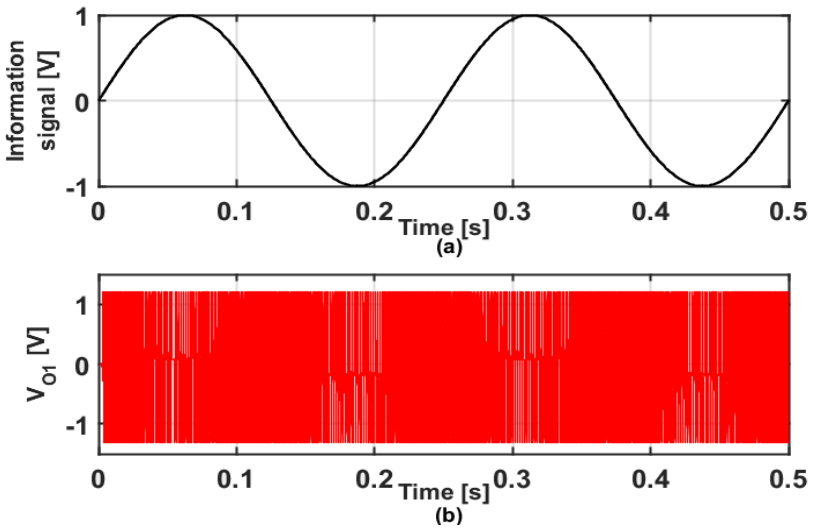

Figure 5.29: Square wave delta modulation with $I_{b1} = I_{b2}$=25 μA, I_{b3}=50 μA and α=0.5 (a) Information signal (b) DM signal

5.4.4.4 Sigma-delta modulator

The delta modulator requires integrator for demodulation process because the output is the differentiated version of the input. To avoid the integrator in demodulator, the information signal must be integrated before modulation. This modified version of delta modulator is known as sigma-delta modulator (SDM). The block diagram of sigma-delta modulator is shown in Fig. 5.30.

To achieve sigma-delta modulator functionality from the proposed fractional-order multivibrator, the negative terminal of OTA_3 should not be grounded, rather than an information signal is applied at this terminal. Now, the difference of information signal and the output signal V_{O1} is fed to the integrator. The rest of the circuit remains same as delta modulator.

In order to get sigma-delta modulated signal, a sinusoidal signal of 4 Hz frequency and 0.085 V peak to peak amplitude is applied as the information signal. The values of I_{b1}, I_{b2} and I_{b3} are taken as 10 μA, 30 μA and 100 μA respectively with α=0.5. The information signal and sigma-delta modulated signal V_{O1} are shown in Fig. 5.31.

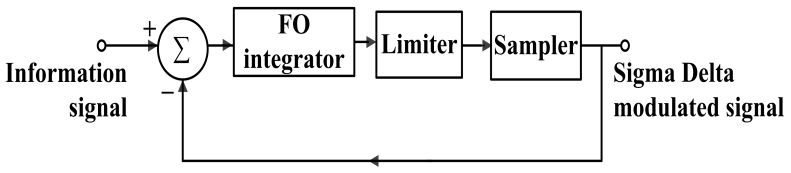

Figure 5.30: Sigma-delta modulator block diagram

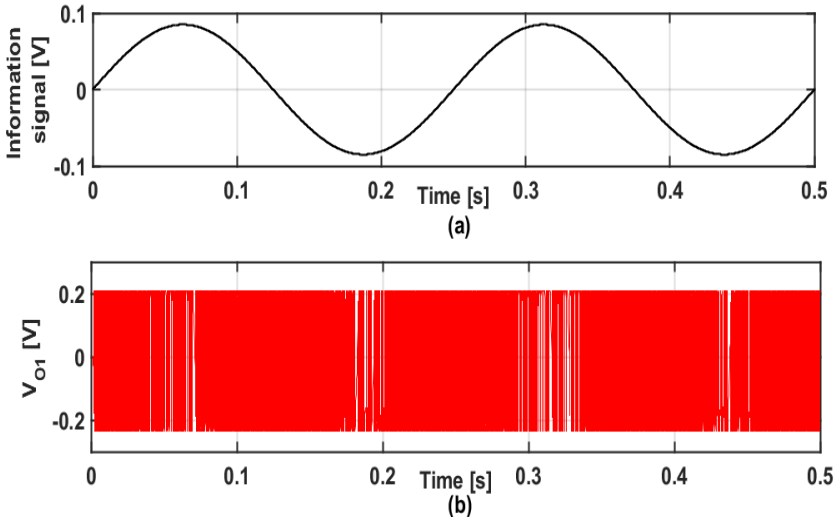

Figure 5.31: Square wave sigma delta modulation with I_{b1}=10 μA, I_{b2}=30 μA and I_{b3}=100 μA and α=0.5 (a) Information signal (b) SDM signal

5.5 Conclusion

In this chapter OTA-based three sinusoidal FOOs and one fractional-order multivibrator are proposed. The first two circuits of the sinusoidal FOO are designed using the trans-admittance mode FAPF with a trans-impedance mode integrator/differentiator. Additionally, the third circuit of the sinusoidal FOO features a unique design that enables independent control of the phase difference between its two output voltages. All the three circuits of sinusoidal FOO are verified through SPICE simulations using 180 nm CMOS technology node. The stability is verified using pole plots with the help of *forlocus* function of MATLAB. The mathematical equations for sensitivity of the oscillation frequency with respect to various circuit parameters has been derived and found that the proposed circuits are lesser sensitive towards higher values of fractional-order α. The robustness of the proposed FOO circuits has also been examined via PVT and Monte-Carlo analyses and no abrupt changes have been found in the transient responses of the proposed circuits. The

sinusoidal FOO circuit I, has also been verified to work in VLF mode.

Further, an electronically tunable fractional-order multivibrator based on OTA has been generalized in fractional domain. The mathematical formula for time period of the proposed fractional-order multivibrator has been derived and verified through SPICE simulations. The oscillation period and the amplitude of the output square wave are electronically tunable and can be controlled independently without affecting the other parameter. The robustness of the circuit is scrutinized through corner and Monte-Carlo analyses. The use of the FOC facilitated the proposed fractional-order multivibrator to have very high frequency of oscillation using standard values of circuit components. The capability of generating high frequency oscillations make the proposed fractional-order multivibrator a superior choice over integer-order multivibrator for the applications such as various modulation techniques. Thus, AM, FM, DM and SDM have been explored and verified as application of the proposed fractional-order multivibrator. The adjustment of the modulation index of analog modulators (AM and FM) has also been examined.

Chapter 6

Realization of Simpler and Higher order FOEs

This chapter presents the results and content of the following papers:

[1] **G. Varshney,** N. Pandey and R. Pandey, "Realization of IIMC based Higher-Order Floating Fractional-Order Element," in First International Conference on Emerging Trends in Industry 4.0 (2021 ETI 4.0). Under publication in IEEE proceedings.

[2] **G. Varshney,** N. Pandey and R. Pandey, "Fractional-order Capacitor Realization Based upon Active Inductor," in 9th International Conference on Signal Processing and Integrated Networks (SPIN 2022). Under publication in "Advanced IoT Sensors, Networks and Systems" part of the book series "Lecture Notes in Electrical Engineering (LNEE, volume 1027)".

6.1 Introduction

As discussed in the previous chapters, FOE is a fundamental component for designing the fractional-order analog circuits. To design fractional-order systems with higher-order, FOE with fractional order α greater than 1 is utilized. The method to realize FOE with fractional order α ($0<\alpha<1$) based on R-C ladder network has already been discussed in Chapter 2.

This chapter is devoted to implement a simpler scheme for the realization of FOC and a floating version of the higher order FOE ($1<\alpha<2$). First, a simple circuit of active inductor is proposed to approximate the behavior of FOC. The circuit is modular in nature, thus allows for the higher order approximations through parallel connection or impedance multiplication to realize FOC. Further, a circuit is presented to implement a floating version of the higher order FOE ($1<\alpha<2$) using OTA-based IIMC [53].

6.2 Simpler Design of FOC Using Active Inductor Circuit

In Fig. 6.1, an active inductor circuit is presented, which employs one NMOS transistor (M_1), two resistors (R_1 and R_2), and a grounded capacitor (C_1). This circuit is the modified version of the one introduced in [46], where a PMOS transistor is used with two resistors and a floating capacitor. However, the proposed circuit is better than the one in [46] because it employs an NMOS transistor,

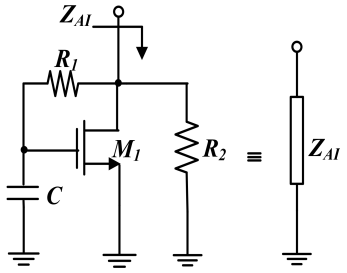

Figure 6.1: Proposed active inductor circuit

which offers advantages in terms of mobility and fabrication process. Moreover, the proposed circuit uses a grounded capacitor, which has simpler fabrication steps than the floating capacitor. Using routine network analysis, the input impedance of the proposed active inductor is obtained and given in (6.1).

$$Z_{AI} = \frac{R_2(1 + sC_1R_1)}{1 + g_{m1}R_2 + sC_1(R_1 + R_2)} \tag{6.1}$$

Here g_{m1} is the small signal transconductance of transistor M_1. Equation (6.1) can be rewritten as:

$$Z_{AI} = \frac{R_1R_2}{R_1 + R_2}.\left[\frac{s + \frac{1}{C_1R_1}}{s + \frac{(1+g_{m1}R_2)}{C_1(R_1+R_2)}}\right] = K.\left[\frac{s + \omega_z}{s + \omega_p}\right] \tag{6.2}$$

The zero and pole frequency of the proposed active inductor are defined as $\omega_z = \frac{1}{C_1R_1}$ and $\omega_p = \frac{(1+g_{m1}R_2)}{C_1(R_1+R_2)}$ respectively.

The input impedance of proposed active inductor, can be utilized to synthesis FOC by appropriately interconnecting multiple such sections, due to its ability to set zero and pole frequencies with certain spacing, allowing for the creation of an unlimited series of alternating roots on the real axis in the complex plane [41].

6.2.1 Higher Order Approximations to Realize FOC

As discussed above that the proposed active inductor can be utilized for the higher order approximations to synthesis FOC. The proposed active inductor can be inteconnected through parallel connection or impedance multiplication to approximate a FOC. According to [116], at least a second-order transfer function is required to approximate a FOC, which is suitable for realizing narrowband applications, such as FOOs [139]. The location of the pole and zero of the proposed active inductor can be adjusted by selecting appropriate values of passive components and transconductance gain of transistor M_1. However, it is important to maintain the pole-zero interlacing, i.e., $\omega_{p1} < \omega_{z1} < \omega_{p2} < \omega_{z2}$ [116]. There are two general methods for higher-order approximations to realize FOC, which are discussed below:

6.2.1.1 Parallel connection of impedances

First method to achieve higher-order approximations to realize a FOC involves parallel connection of n stages of the proposed active inductor, as illustrated in Fig. 6.2 (a). Each stage contributes a pair of pole and zero, and at least two poles and two zeros are required to approximate a FOC. These poles and zeros should be placed alternatively. The total input admittance of this scheme is given as:

$$Y_{in} = \Sigma_{i=1}^{n} \frac{1}{Z_{AIi}}, \qquad i = 1, 2...n \tag{6.3}$$

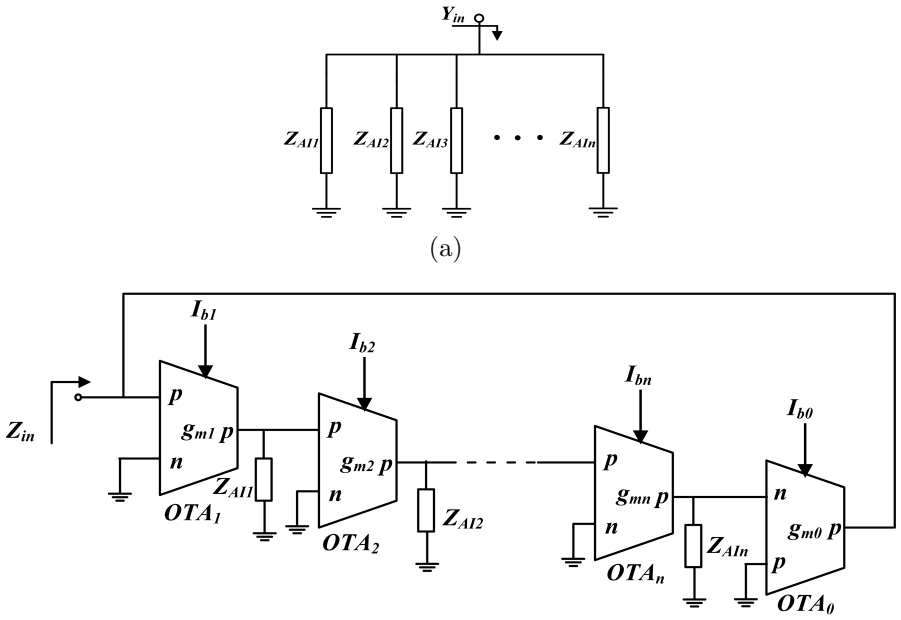

Figure 6.2: Higher order approximation of FOC (a) Parallel connection of impedances (b) Impedance multiplication

Z_{AI} is given in (6.2).

6.2.1.2 Impedance multiplication

Another method involves multiplying n stages of the proposed active inductor using a generic circuit of impedance multiplier shown in Fig. 6.2 (b). This impedance multiplier circuit is based on OTA and is inspired by [53]. It has several advantages over Opamp based GICs, such as all impedances are grounded, and it can multiply n numbers of impedances. The total input impedance of this scheme is given as:

$$Z_{in} = \frac{1}{g_{m0}\Pi_{i=1}^{n} g_{mi} Z_{AIi}}, \qquad i = 1, 2...n \tag{6.4}$$

Z_{AI} is given in (6.2).

The order of approximation required to realize the FOC can be set by setting the value of n; e.g. for a second order approximation of FOC, n is set as 2. To calculate the values of poles and zeros of the approximated FOC of the required magnitude and phase, the Valsa's algorithm [116] is used (refer chapter 2).

6.2.2 Functional Verification

To validate the performance of the approximated FOC based on proposed active inductor, SPICE simulations are conducted using 180 nm CMOS technology parameters. Figures 6.3 (a) and (b) show the magnitude and phase responses of a second-order approximation of FOC using the first method, which involves parallel connection of two active inductors (n=2 in Fig. 6.2 (a)), for phase angles (ϕ)= $-$ 30° and $-45°$, respectively. The values of various components used to realize the FOCs with ϕ= $-30°$ and $-45°$ are provided in Table 6.1. The theoretical slopes of the magnitude response iare -6.66 dB/decade and -10 dB/decade for ϕ=$-30°$ and $-45°$ respectively, while the simulated slopes are -7.1 dB/decade and -9.6 dB/decade, for ϕ= $-$ 30° and $-45°$, respectively. The percentage error in the slope is within 6% and the error in the phase response is within 5% for both the cases, indicating good agreement between the simulated and theoretical results.

Further, second-order approximation of FOC using the second method to realize higher order approximation (i.e., impedance multiplier) has been implemented,

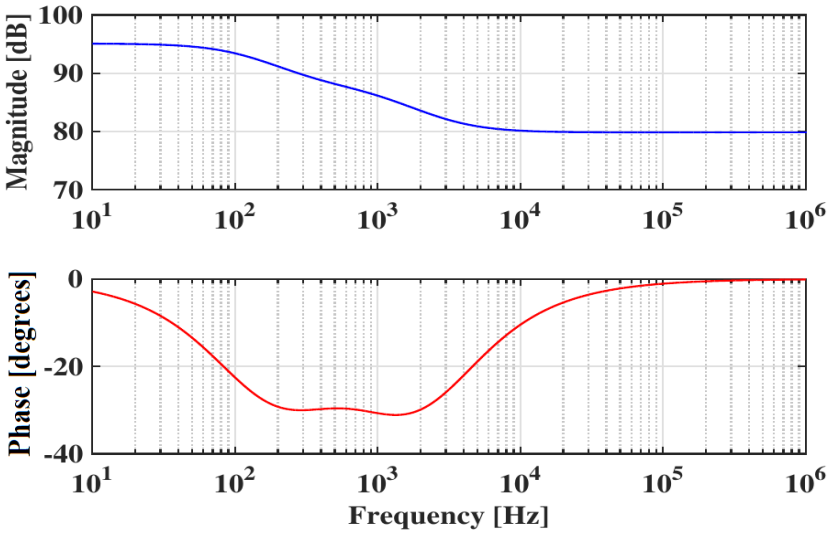

(a)

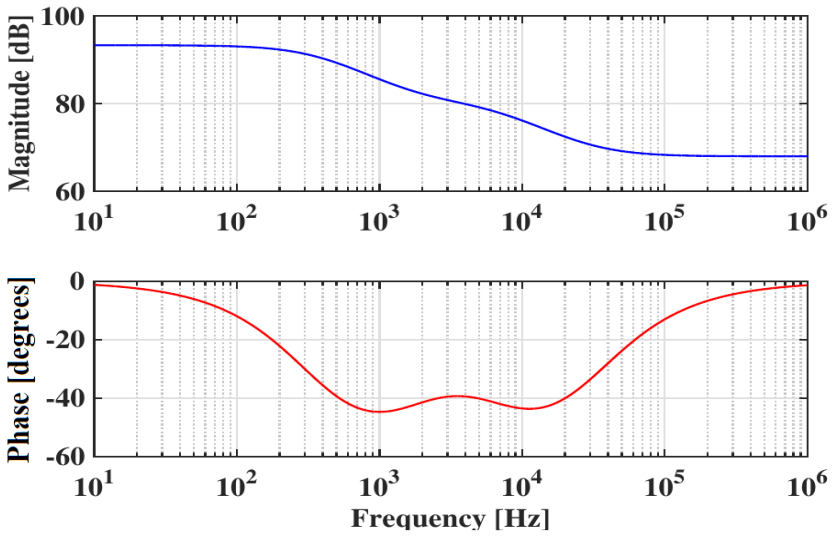

(b)

Figure 6.3: Simulation results for second order approximation of FOC based upon two stage parallel connection of active inductor for (a) $\phi = -30°$ (b) $\phi = -45°$

Table 6.1: Simulation settings for two stage parallel connection of active inductor to realize FOC

# Stage	Component	$\phi = -30°$ (α=1/3)	$\phi = -45°$ (α=1/2)
-	$(W/L)_{1,2}$	10	10
Z_{AI1}	C	17.5 nF	7 nF
	R_1	40 $k\Omega$	15 $k\Omega$
	R_2	140 $k\Omega$	130 $k\Omega$
Z_{AI2}	C	5 nF	1.9 nF
	R_1	13 $k\Omega$	3 $k\Omega$
	R_2	70 $k\Omega$	65 $k\Omega$

again the value of n is taken as 2 in Fig. 6.2 (b). Section 2.4 provides the aspect ratios of the transistors used in OTA, and its corresponding CMOS schematic is depicted in Fig. 2.8 (b). The transconductance values of all three OTAs are set to be the same, with a value of 61 $\mu A/V$. The component settings to realize the FOC with $\phi = -30°$ and $-45°$ are given in Table 6.2. The magnitude and phase responses are shown in Figs. 6.4 (a) and (b) for phase angle $\phi = -30°$ and $-45°$ respectively. The theoretical slopes of the magnitude response are -6.66 dB/decade and -10 dB/decade for $\phi = -30°$ and $-45°$ respectively, while the simulated slopes are -7 dB/decade and -9.3 dB/decade for $\phi = -30°$ and $-45°$ respectively. The percentage error in the slope is within 6%. The error in the phase response is within 7% for both the cases.

6.2.3 Application as in FOO

The proposed FOC (two stage parallel connection of active inductor with $\phi = -45°$) has been tested for the functionality, by using it in an OTA-based FOO application (proposed in section 5.3), as shown in Fig. 6.5 for quick reference. The phase

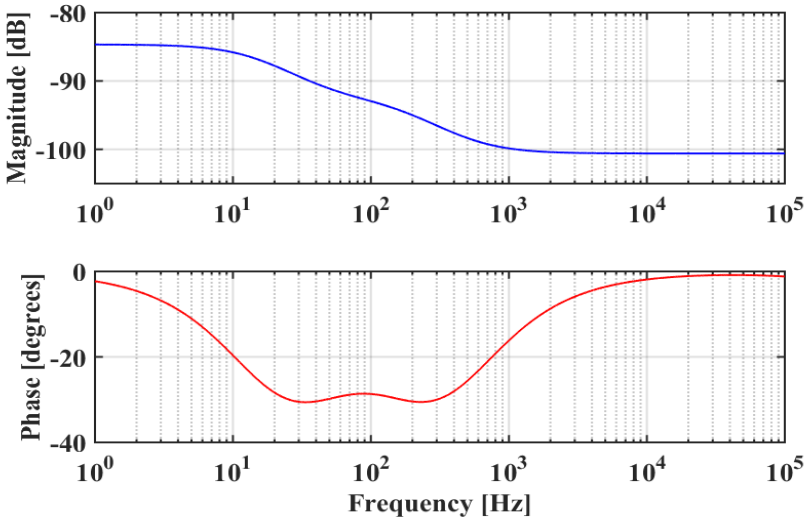

(a)

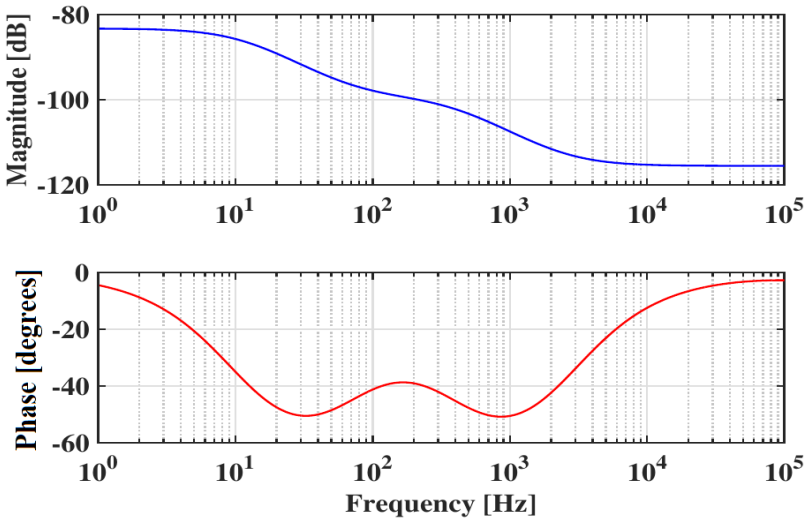

(b)

Figure 6.4: Simulation results for second order approximation of FOC based upon impedance multiplication of two active inductor for (a) $\phi = -30°$ (b) $\phi = -45°$

difference between two output voltages (V_{O1} and V_{O2}) is equal to $\frac{\beta\pi}{2}$. The FOO's frequency of oscillation (FO) and condition of oscillation (CO) are given below:

$$\textbf{FO:} \quad \omega_0 = \left[\frac{g_{m1}\ sin\frac{\beta\pi}{2}}{C_\alpha \sin\frac{(\alpha+\beta)\pi}{2}}\right]^{\frac{1}{\alpha}} \tag{6.5}$$

Table 6.2: Simulation settings for two stage impedance multiplier circuit of realize FOC

# Stage	Component	$\phi = -30^\circ$ (α=1/3)	$\phi = -45^\circ$ (α=1/2)
-	$(W/L)_{1,2}$	10	10
Z_{AI1}	C	49 nF	33 nF
	R_1	7 $k\Omega$	2.4 $k\Omega$
	R_2	18 $k\Omega$	10 $k\Omega$
Z_{AI2}	C	220 nF	480 nF
	R_1	10 $k\Omega$	4.8 $k\Omega$
	R_2	27 $k\Omega$	25 $k\Omega$

$$\textbf{CO:} \qquad g_{m1} = \left[\frac{C_\alpha \ sin\frac{(\alpha+\beta)\pi}{2}}{sin\frac{\beta\pi}{2}}\right]\left[\frac{g_{m2}}{C_\beta\left(cos\frac{\beta\pi}{2} - \frac{sin\frac{\beta\pi}{2}}{tan\frac{\alpha+\beta\pi}{2}}\right)}\right]^{\frac{\alpha}{\beta}} \tag{6.6}$$

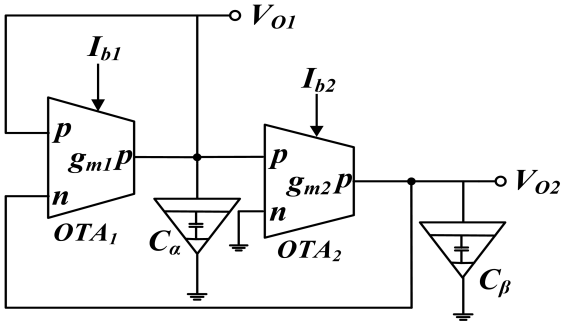

Figure 6.5: Circuit diagram of fractional-order oscillator (FOC used is two stage parallel connection of active inductor with $\phi = -45^\circ$)

The FOO is designed for FO=1 kHz and a phase difference of 45° between V_{O1} and V_{O2}. The values of C_α and C_β are set to be same and equal to 1.65 $\mu\mho sec^\alpha$ with α=β=0.5. The value of g_{m1} is set as 185 μA/V and the value of g_{m2} required to satisfy the CO is calculated as 92.5 μA/V. The transient response and frequency spectrum of the FOO are shown in Fig. 6.6. The simulated FO is observed as 1069 Hz. The error between the simulated and designed value of FO is within 7%. The transient response of V_{O1} and V_{O2} is shown in Fig. 6.7, which verifies that the phase difference between the two voltages is 44°. The error between the simulated

and theoretical value of phase difference is 2.22%.

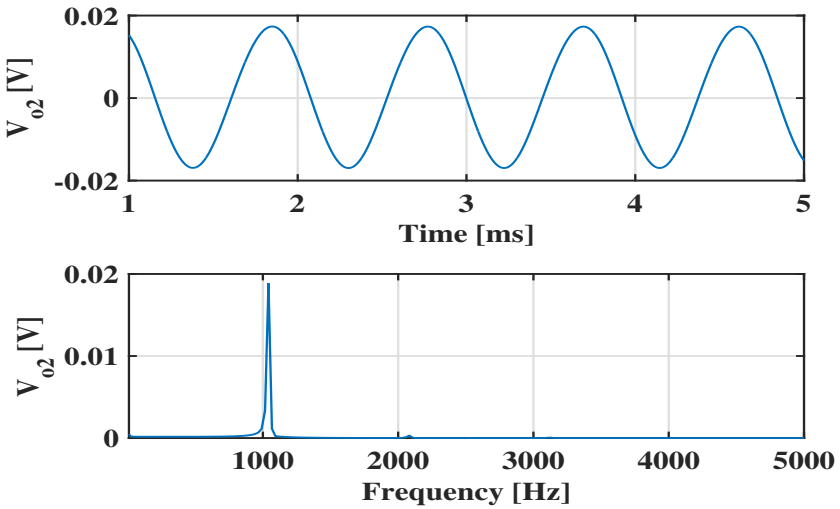

Figure 6.6: FOO's transient response and frequency spectrum for α=β=0.5

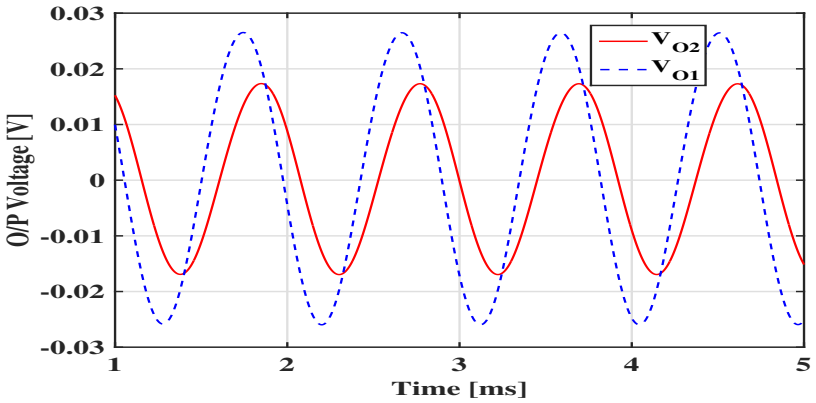

Figure 6.7: Transient response of V_{O1} and V_{O2} for α=β=0.5

6.3 Floating Higher-Order FOEs Using IIMC Structure

In this section, a floating higher-order FOE using the inverted impedance multiplier circuit (IIMC) is presented. The grounded IIMC structure [53] is modified to realize a floating IIMC structure, which is shown in Fig. 6.8. By taking into account the port relationships of the OTA and performing routine network analysis,

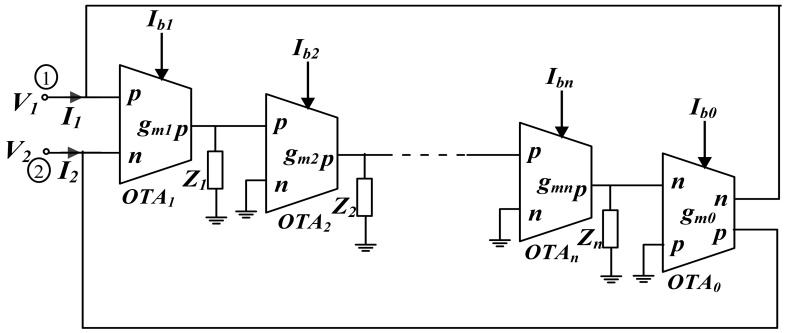

Figure 6.8: Generalized floating IIMC

the input impedance between its input terminal (i.e., terminals 1 and 2) is given as:

$$Z_{in(1-2)} = \frac{1}{g_{m0}(g_{m1}g_{m2}...g_{mn})(Z_1Z_2...Z_n)} \tag{6.7}$$

Where g_{m0}, g_{m1}, $g_{m2}...g_{mn}$ are the transconductance gains of respective OTAs. When Z_1 is replaced with FOC ($C_{1\alpha}$) and other impedances are replaced with integer-order capacitances, the input impedance given by (6.7) is modified. The modified input impedance is given as:

$$Z_{in(1-2)} = \frac{s^{n-1+\alpha}C_{1\alpha}C_2...C_n}{g_{m0}(g_{m1}g_{m2}\cdots g_{mn})} \tag{6.8}$$

Equation (6.8) represents the input impedance of a FOI with fractional order $(n-1+\alpha)$. By taking n=2, FOI with fractional order $(1+\alpha)$ can be realized, which is shown in Fig. 6.9 (a). To realize FOC with fractional order $(1+\alpha)$, the impedance inverter circuit of Fig. 6.9 (b) is used, where Z_L is replaced with the FOI of the same fractional order. Equations (6.9) and (6.10) provide the magnitudes of the input impedance for the FOI and FOC shown in Figs. 6.9 (a)

and (b), respectively.

$$L_{1+\alpha(1-2)} = \frac{C_{1\alpha}C_2}{g_{m0}g_{m1}g_{m2}} \tag{6.9}$$

$$C_{1+\alpha(1-2)} = \frac{g_{m3}g_{m4}C_{1\alpha}C_2}{g_{m0}g_{m1}g_{m2}} \tag{6.10}$$

6.3.1 Functional Verification

To verify the functionality of the proposed circuits of floating FOC and FOI with fractional order $(1+\alpha)$, SPICE simulations have been carried out with 180 nm CMOS technology model parameters. The supply voltages are taken as $\pm 1.8\ V$. Section 2.4 provides the aspect ratios of the transistors used in OTA, and its corresponding CMOS schematic is depicted in Fig. 2.8 (b). The FOC ($C_{1\alpha}$) with fractional order α, used in the proposed circuits of Fig. 6.9, is realized using the R-C ladder network based on 12^{th} order CFE approximation [35] shown in Fig. 6.10. The values of R_0, R_i and C_i (i=1, 2, ...11) to emulate FOC with C_α=3.75 $\mu\mho sec^\alpha$ and α=0.5 can be referred from Sect. 3.3.1.

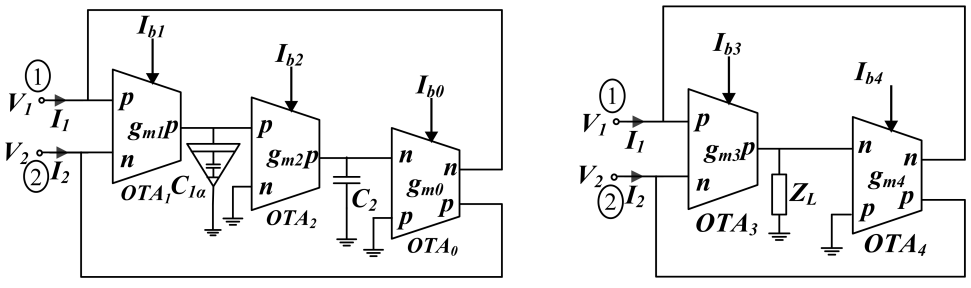

Figure 6.9: Proposed IIMC based floating FOEs of order $(1+\alpha)$ (a) IIMC circuit realizing FOI (b) Impedance inverter circuit realizing FOC, with Z_L as FOI

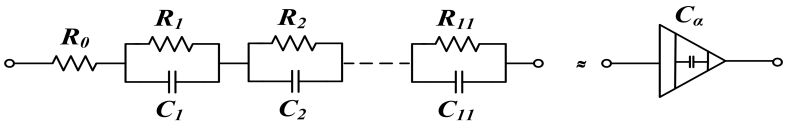

Figure 6.10: 12^{th} order R-C ladder network (based upon CFE approximation) realizing FOC

Bias currents for all the OTAs are taken same and equal to 8.32 μA correspond to the transconductance gain (g_m) of 100 $\mu A/V$. The value of integer-order capacitor C_2 is taken as 10 nF. Figures 6.11 (a) and (b) show simulated and theoretical frequency response of (1+α) order FOI and FOC respectively. The theoretical magnitudes of FOI and FOC of fractional order 1.5 are calculated as 37.5 $m\Omega sec^{1.5}$ and 0.375 $n\mho sec^{1.5}$ respectively, while the magnitudes through simulations have been measured as 36.8 $m\Omega sec^{1.5}$ and 0.371 $n\mho sec^{1.5}$ respectively. The errors between theoretical and simulated magnitudes lie within 2%. Table 6.3 presents the frequency range of operation for FOI and FOC, taking into account a maximum deviation of $\pm 5dB$ and $\pm 5^{\circ}$ in impedance magnitude and phase, respectively.

Table 6.3: Frequency range of operation for proposed floating FOEs

Impedance response	Valid frequency range for FOI	Valid frequency range for FOC
Magnitude	10 Hz - 7.7 kHz	10 Hz - 10 kHz
Phase	84 Hz - 1.4 kHz	11 Hz - 2.9 kHz

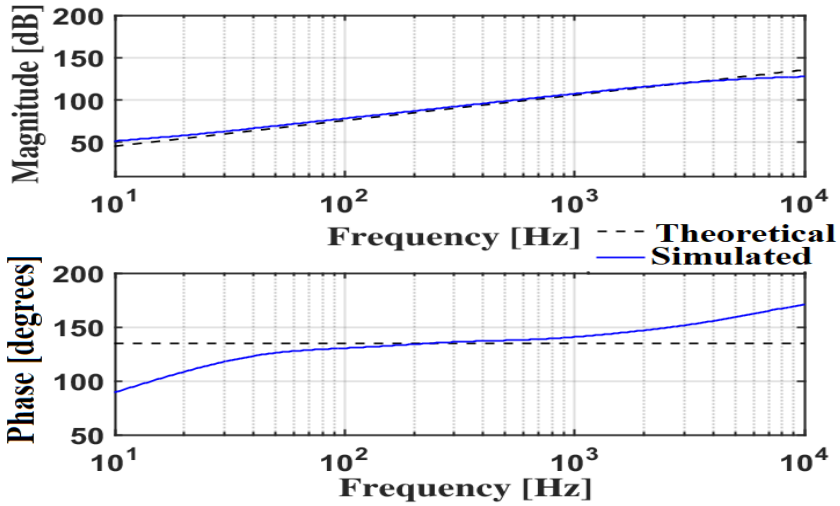

(a)

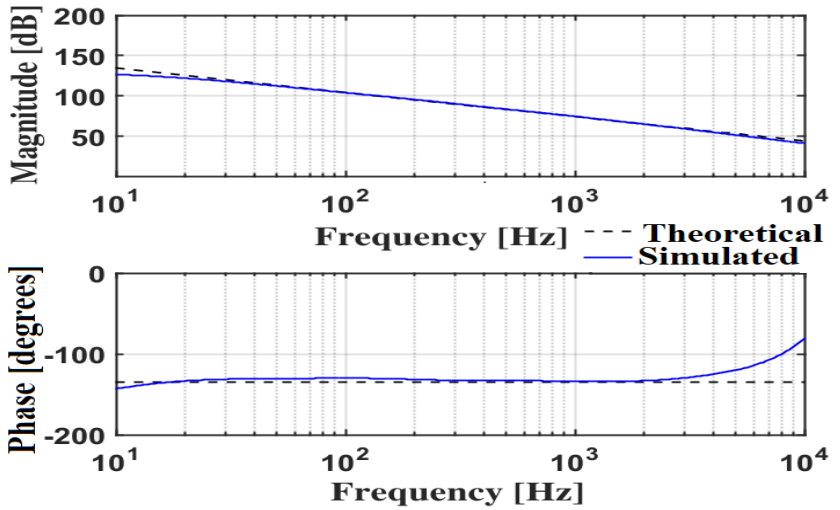

(b)

Figure 6.11: Magnitude and phase response for floating FOEs of order 1.5 (a) FOI (b) FOC

6.4 Conclusion

In the present chapter, a simpler scheme based upon active inductor to approximate the behaviour of FOC has been proposed. Proposed structure enables higher order approximation through parallel connection or impedance multiplication to realize FOC. The behaviour of the proposed FOC has been verified through SPICE

simulations with 180 nm CMOS technology model parameters and the errors are found within 6% for slope of the magnitude. Moreover, a FOO has been demonstrated as an application of the proposed FOC.

Further, a circuit to realize higher order floating FOE based on IIMC circuit is proposed. The proposed circuit can be used to realize floating FOI and floating FOC of fractional order α greater than 1. The magnitude of the proposed FOI and FOC can be controlled electronically by using external bias currents of OTAs. Workability of the proposed FOI and FOC of fractional order $(1 + \alpha)$ is verified using SPICE simulations with 180 nm CMOS technology model parameters and found that the errors between theoretical and simulated magnitudes of FOI and FOC with fractional order 1.5 lie within 2%.

Chapter 7

Conclusions and Suggestions for Future Work

The use of fractional calculus in modeling physical systems and processes has become increasingly popular due to its ability to provide an additional degree of freedom for modeling control mechanisms of physical phenomena. This approach allows for more precise modeling of real-world objects and natural processes.
The main focus of this thesis is to design a range of signal processing and signal generating circuits using fractional-order design equations that are based on generalized versions of integer-order design principles. This chapter provides a comprehensive summary of the significant findings and contributions presented throughout the various chapters of the thesis.

7.1 Summary of Work done

The introduction chapter of the thesis provided a literature survey on fractional order elements and fractional-order signal processing and signal generating circuits. This review helped to identify significant research gaps in the field and led to the identification of areas where further research could be conducted. The organization of thesis was also presented in this chapter.

Chapter 2 presented review of the approximated FOC realization techniques, specifically focusing on the use of the CFE approximation and Valsa's algorithm. The discussion also covered the circuit implementation for emulating FOC with different values of α, specifically 0.2, 0.5, and 0.8, using 5^{th}-order CFE approximation and 7^{th}-order Valsa's algorithm. Additionally, the chapter presented stability analysis of fractional-order systems and included preliminary analysis of the active

block used in this work, that is OTA. The functionality of the circuits presented in this chapter was also verified through SPICE simulations.

In chapter 3 an α-order multifunction TAM FOF was proposed for the very first time. The proposed TAM FOF offered FLPF, FHPF, and FAPF filter functions. The proposed structure's effectiveness was verified through both SPICE simulations and experimental testing, and found that results fit in the theoretical predictions very well. Additionally, the electronic tunability of the pole frequency has been confirmed through SPICE simulations. The sensitivity of the proposed TAM FOF was analyzed using MATLAB, and the structure's robustness was verified through PVT and Monte Carlo analysis.

Chapter 4 generalized the theory of integer-order shadow filters to fractional domain. Mathematical equations were drafted to determine the pole frequency and pole quality factor of shadow FOF for different types of feedback signals applied to the external amplifier in the feedback loop and demonstrated using MATLAB simulations. The proposed theory was verified utilizing two active shadow FOF circuits through SPICE simulations using 180 nm CMOS technology node. It was found that results fit in the theoretical predictions very well. The shadow FOF's parameters such as pole frequency and pole quality factor were tuned with the help of external amplifier's gain, without changing the active or passive components of the basic FOF. For both of the shadow FOF circuits the THD was found to be below 4%. Further, corner and Monte-Carlo analysis were performed to verify the robustness of the shadow FOF circuits.

In chapter 5 OTA-based three sinusoidal FOOs and one fractional-order multivibrator were proposed. The first two circuits of the sinusoidal FOO were designed using the trans-admittance mode FAPF with a trans-impedance mode integrator/differentiator. Additionally, the third circuit of the sinusoidal FOO featured a unique design that enables independent control of the phase difference between its two output voltages. All the three circuits of sinusoidal FOO were verified through SPICE simulations using 180 nm CMOS technology node. The stability was verified using pole plots with the help of *forlocus* function of MATLAB. The mathematical equations for sensitivity of the oscillation frequency with respect to various circuit parameters had been derived and found that the proposed circuits were lesser sensitive towards higher values of fractional-order α. The robustness of the proposed FOO circuits had also been examined via PVT and Monte-Carlo analyses and no abrupt changes were found in the transient responses of the proposed circuits. The sinusoidal FOO circuit I, had also been verified to work in VLF mode.

Further, an electronically tunable fractional-order multivibrator based on OTA was generalized in fractional domain. The mathematical formula for time period of the proposed fractional-order multivibrator was derived and verified through SPICE simulations. The robustness of the circuit was scrutinized through Monte-Carlo and corner analyses. The use of the FOC facilitated the proposed fractional-order multivibrator to have very high frequency of oscillation using standard circuit components' values. The capability of generating high frequency oscillation makes the proposed fractional-order multivibrator a superior choice over integer-order multivibrator for the applications such as various modulation techniques. So, AM, FM, DM and SDM had been explored and verified as application of the proposed

fractional-order multivibrator in this chapter. The adjustment of the modulation index of analog modulators (AM and FM) were also examined.

In chapter 6, a simpler scheme based upon active inductor to approximate the behaviour of FOC was proposed. Proposed structure enables higher order approximation of FOC either by parallel connection or by impedance multiplication method. The behaviour of the proposed FOC was verified through SPICE simulations with 180 nm CMOS technology model parameters and the errors were found within 6% for slope of the magnitude. Moreover, a FOO was demonstrated as an application of the proposed FOC.

Further, a circuit to realize higher order floating FOE based on IIMC circuit was also proposed. The proposed circuit had been used to realize floating FOI and floating FOC of fractional order α ($1 < \alpha < 2$). The magnitude of the proposed FOI and FOC can be adjusted electronically by using external bias currents of OTAs. Workability of the proposed FOI and FOC of fractional order $(1 + \alpha)$ was verified using SPICE simulations with 180 nm CMOS technology model parameters and found that results fit in the theoretical predictions with a maximum deviation of ± 5 dB and $\pm 5^{\circ}$ in impedance magnitude and phase respectively.

7.2 Suggestions for Future Work

The fractional domain is a highly interdisciplinary field with numerous research opportunities for exploration. Throughout this thesis, the candidate delved into

topics such as the development of electronically tunable FOFs and FOOs based on OTA as well as simpler and higher order designs of FOE. However, there are several potential directions in which the research can be expanded upon.

Firstly, it would be valuable to assess the performance of the developed FOFs and FOOs across diverse operating conditions and environments. This analysis will provide a comprehensive understanding of their behaviour and potential limitations in different scenarios. Another avenue to explore is the utilization of more efficient building blocks in the design of FOFs and FOOs. By considering different building block options, novel circuit configurations can be developed to enhance performance and expand the design possibilities.

In addition, the thesis has discussed a compact structure for realizing FOCs using active inductors. However, further investigations can be conducted to explore the tuning of magnitude and order in the structure. Lastly, the potential applications of FOFs and FOOs in various feilds such as biomedical signal processing, speech recognition, and image processing may be explored.

Overall, the field of fractional-order signal processing and signal generation is a promising area for future research, with potential applications in a wide range of fields and technologies.

References

[1] F. Mainardi, *Fractional Calculus: Theory and Applications*. MDPI, Sep. 2018. DOI: 10.3390/books978-3-03897-207-5. [Online]. Available: https://doi.org/10.3390%2Fbooks978-3-03897-207-5.

[2] A. S. Elwakil, "Fractional-order circuits and systems: An emerging interdisciplinary research area," *IEEE Circuits and Systems Magazine*, vol. 10, no. 4, pp. 40–50, 2010. DOI: 10.1109/MCAS.2010.938637.

[3] L. Debnath, "Recent applications of fractional calculus to science and engineering," *International Journal of Mathematics and Mathematical Sciences*, pp. 3413–3442, 2003. DOI: https://doi.org/10.1155/S0161171203301486.

[4] Y. Chen, I. Petras, and D. Xue, "Fractional order control - a tutorial," in *2009 American Control Conference (ACC)*, 2009, pp. 1397–1411.

[5] T. Suksang, W. Loedhammacakra, and V. Pirajnanchai, "Implement the fractional-order, half integrator and differentiator on the OTA base $PI^{\lambda}D^{\mu}$ controller circuit," in *2012 9th International Conference on Electrical Engineering/Electro Computer, Telecommunications and Information Technology*, IEEE, May 2012. DOI: 10.1109/ecticon.2012.6254136.

[6] G. Tsirimokou, C. Psychalinos, and A. S. Elwakil, *Design of CMOS Analog Integrated Fractional-Order Circuits, Applications in Medicine and Biology*. Springer Cham, 2017, 114 pp. DOI: 10.1007/978-3-319-55633-8.

[7] A. C. Faria, J. Veiga, A. J. Lopes, and P. L. Melo, "Forced oscillation, integer and fractional-order modeling in asthma," *Computer Methods and Programs in Biomedicine*, vol. 128, pp. 12–26, May 2016. DOI: 10.1016/j.cmpb.2016.02.010.

[8] P. Bertsias, M. Mohsen, L. A. Said, A. S. Elwakil, C. Psychalinos, and A. G. Radwan, "Design and implementation of an optimized artificial human eardrum model," *Circuits, Systems, and Signal Processing*, vol. 39, no. 6, pp. 3219–3233, Nov. 2019. DOI: 10.1007/s00034-019-01308-6.

[9] S. Das and I. Pan, "Fractional order statistical signal processing," in *Fractional Order Signal Processing*, Springer Berlin Heidelberg, Sep. 2011, pp. 83–96. DOI: 10.1007/978-3-642-23117-9_6.

[10] H. Sheng, Y. Chen, and T. Qiu, "An overview of fractional processes and fractional-order signal processing techniques," in *Fractional Processes and Fractional-Order Signal Processing*, Springer London, 2012, pp. 31–46. DOI: 10.1007/978-1-4471-2233-3_2.

[11] E. M. Hamed, L. A. Said, A. H. Madian, and A. G. Radwan, "On the approximations of CFOA-based fractional-order inverse filters," *Circuits, Systems, and Signal Processing*, vol. 39, no. 1, pp. 2–29, Jun. 2019. DOI: 10.1007/s00034-019-01155-5.

[12] C. Muniz-Montero, L. A. Sanchez-Gaspariano, C. Sanchez-Lopez, V. R. Gonzalez-Diaz, and E. Tlelo-Cuautle, "On the electronic realizations of fractional-order phase-lead-lag compensators with OpAmps and FPAAs," in *Fractional Order Control and Synchronization of Chaotic Systems*, Springer International Publishing, 2017, pp. 131–164. DOI: 10.1007/978-3-319-50249-6_5.

[13] E. Tlelo-Cuautle, A. D. Pano-Azucena, O. Guillen-Fernandez, and A. Silva-Juarez, *Analog/Digital Implementation of Fractional Order Chaotic Circuits and Applications*. Springer Cham, 2020, 212 pp. DOI: 10.1007/978-3-030-31250-3.

[14] W. S. Sayed and A. G. Radwan, "Generalized switched synchronization and dependent image encryption using dynamically rotating fractional-order chaotic systems," *AEU - International Journal of Electronics and Communications*, vol. 123, p. 153 268, Aug. 2020. DOI: 10.1016/j.aeue.2020.153268.

[15] T. F. Nonnenmacher and R. Metzler, "On the riemann-liouville fractional calculus and some recent applications," *Fractals*, vol. 03, no. 03, pp. 557–566, Sep. 1995. DOI: 10.1142/s0218348x95000497.

[16] M. N. and Kazuyuki Sorimachi, "Basic characteristics of a fractance device," *IEICE TRANSACTIONS on Fundamentals of Electronics, Communications and Computer Sciences*, vol. E75-A, no. 12, pp. 1814–1819, Dec. 1992.

[17] A. G. Radwan, A. M. Soliman, and A. S. Elwakil, "First-order filters generalized to the fractional domain," *Journal of Circuits, Systems and Computers*, vol. 17, no. 01, pp. 55–66, Feb. 2008. DOI: 10.1142/s0218126608004162.

[18] A. Kartci, A. Agambayev, M. Farhat, *et al.*, "Synthesis and optimization of fractional-order elements using a genetic algorithm," *IEEE Access*, vol. 7, pp. 80 233–80 246, 2019. DOI: 10.1109/access.2019.2923166.

[19] I. Podlubny, I. Petras, B. M. Vinagre, P. O'Leary, and L. Dorcak, "Analogue realizations of fractional-order controllers," *Nonlinear Dynamics*, vol. 29, pp. 281–296, Jul. 2002. DOI: 10.1023/A:1016556604320.

[20] G. W. Bohannan, "Analog fractional order controller in temperature and motor control applications," *Journal of Vibration and Control*, vol. 14, no. 9-10, pp. 1487–1498, Sep. 2008. DOI: 10.1177/1077546307087435.

[21] T. C. Haba, G. Ablart, T. Camps, and F. Olivie, "Influence of the electrical parameters on the input impedance of a fractal structure realised on silicon," *Chaos, Solitons &amp Fractals*, vol. 24, no. 2, pp. 479–490, Apr. 2005. DOI: 10.1016/j.chaos.2003.12.095.

[22] K. Biswas, S. Sen, and P. Dutta, "Realization of a constant phase element and its performance study in a differentiator circuit," *IEEE Transactions on Circuits and Systems II: Express Briefs*, vol. 53, no. 9, pp. 802–806, Sep. 2006. DOI: 10.1109/tcsii.2006.879102.

[23] I. S. Jesus and J. A. T. Machado, "Development of fractional order capacitors based on electrolyte processes," *Nonlinear Dynamics*, vol. 56, no. 1-2, pp. 45–55, Jun. 2008. DOI: 10.1007/s11071-008-9377-8.

[24] M. S. Krishna, S. Das, K. Biswas, and B. Goswami, "Fabrication of a fractional order capacitor with desired specifications: A study on process identification and characterization," *IEEE Transactions on Electron Devices*, vol. 58, no. 11, pp. 4067–4073, Nov. 2011. DOI: 10.1109/ted.2011.2166763.

[25] K. Biswas, S. Sen, and P. K. Dutta, "Modeling of a capacitive probe in a polarizable medium," *Sensors and Actuators A: Physical*, vol. 120, no. 1, pp. 115–122, Apr. 2005. DOI: 10.1016/j.sna.2004.11.025.

[26] D. Mondal and K. Biswas, "Packaging of single-component fractional order element," *IEEE Transactions on Device and Materials Reliability*, vol. 13, no. 1, pp. 73–80, Mar. 2013. DOI: 10.1109/tdmr.2012.2212020.

[27] A. M. Elshurafa, M. N. Almadhoun, K. N. Salama, and H. N. Alshareef, "Microscale electrostatic fractional capacitors using reduced graphene oxide percolated polymer composites," *Applied Physics Letters*, vol. 102, no. 23, p. 232 901, Jun. 2013. DOI: 10.1063/1.4809817.

[28] A. Agambayev, S. P. Patole, M. Farhat, A. Elwakil, H. Bagci, and K. N. Salama, "Ferroelectric fractional-order capacitors," *ChemElectroChem*, vol. 4, no. 11, pp. 2807–2813, Aug. 2017. DOI: 10.1002/celc.201700663.

[29] A. Agambayev, S. P. Patole, M. Farhat, A. Elwakil, H. Bagci, and K. N. Salama, "Ferroelectric fractional-order capacitors," *ChemElectroChem*, vol. 4, no. 11, pp. 2807–2813, Aug. 2017. DOI: 10.1002/celc.201700663.

[30] K. Biswas, R. Caponetto, G. D. Pasquale, S. Graziani, A. Pollicino, and E. Murgano, "Realization and characterization of carbon black based fractional order element," *Microelectronics Journal*, vol. 82, pp. 22–28, Dec. 2018. DOI: 10.1016/j.mejo.2018.10.008.

[31] A. Buscarino, R. Caponetto, S. Graziani, and E. Murgano, "Realization of fractional order circuits by a constant phase element," *European Journal of Control*, vol. 54, pp. 64–72, Jul. 2020. DOI: 10.1016/j.ejcon.2019.11.009.

[32] B. M. Vinagre, I. Podlubny, A. Hernández, and V. Feliu, "Some approximations of fractional order operators used in control theory," *Fractional Calculus and Applied Analysis*, vol. 3, no. 3, pp. 1–17, Jan. 2000.

[33] D. Xue, C. Zhao, and Y. Chen, "A modified approximation method of fractional order system," in *2006 International Conference on Mechatronics and Automation*, IEEE, Jun. 2006. DOI: 10.1109/icma.2006.257769.

[34] G. Tsirimokou, "A systematic procedure for deriving RC networks of fractional-order elements emulators using MATLAB," *AEU - International Journal of Electronics and Communications*, vol. 78, pp. 7–14, Aug. 2017. DOI: 10.1016/j.aeue.2017.05.003.

[35] A. Adhikary, P. Sen, S. Sen, and K. Biswas, "Design and performance study of dynamic fractors in any of the four quadrants," *Circuits, Systems, and Signal Processing*, vol. 35, no. 6, pp. 1909–1932, Dec. 2015. DOI: 10.1007/s00034-015-0213-3.

[36] G. Tsirimokou, C. Psychalinos, A. S. Elwakil, and K. N. Salama, "Experimental behavior evaluation of series and parallel connected constant phase elements," *AEU - International Journal of Electronics and Communications*, vol. 74, pp. 5–12, Apr. 2017. DOI: 10.1016/j.aeue.2017.01.010.

[37] G. Tsirimokou, C. Psychalinos, A. S. Elwakil, and K. N. Salama, "Experimental verification of on-chip CMOS fractional-order capacitor emulators," *Electronics Letters*, vol. 52, no. 15, pp. 1298–1300, Jul. 2016. DOI: 10.1049/el.2016.1457.

[38] G. Tsirimokou, C. Psychalinos, and A. S. Elwakil, "Emulation of a constant phase element using operational transconductance amplifiers," *Analog Integrated Circuits and Signal Processing*, vol. 85, no. 3, pp. 413–423, Sep. 2015. DOI: 10.1007/s10470-015-0626-8.

[39] G. Tsirimokou, C. Psychalinos, A. S. Elwakil, and K. N. Salama, "Electronically tunable fully integrated fractional-order resonator," *IEEE Transactions on Circuits and Systems II: Express Briefs*, vol. 65, no. 2, pp. 166–170, Feb. 2018. DOI: 10.1109/tcsii.2017.2684710.

[40] S. Kapoulea, G. Tsirimokou, C. Psychalinos, and A. S. Elwakil, "Generalized fully adjustable structure for emulating fractional-order capacitors and inductors of orders less than two," *Circuits, Systems, and Signal Processing*, vol. 39, no. 4, pp. 1797–1814, Sep. 2019. DOI: 10.1007/s00034-019-01252-5.

[41] R. Sotner, J. Jerabek, J. Petrzela, O. Domansky, G. Tsirimokou, and C. Psychalinos, "Synthesis and design of constant phase elements based on the multiplication of electronically controllable bilinear immittances in practice," *AEU - International Journal of Electronics and Communications*, vol. 78, pp. 98–113, Aug. 2017. DOI: 10.1016/j.aeue.2017.05.013.

[42] R. Sotner, L. Polak, J. Jerabek, and J. Petrzela, "Simple two operational transconductance amplifiers-based electronically controllable bilinear two port for fractional-order synthesis," *Electronics Letters*, vol. 54, no. 20, pp. 1164–1166, Oct. 2018. DOI: 10.1049/el.2018.5575.

[43] R. Sotner, J. Jerabek, J. Petrzela, and T. Dostal, "Simple approach for synthesis of fractional-order grounded immittances based on OTAs," in *2016 39th International Conference on Telecommunications and Signal Processing (TSP)*, IEEE, Jun. 2016. DOI: 10.1109/tsp.2016.7760944.

[44] J. Petrzela, "Fundamental analog cells for fractional-order two-port synthesis," in *2013 23rd International Conference Radioelektronika (RADIOELEKTRONIKA)*, IEEE, Apr. 2013. DOI: 10.1109/radioelek.2013.6530912.

[45] S. Kapoulea, C. Psychalinos, and A. S. Elwakil, "Realizations of simple fractional-order capacitor emulators with electronically-tunable capacitance," *Integration*, vol. 69, pp. 225–233, Nov. 2019. DOI: 10.1016/j.vlsi.2019.04.004.

[46] M. E. Fouda, A. AboBakr, A. S. Elwakil, A. G. Radwan, and A. M. Eltawil, "Simple MOS transistor-based realization of fractional-order capacitors," in *2019 IEEE International Symposium on Circuits and Systems (ISCAS)*, IEEE, May 2019. DOI: 10.1109/iscas.2019.8702341.

[47] P. Bertsias, C. Psychalinos, A. S. Elwakil, and A. G. Radwan, "Low-voltage and low-power fractional-order parallel tunable resonator," *Microelectronics Journal*, vol. 88, pp. 108–116, Jun. 2019. DOI: 10.1016/j.mejo.2019.05.002.

[48] P. Bertsias, C. Psychalinos, A. G. Radwan, and A. S. Elwakil, "High-frequency capacitorless fractional-order CPE and FI emulator," *Circuits, Systems, and Signal Processing*, vol. 37, no. 7, pp. 2694–2713, Oct. 2017. DOI: 10.1007/s00034-017-0697-0.

[49] P. Bertsias, C. Psychalinos, A. Elwakil, and B. Maundy, "Current-mode capacitorless integrators and differentiators for implementing emulators of fractional-order elements," *AEU - International Journal of Electronics and Communications*, vol. 80, pp. 94–103, Oct. 2017. DOI: 10.1016/j.aeue.2017.06.036.

[50] G. Tsirimokou, C. Psychalinos, T. J. Freeborn, and A. S. Elwakil, "Emulation of current excited fractional-order capacitors and inductors using OTA topologies," *Microelectronics Journal*, vol. 55, pp. 70–81, Sep. 2016. DOI: 10.1016/j.mejo.2016.06.008.

[51] A. Adhikary, S. Sen, and K. Biswas, "Practical realization of tunable fractional order parallel resonator and fractional order filters," *IEEE Transactions on Circuits and Systems I: Regular Papers*, vol. 63, no. 8, pp. 1142–1151, Aug. 2016. DOI: 10.1109/tcsi.2016.2568262.

[52] A. S. E. Todd J. Freeborn Brent Maundy, "Fractional resonance-based $RL_\beta C_\alpha$ filters," *Mathematical Problems in Engineering*, vol. 2013, pp. 1–10, Feb. 2013. DOI: 10.1155/2013/726721.

[53] R. Verma, N. Pandey, and R. Pandey, "Realization of a higher fractional order element based on novel OTA based IIMC and its application in filter," *Analog Integrated Circuits and Signal Processing*, vol. 97, no. 1, pp. 177–191, Aug. 2018. DOI: 10.1007/s10470-018-1315-1.

[54] P. Ahmadi, B. Maundy, A. Elwakil, and L. Belostotski, "High-quality factor asymmetric-slope band-pass filters: A fractional-order capacitor approach," *IET Circuits, Devices & Systems*, vol. 6, no. 3, pp. 187–197, 2012. DOI: 10.1049/iet-cds.2011.0239.

[55] A. Soltan, A. M. Soliman, and A. G. Radwan, "Fractional-order impedance transformation based on three port mutators," *AEU - International Journal of Electronics and Communications*, vol. 81, pp. 12–22, Nov. 2017. DOI: 10.1016/j.aeue.2017.06.012.

[56] S. Kapoulea, C. Psychalinos, A. S. Elwakil, and A. G. Radwan, "One-terminal electronically controlled fractional-order capacitor and inductor emulator," *AEU - International Journal of Electronics and Communications*, vol. 103, pp. 32–45, May 2019. DOI: 10.1016/j.aeue.2019.03.002.

[57] A. G. Radwan, A. S. ElWakil, and A. M. Soliman, "On the generalization of second-order filters to the fractional-order domain," *Journal of Circuits, Systems and Computers*, vol. 18, no. 02, pp. 361–386, Apr. 2009. DOI: 10.1142/s0218126609005125.

[58] T. J. Freeborn, B. Maundy, and A. S. Elwakil, "Fractional-step tow-thomas biquad filters," *Nonlinear Theory and Its Applications, IEICE*, vol. 3, no. 3, pp. 357–374, 2012. DOI: 10.1587/nolta.3.357.

[59] T. J. Freeborn, "Comparison of $(1+\alpha)$ fractional-order transfer functions to approximate lowpass butterworth magnitude responses," *Circuits, Systems, and Signal Processing*, vol. 35, no. 6, pp. 1983–2002, Dec. 2015. DOI: 10.1007/s00034-015-0226-y.

[60] M. C. Tripathy, K. Biswas, and S. Sen, "A design example of a fractional-order kerwin-huelsman-newcomb biquad filter with two fractional capacitors of different order," *Circuits, Systems, and Signal Processing*, vol. 32, no. 4, pp. 1523–1536, Jan. 2013. DOI: 10.1007/s00034-012-9539-2.

[61] E. M. Hamed, A. M. AbdelAty, L. A. Said, and A. G. Radwan, "Effect of different approximation techniques on fractional-order KHN filter design," *Circuits, Systems, and Signal Processing*, vol. 37, no. 12, pp. 5222–5252, May 2018. DOI: 10.1007/s00034-018-0833-5.

[62] A. Soltan, A. G. Radwan, and A. M. Soliman, "Fractional order sallen–key and KHN filters: Stability and poles allocation," *Circuits, Systems, and Signal Processing*, vol. 34, no. 5, pp. 1461–1480, Nov. 2014. DOI: 10.1007/s00034-014-9925-z.

[63] D. Kubanek, T. Freeborn, and J. Koton, "Fractional-order band-pass filter design using fractional-characteristic specimen functions," *Microelectronics Journal*, vol. 86, pp. 77–86, Apr. 2019. DOI: 10.1016/j.mejo.2019.02.020.

[64] A. M. AbdelAty, A. Soltan, W. A. Ahmed, and A. G. Radwan, "Fractional order chebyshev-like low-pass filters based on integer order poles," *Microelectronics Journal*, vol. 90, pp. 72–81, Aug. 2019. DOI: 10.1016/j.mejo.2019.05.016.

[65] T. Freeborn, B. Maundy, and A. S. Elwakil, "Approximated fractional order chebyshev lowpass filters," *Mathematical Problems in Engineering*, vol. 2015, pp. 1–7, 2015. DOI: 10.1155/2015/832468.

[66] N. Herencsar, R. Sotner, A. Kartci, and K. Vrba, "A novel pseudo-differential integer/ fractional-order voltage-mode all-pass filter," in *2018 IEEE International Symposium on Circuits and Systems (ISCAS)*, IEEE, May 2018. DOI: 10.1109/iscas.2018.8351520.

[67] M. V. Bhat, S. S. Bhat, and D. Kamath, "G_m-c current mode fractional all pass filter of order $(0 < \alpha < 1)$," in *2019 3rd International conference on Electronics, Communication and Aerospace Technology (ICECA)*, IEEE, Jun. 2019. DOI: 10.1109/iceca.2019.8822183.

[68] J. Dvorak, J. Jerabek, Z. Polesakova, D. Kubanek, and P. Blazek, "Multifunctional electronically reconfigurable and tunable fractional-order filter," *Elektronika ir Elektrotechnika*, vol. 25, no. 1, Feb. 2019. DOI: 10.5755/j01.eie.25.1.22732.

[69] S. K. Mishra, M. Gupta, and D. K. Upadhyay, "Active realization of fractional order butterworth lowpass filter using DVCC," *Journal of King Saud University - Engineering Sciences*, vol. 32, no. 2, pp. 158–165, Feb. 2020. DOI: 10.1016/j.jksues.2018.11.005.

[70] P. Bertsias, C. Psychalinos, A. S. Elwakil, and B. Maundy, "Simple multi-function fractional-order filter designs," in *2019 8th International Conference on Modern Circuits and Systems Technologies (MOCAST)*, IEEE, May 2019. DOI: 10.1109/mocast.2019.8741674.

[71] R. Verma, N. Pandey, and R. Pandey, "Electronically tunable fractional order filter," *Arabian Journal for Science and Engineering*, vol. 42, no. 8, pp. 3409–3422, Apr. 2017. DOI: 10.1007/s13369-017-2500-8.

[72] G. Kaur, A. Ansari, and M. Hashmi, "Fractional order multifunction filter with 3 degrees of freedom," *AEU - International Journal of Electronics and Communications*, vol. 82, pp. 127–135, Dec. 2017. DOI: 10.1016/j.aeue.2017.08.010.

[73] T. J. Freeborn, A. S. Elwakil, and B. Maundy, "Approximated fractional-order inverse chebyshev lowpass filters," *Circuits, Systems, and Signal Processing*, vol. 35, no. 6, pp. 1973–1982, Dec. 2015. DOI: 10.1007/s00034-015-0222-2.

[74] A. Soltan, A. G. Radwan, and A. M. Soliman, "CCII based fractional filters of different orders," *Journal of Advanced Research*, vol. 5, no. 2, pp. 157–164, Mar. 2014. DOI: 10.1016/j.jare.2013.01.007.

[75] L. A. Said, S. M. Ismail, A. G. Radwan, A. H. Madian, M. F. A. El-Yazeed, and A. M. Soliman, "On the optimization of fractional order low-pass filters," *Circuits, Systems, and Signal Processing*, vol. 35, no. 6, pp. 2017–2039, Jun. 2016. DOI: 10.1007/s00034-016-0258-y.

[76] B. Maundy, A. Elwakil, and T. Freeborn, "On the practical realization of higher-order filters with fractional stepping," *Signal Processing*, vol. 91, no. 3, pp. 484–491, Mar. 2011. DOI: 10.1016/j.sigpro.2010.06.018.

[77] J. Jerabek, R. Sotner, J. Dvorak, L. Langhammer, and J. Koton, "Fractional-order high-pass filter with electronically adjustable parameters," in *2016 International Conference on Applied Electronics (AE)*, IEEE, Sep. 2016. DOI: 10.1109/ae.2016.7577253.

[78] J. Jerabek, R. Sotner, J. Dvorak, *et al.*, "Reconfigurable fractional-order filter with electronically controllable slope of attenuation, pole frequency and type of approximation," *Journal of Circuits, Systems and Computers*, vol. 26, no. 10, p. 1 750 157, Mar. 2017. DOI: 10.1142/s0218126617501572.

[79] J. Koton, D. Kubanek, O. Sladok, K. Vrba, A. Shadrin, and P. Ushakov, "Fractional-order low- and high-pass filters using UVCs," *Journal of Circuits, Systems and Computers*, vol. 26, no. 12, p. 1 750 192, Aug. 2017. DOI: 10.1142/s0218126617501924.

[80] G. Tsirimokou, S. Koumousi, and C. Psychalinos, "Design of fractional-order filters using current feedback operational amplifiers," *Journal of Engineering Science and Technology Review*, vol. 9, no. 4, pp. 77–81, Jan. 2016. DOI: 10.25103/jestr.094.12.

[81] J. Dvorak, L. Langhammer, J. Jerabek, J. Koton, R. Sotner, and J. Polak, "Electronically tunable fractional-order low-pass filter with current followers," in *2016 39th International Conference on Telecommunications and Signal Processing (TSP)*, IEEE, Jun. 2016. DOI: 10.1109/tsp.2016.7760949.

[82] L. Langhammer, R. Sotner, J. Dvorak, J. Jerabek, and J. Polak, "Fully-differential tunable fractional-order filter with current followers and current amplifiers," in *2017 27th International Conference Radioelektronika (RADIOELEKTRONIKA)*, IEEE, Apr. 2017. DOI: 10.1109/radioelek.2017.7937576.

[83] J. Dvorak, L. Langhammer, J. Jerabek, J. Koton, R. Sotner, and J. Polak, "Synthesis and analysis of electronically adjustable fractional-order low-pass filter," *Journal of Circuits, Systems and Computers*, vol. 27, no. 02, p. 1 850 032, Sep. 2017. DOI: 10.1142/s0218126618500329.

[84] J. Dvorak, Z. Polesakova, J. Jerabek, L. Langhammer, A. Kartci, and J. Koton, "Non-integer-order low-pass filter with electronically controllable parameters," in *2018 IEEE International Symposium on Circuits and Systems (ISCAS)*, IEEE, May 2018. DOI: 10.1109/iscas.2018.8351488.

[85] G. Tsirimokou and C. Psychalinos, "Ultra-low voltage fractional-order circuits using current mirrors," *International Journal of Circuit Theory and Applications*, vol. 44, no. 1, pp. 109–126, Feb. 2015. DOI: 10.1002/cta.2066.

[86] R. Verma, N. Pandey, and R. Pandey, "CFOA based low pass and high pass fractional step filter realizations," *AEU - International Journal of Electronics and Communications*, vol. 99, pp. 161–176, Feb. 2019. DOI: 10.1016/j.aeue.2018.11.032.

[87] L. Langhammer, J. Dvorak, R. Sotner, and J. Jerabek, "Electronically tunable fully-differential fractional-order low-pass filter," *Elektronika ir Elektrotechnika*, vol. 23, no. 3, Jun. 2017. DOI: 10.5755/j01.eie.23.3.18332.

[88] L. Langhammer, J. Dvorak, J. Jerabek, J. Koton, and R. Sotner, "Fractional-order low-pass filter with electronic tunability of its order and pole frequency," *Journal of Electrical Engineering*, vol. 69, no. 1, pp. 3–13, Jan. 2018. DOI: 10.1515/jee-2018-0001.

[89] F. Khateb, D. Kubanek, G. Tsirimokou, and C. Psychalinos, "Fractional-order filters based on low-voltage DDCCs," *Microelectronics Journal*, vol. 50, pp. 50–59, Apr. 2016. DOI: 10.1016/j.mejo.2016.02.002.

[90] L. Langhammer, R. Sotner, J. Dvorak, and T. Dostal, "Fully-differential multifunctional electronically configurable fractional-order filter with electronically adjustable parameters," *Elektronika ir Elektrotechnika*, vol. 24, no. 5, Oct. 2018. DOI: 10.5755/j01.eie.24.5.21841.

[91] O. I. Ahmed, H. M. Yassin, L. A. Said, C. Psychalinos, and A. G. Radwan, "Implementation and analysis of tunable fractional-order band-pass filter of order 2α," *AEU - International Journal of Electronics and Communications*, vol. 124, p. 153 343, Sep. 2020. DOI: 10.1016/j.aeue.2020.153343.

[92] G. Kaur, A. Q. Ansari, and M. S. Hashmi, "Analysis and investigation of CDBA based fractional-order filters," *Analog Integrated Circuits and Signal Processing*, vol. 105, no. 1, pp. 111–124, Jul. 2020. DOI: 10.1007/s10470-020-01683-0.

[93] S. Mahata, S. K. Saha, R. Kar, and D. Mandal, "Optimal design of fractional order low pass butterworth filter with accurate magnitude response," *Digital Signal Processing*, vol. 72, pp. 96–114, Jan. 2018. DOI: 10.1016/j.dsp.2017.10.001.

[94] W. Ahmad, R. El-khazali, and A. Elwakil, "Fractional-order wien-bridge oscillator," *Electronics Letters*, vol. 37, no. 18, p. 1110, 2001. DOI: 10.1049/el:20010756.

[95] A. G. Radwan, A. S. Elwakil, and A. M. Soliman, "Fractional-order sinusoidal oscillators: Design procedure and practical examples," *IEEE Transactions on Circuits and Systems I: Regular Papers*, vol. 55, no. 7, pp. 2051–2063, Aug. 2008. DOI: 10.1109/tcsi.2008.918196.

[96] A. G. Radwan, A. M. Soliman, and A. S. Elwakil, "Design equations for fractional-order sinusoidal oscillators: Practical circuit examples," in *2007 Internatonal Conference on Microelectronics*, IEEE, Dec. 2007. DOI: 10.1109/icm.2007.4497668.

[97] L. A. Said, A. G. Radwan, A. H. Madian, and A. M. Soliman, "Fractional order two port network oscillator with equal order," in *2014 26th International Conference on Microelectronics (ICM)*, IEEE, Dec. 2014. DOI: 10.1109/icm.2014.7071830.

[98] L. A. Said, A. G. Radwan, A. H. Madian, and A. M. Soliman, "Three fractional-order-capacitors-based oscillators with controllable phase and frequency," *Journal of Circuits, Systems and Computers*, vol. 26, no. 10, p. 1 750 160, Apr. 2017. DOI: 10.1142/s0218126617501602.

[99] O. Elwy, L. A. Said, A. H. Madian, and A. G. Radwan, "All possible topologies of the fractional-order wien oscillator family using different approximation techniques," *Circuits, Systems, and Signal Processing*, vol. 38, no. 9, pp. 3931–3951, Feb. 2019. DOI: 10.1007/s00034-019-01057-6.

[100] B. Maundy, A. S. Elwakil, and S. Gift, "On the realization of multiphase oscillators using fractional-order allpass filters," *Circuits, Systems, and Signal Processing*, vol. 31, no. 1, pp. 3–17, Dec. 2010. DOI: 10.1007/s00034-010-9235-z.

[101] M. E. Fouda, A. Soltan, A. G. Radwan, and A. M. Soliman, "Fractional-order multi-phase oscillators design and analysis suitable for higher-order PSK applications," *Analog Integrated Circuits and Signal Processing*, vol. 87, no. 2, pp. 301–312, Mar. 2016. DOI: 10.1007/s10470-016-0716-2.

[102] A. M. EL-Naggar, L. A. Said, A. G. Radwan, A. H. Madian, and A. M. Soliman, "Fractional order four-phase oscillator based on double integrator topology," in *2017 6th International Conference on Modern Circuits and Systems Technologies (MOCAST)*, IEEE, May 2017. DOI: 10.1109/mocast.2017.7937685.

[103] G. Tsirimokou, C. Psychalinos, A. S. Elwakil, and B. Maundy, "Fractional-order multiphase sinusoidal oscillator design using current-mirrors," in *2018 41st International Conference on Telecommunications and Signal Processing (TSP)*, IEEE, Jul. 2018. DOI: 10.1109/tsp.2018.8441399.

[104] L. A. Said, A. G. Radwan, A. H. Madian, and A. M. Soliman, "Fractional order oscillators based on operational transresistance amplifiers," *AEU - International Journal of Electronics and Communications*, vol. 69, no. 7, pp. 988–1003, Jul. 2015. DOI: 10.1016/j.aeue.2015.03.003.

[105] D. Kubanek, F. Khateb, G. Tsirimokou, and C. Psychalinos, "Practical design and evaluation of fractional-order oscillator using differential voltage current conveyors," *Circuits, Systems, and Signal Processing*, vol. 35, no. 6, pp. 2003–2016, Jan. 2016. DOI: 10.1007/s00034-016-0243-5.

[106] T. Comedang and P. Intani, "Current-controlled CFTA based fractional order quadrature oscillators," *Circuits and Systems*, vol. 07, no. 13, pp. 4201–4212, 2016. DOI: 10.4236/cs.2016.713345.

[107] A. Kartci, N. Herencsar, J. Koton, and C. Psychalinos, "Compact MOS-RC voltage-mode fractional-order oscillator design," in *2017 European Conference on Circuit Theory and Design (ECCTD)*, IEEE, Sep. 2017. DOI: 10.1109/ecctd.2017.8093281.

[108] A. Pradhan and R. K. Sharma, "Generalised fractional-order oscillators using OTA," in *2018 5th International Conference on Signal Processing and Integrated Networks (SPIN)*, IEEE, Feb. 2018. DOI: 10.1109/spin.2018.8474177.

[109] S. K. Mishra, M. Gupta, and D. K. Upadhyay, "Design and implementation of DDCC-based fractional-order oscillator," *International Journal of Electronics*, vol. 106, no. 4, pp. 581–598, Nov. 2018. DOI: 10.1080/00207217.2018.1545260.

[110] R. Kengne, F. H. Bertrand, A. T. Azar, and K. S. T. Alain, "Stability analysis and robust synchronisation of fractional-order modified colpitts oscillators," *International Journal of Automation and Control*, vol. 14, no. 1, p. 52, 2020. DOI: 10.1504/ijaac.2020.10025261.

[111] A. G. Radwan, "Stability analysis and robust synchronisation of fractional-order modified colpitts oscillators," *Journal of Fractional Calculus and Applications*, vol. 3, no. 1, pp. 1–15, Jul. 2012. DOI: 10.21608/JFCA.2012.283761.

[112] B. Maundy, A. S. Elwakil, and S. Gift, "On a multivibrator that employs a fractional capacitor," *Analog Integrated Circuits and Signal Processing*, vol. 62, no. 1, pp. 99–103, Jun. 2009. DOI: 10.1007/s10470-009-9329-3.

[113] A. S. Elwakil, A. Allagui, B. Maundy, and C. Psychalinos, "A low frequency oscillator using a super-capacitor," *AEU - International Journal of Electronics and Communications*, vol. 70, no. 7, pp. 970–973, Jul. 2016. DOI: 10.1016/j.aeue.2016.03.020.

[114] O. Elwy, A. M. AbdelAty, L. A. Said, A. H. Madian, and A. G. Radwan, "Two implementations of fractional-order relaxation oscillators," *Analog Integrated Circuits and Signal Processing*, vol. 106, no. 2, pp. 421–432, May 2020. DOI: 10.1007/s10470-020-01640-x.

[115] İ. E. Saçu and M. Alçı, "An electronically controllable fractional multivibrator," *IETE Journal of Research*, vol. 67, no. 3, pp. 313–321, Dec. 2018. DOI: 10.1080/03772063.2018.1548909.

[116] F. M. Valsa J Dvorak P, "Network model of the cpe," *Radioengineering*, vol. 20, pp. 619–626, 2011.

[117] A. G. Radwan, A. M. Soliman, A. S. Elwakil, and A. Sedeek, "On the stability of linear systems with fractional-order elements," *Chaos, Solitons & Fractals*, vol. 40, no. 5, pp. 2317–2328, Jun. 2009. DOI: 10.1016/j.chaos.2007.10.033.

[118] T. Tsukutani, Y. Sumi, and Y. Fukui, "Electronically controlled currentmode oscillators using MO-OTAs and grounded capacitors," *Frequenz*, vol. 60, no. 11-12, Jan. 2006. DOI: 10.1515/freq.2006.60.11-12.220.

[119] A. N. Khovanskii, *The Application of Continued Fractions and their Generalizations to Problems in Approximation Theory*. P. Noordhoff, 1963, 212 pp.

[120] B. Krishna, "Studies on fractional order differentiators and integrators: A survey," *Signal Processing*, vol. 91, no. 3, pp. 386–426, Mar. 2011. DOI: 10.1016/j.sigpro.2010.06.022.

[121] F. F. Kuo, *Network Analysis and Synthesis*, 2nd ed. Wiley International, 1968, 515 pp.

[122] Z. Li. "Fractional order root locus." (2015), [Online]. Available: http://www.%20mathworks.com/matlabcentral/fileexchange/50458.

[123] A. Toker, O. ÇiÇekoglu, S. Özcan, and H. Kuntman, "High-output-impedance transadmittance type continuous-time multifunction filter with minimum active elements," *International Journal of Electronics*, vol. 88, no. 10, pp. 1085–1091, Oct. 2001. DOI: 10.1080/00207210110071260.

[124] B. Chaturvedi and A. Kumar, "Electronically tunable first-order filters and dual-mode multiphase oscillator," *Circuits, Systems, and Signal Processing*, vol. 38, no. 1, pp. 2–25, May 2018. DOI: 10.1007/s00034-018-0849-x.

[125] D. Nand and N. Pandey, "Transadmittance mode first order LP/HP/AP filter and its application as an oscillator," *IOP Conference Series: Materials Science and Engineering*, vol. 225, p. 012 150, Aug. 2017. DOI: 10.1088/1757-899x/225/1/012150.

[126] M. E. V. Valkenburg, *Analog Filter Design*. Oxford University Press, 1982, 608 pp., ISBN: 0195107349, 9780195107340.

[127] Y. Lakys and A. Fabre, "Shadow filters – new family of second-order filters," *Electronics Letters*, vol. 46, no. 4, p. 276, 2010. DOI: 10.1049/el.2010.3249.

[128] Y. Lakys and A. Fabre, "Shadow filters generalisation to nth-class," *Electronics Letters*, vol. 46, no. 14, p. 985, 2010. DOI: 10.1049/el.2010.0452.

[129] S. C. D. Roy, "'shadow' filters—a new family of electronically tunable filters," in *Topics in Signal Processing*, Springer Singapore, Oct. 2019, pp. 125–130. DOI: 10.1007/978-981-13-9532-1_14.

[130] M. T. Abuelma'atti and N. R. Almutairi, "New current-feedack operational-amplifier based shadow filters," *Analog Integrated Circuits and Signal Processing*, vol. 86, no. 3, pp. 471–480, Jan. 2016. DOI: 10.1007/s10470-016-0691-7.

[131] P. Huaihongthong, A. Chaichana, P. Suwanjan, *et al.*, "Single-input multiple-output voltage-mode shadow filter based on VDDDAs," *AEU - International Journal of Electronics and Communications*, vol. 103, pp. 13–23, May 2019. DOI: 10.1016/j.aeue.2019.02.013.

[132] D. Singh and S. K. Paul, "Realization of current mode universal shadow filter," *AEU - International Journal of Electronics and Communications*, vol. 117, p. 153 088, Apr. 2020. DOI: 10.1016/j.aeue.2020.153088.

[133] G. Kennedy, *Electronic Communication Systems*. McGraw-Hill Education (India) Pvt Limited, 1999, 763 pp., ISBN: 0074636820, 9780074636824.

[134] D. Wen, Y. Zhou, and X. Li, "A critical review: Coupling and synchronization analysis methods of EEG signal with mild cognitive impairment," *Frontiers in Aging Neuroscience*, vol. 7, Apr. 2015. DOI: 10.3389/fnagi.2015.00054.

[135] M. E. Fouda, A. Soltan, A. G. Radwan, and A. M. Soliman, "Fractional-order multi-phase oscillators design and analysis suitable for higher-order PSK applications," *Analog Integrated Circuits and Signal Processing*, vol. 87, no. 2, pp. 301–312, Mar. 2016. DOI: 10.1007/s10470-016-0716-2.

[136] A. S. Elwakil and W. M. Ahmad, "On the necessary and sufficient conditions for latch-up in sinusoidal oscillators," *International Journal of Electronics*, vol. 89, no. 3, pp. 197–206, Mar. 2002. DOI: 10.1080/00207210210126952.

[137] W. Chung, H. Kim, H. Cha, and H. Kim, "Triangular/square-wave generator with independently controllable frequency and amplitude," *IEEE Transactions on Instrumentation and Measurement*, vol. 54, no. 1, pp. 105–109, Feb. 2005. DOI: 10.1109/tim.2004.840238.

[138] P. Tuwanut, J. Koseeyapom, and P. Wardkein, "A novel versatile modulator circuit," in *IEEE International Symposium on Communications and Information Technology, 2005. ISCIT 2005.*, IEEE. DOI: 10.1109/iscit.2005.1567044.

[139] S. K. Mishra, D. K. Upadhyay, and M. Gupta, "An approach to improve the performance of fractional-order sinusoidal oscillators," *Chaos, Solitons & Fractals*, vol. 116, pp. 126–135, Nov. 2018. DOI: 10.1016/j.chaos.2018.09.015.